VALIDATION OF CONCENTRATIONS ESTIMATED FROM AIR DISPERSION MODELING FOR SOURCE-RECEPTOR DISTANCES OF LESS THAN 100 METERS

FINAL REPORT
CONTRACT NO. 99-319

PREPARED FOR:

CALIFORNIA AIR RESOURCES BOARD
RESEARCH DIVISION
1001 I STREET
SACRAMENTO, CALIFORNIA 95814

PREPARED BY:

AKULA VENKATRAM

DEPARTMENT OF MECHANICAL ENGINEERING
UNIVERSITY OF CALIFORNIA, RIVERSIDE
RIVERSIDE, CALIFORNIA 92521

IN COLLABORATION WITH
JOSEPH KLEWICKI
DEPARTMENT OF MECHANICAL ENGINEERING
UNIVERSITY OF UTAH
SALT LAKE CITY, UT

MAY, 2003

For more information about the ARB's, Research Division's research and activities, please visit our Website:

http://www.arb.ca.gov/research/research.htm

DISCLAIMER

The statements and conclusions in the Report are those of the contractor and not necessarily those of the California Air Resources Board. The mention of commercial products, their source, or their use in connection with material reported herein is not to be construed as actual or implied endorsement of such products.

ACKNOWLEDGEMENTS

The project team from UCR consisted of David Pankratz, Jing Yuan, James Heumann, Jeetendra Kumar Upadhyay, Dennis Fitz, and Akula Venkatram. The University of Utah team included Joseph Klewicki and Heidi Miner. The project members would like to thank Jim Pederson, the ARB project manager, for his support of this project.

We would like to thank Chris Biltoft of the US Army for providing both technical and material support at Dugway Proving Ground, Utah. Vlad Isakov, ARB, played an active role in study design, data analysis, and modeling aspects of this project. He took the initiative to apply a version of the new model to a real case study involving release of Chromium VI near a plating facility in Barrio Logan, San Diego. His contributions were important to the success of this project. We also want to thank Andrew Ranzieri, ARB, for his technical input to the project.

This Report was submitted in fulfillment of ARB contract number 99-319, "Validation of concentrations estimated from air dispersion modeling for source-receptor distances of less than 100 meters", under the sponsorship of the California Air Resources Board. Work was completed as of December 17, 2002.

ABSTRACT

Currently available dispersion models used to estimate dispersion in urban areas were developed using data from experiments conducted at source-receptor distances ranging from 50 m to 16 km. The rural dispersion curves are based on the Prairie Grass experiment (Barad, 1958) where the source-receptor distances ranged from 50 m to 800 m. The urban dispersion curves are based on the St. Louis Dispersion Study (McElroy and Pooler, 1968) where the nearest receptor was 800 m from the source. Regulatory programs require the assessment of potential health impacts from exposures to air toxics from urban sources, such as gasoline stations, dry cleaners, and automotive repair facilities, where human receptors are typically within fifty meters from the source. Because such sources represent about 30,000 small businesses in California, there is a critical need to validate dispersion tools at this distance. ARB has responded to this need by sponsoring UCR to develop a new dispersion model that can be used to estimate the impact of urban sources at source-receptor distances of tens of meters. The model has been developed using data from the Prairie Grass experiment (Barad, 1958), and an experiment conducted in a model urban area at the Dugway Proving Ground, Utah. Estimates from the model proposed in this project have been compared with tracer concentrations measured under a variety of meteorological conditions in the vicinity of an urban source located at a parking lot on the College of Engineering, Center for Environmental Research and Technology (CE-CERT) at the University of California, Riverside. In addition, the performance of the model has been compared with those of ISC, ISC-PRIME, and AERMOD-PRIME, models that are currently used in regulatory practice. The statistics used to quantify model performance ranks the models in the following order: Proposed model, AERMOD-PRIME, ISC, and ISC-PRIME. The relative performance of these models indicates that a reliable model for near source dispersion in urban areas needs to use site-specific meteorology, incorporate upwind dispersion under low wind speed conditions, and reduce source height to account for building downwash.

TABLE OF CONTENTS

LIST OF FIGURES

LIST OF TABLES

1. EXECUTIVE SUMMARY

BACKGROUND

Dispersion models used for regulatory applications, such as ISC, use two sets of dispersion curves, one for rural areas, and the other for urban areas. The rural curves are based on the Pasquill-Gifford dispersion curves, which were derived from experiments conducted in 1956 at O'Neill, Nebraska (Barad, 1958). Because the closest receptor in this experiment was 50 meters from the source, concentrations at smaller distances rely on extrapolation of empirical dispersion curves. The dispersion curves applicable to urban areas were derived from the St. Louis Dispersion Study (McElroy and Pooler, 1968) where the closest receptor was 800 m.

Regulatory programs require the assessment of potential health impacts from exposure to air toxics from urban sources, such as gasoline stations, dry cleaners, and automotive repair facilities, where human receptors are typically within 10 meters from the source. Because such sources represent about 30,000 small businesses in California, there is a critical need to validate dispersion tools at distances within 50 meters. ARB has responded to this need by sponsoring UCR to develop a new dispersion model that can be used to estimate the impact of urban sources at source-receptor distances of tens of meters.

METHODS

The development of the dispersion model consisted of the following steps:

1. Formulate initial model.
2. Evaluate model with Prairie Grass data, and modify formulation.
3. Design and conduct field study in model urban area.
4. Evaluate model with data from field study.
5. Evaluate model with data from source in urban setting.
6. Compare the performance of the proposed model with those of existing regulatory models.
7. Develop user-friendly code for model.

In step 3, UCR in collaboration with the University of Utah, conducted a field study at Dugway Proving Grounds, Utah, from July 12th to July 26th 2001. In this study, the urban canopy was simulated with a 5 × 9 rectangular array of 45 barrels with a height of 0.91 m and a diameter of 0.57 m, and a center-to-center spacing of 1.8 m. If we assume an average urban building height of 5 m, the experiment corresponds roughly to a length scale ratio of 1:5 and plan area density of 16%, which is typical of an urban canopy (Britter and Hanna, 2003). Propylene (C_2H_6), a tracer, was released through a 25.4 mm diameter pipe, both upstream and within the barrel array. This experiment was designed to provide information on the effects of source-geometry on dispersion in the near field.

In step 5, we evaluated the proposed model with data from a tracer experiment sponsored by the California Air Resources Board (ARB contract #00-720) at a parking lot of the College of Engineering's Center for Environmental Research and Technology. SF_6 was released from a line source from the top of trailer situated in a parking lot surrounded by buildings. This arrangement mimics a small source on the top of a building in an urban area. The data was collected over the

two-week period between June 11th and June 28th 2001. This data was also used to evaluate the performance of currently available regulatory models, ISCST, ISCST-PRIME, and AERMOD-PRIME.

RESULTS

We have developed a dispersion formulation that uses onsite turbulence information to estimate vertical and horizontal plume spreads. The model was evaluated and calibrated with data from the Prairie Grass experiment (Barad, 1958). We found that the new model described the essential features of the data from the Dugway experiment without modification to account for source geometry.

The evaluation of the regulatory models and the proposed model with data from the CE-CERT experiment indicates that ISC-PRIME, AERMOD-PRIME, and the proposed model overestimate the high concentrations at the 95th percentile. However, the 95th percentiles estimated by the proposed model are generally within a factor of two of the observed values. The regulatory models generally underestimate both the median and the lower part of the distribution of observed concentrations, signified by the 25th percentiles. ISC generally underestimates the concentrations over the entire range of observed concentrations. The statistics used to quantify model performance ranks the models in the following order: Proposed model, AERMOD-PRIME, ISC, ISC-PRIME.

This project utilized two comprehensive databases from the Dugway and the CE-CERT experiments. The scope of the current project has allowed us to examine only a part of this data. It is clear that much more information in these databases can be used by investigators to understand dispersion in urban areas.

CONCLUSIONS

The major conclusions of the study are:

1. It is possible to estimate near source concentrations in urban areas with a relatively simple model and knowledge of the mean flow and turbulence levels in the vicinity of the source. Results from the Dugway experiment indicate that it is not necessary to model the details of the flow field near the source to estimate concentrations because turbulence levels measured in the vicinity of the source building are likely to automatically reflect the effects of the building.
2. The use of near source turbulence information in the new model and AERMOD-PRIME explains the performance of these models relative to ISC and ISC-PRIME, which are based on generic McElroy-Pooler (McElroy and Pooler, 1968) dispersion curves derived from the St. Louis Dispersion Study.
3. The relative performance of the models in explaining observations indicates that the PRIME component of both AERMOD and ISC overestimated ground-level concentrations observed at CE-CERT within a few building heights of the source. The good performance of the proposed model for receptors less than 5 m from the source suggests that it might be possible to account for downwash by reducing the source height by a factor (0.5 in our case).
4. A dispersion model designed to estimate concentrations at distances of tens of meters from an urban source needs to include a method to account for upwind dispersion. This is

because turbulence levels in the urban canopy can be of the same order of magnitude as the mean winds. The incorporation of upwind dispersion in the proposed model and in AERMOD-PRIME is responsible for the improved performance of these models relative to ISC and ISC-PRIME.

5. Among those regulatory models currently accepted by the USEPA, the model performance statistics suggest AERMOD-PRIME as the preferred model for estimating the near field concentrations for conditions similar to those observed at CE-CERT. AERMOD-PRIME accepts site-specific turbulence information, and accounts for upwind dispersion. The inclusion of these features explains its relative performance in explaining the CE-CERT data. We point out that the use of PRIME might lead to overestimation of maximum concentrations (95^{th} percentile) near the source.

RECOMMENDATIONS

It needs to be stressed that successful application of models for near-source dispersion requires onsite data or an estimate of micrometeorology that includes the general effects of urban obstacles on turbulence. Based on the locations of the meteorological measurements made in the Dugway and the CE-CERT experiments, we suggest that model inputs be derived from meteorological instrumentation, preferably sonic anemometers, located between 1 and 10 building heights from the source below the top of the urban canopy. This is only empirical guidance, which needs to be examined further in future studies.

The basic assumption that underlies the use of turbulence measurements is that horizontal variations in turbulence within a uniform urban canopy are relatively small. But, in a real urban area, we do expect variations in turbulence. Thus, at this point, it is not clear how model results depend on the location of these measurements relative to the source. It is necessary to conduct a study in which sonic anemometers measure flow at several locations within an urban canopy. We can then understand how differences in measured turbulence levels affect modeled concentrations. We might be able to obtain preliminary understanding of these effects by examining measurements made in the Dugway experiment. However, the experiment did not include simultaneous measurements at several locations within the canopy. Measurements were made inside and outside the canopy. Differences between these measurements are likely to be much larger than those within locations inside the canopy. Thus, any results from the Dugway experiment will only be suggestive of the effects of horizontal variations of turbulence levels.

Hanna et al. (2000) have proposed methods to estimate turbulence levels within urban canopies from measurements above the canopy level at rural locations, such as airports. In view of the importance of on-site data in the proposed modeling approach, the applicability of such methods needs to be examined in detail. The Dugway experiment collected an extensive data set on turbulence and flow both inside and outside the model urban canopy. This data can be used in a future project to provide guidance on inferring urban canopy turbulence from measurements made at higher levels.

The model contains three empirical parameters that have been obtained by fitting model estimates to observations. We have not conducted the range of sensitivity studies required to determine whether the chosen values are unique in some sense. Theoretical research is also likely to provide more insight into the values of these parameters.

2. INTRODUCTION

2.1 PURPOSE OF REPORT

Dispersion models used for regulatory applications, such as ISC, use two sets of dispersion curves, one for rural areas, and the other for urban areas. The rural curves are based on the Pasquill-Gifford dispersion curves, which were derived from experiments conducted in 1956 at O'Neill, Nebraska (Barad, 1958). Because the closest receptor in this experiment was 50 meters from the source, concentrations at smaller distances rely on extrapolation of empirical dispersion curves. The dispersion curves applicable to urban areas were derived from the St. Louis Dispersion Study (McElroy and Pooler, 1968) where the closest receptor was 800 m.

Regulatory programs require the assessment of potential health impacts from exposure to air toxics from urban sources, such as gasoline stations, dry cleaners, and automotive repair facilities, where human receptors are typically within 10 meters from the source. Because such sources represent about 30,000 small businesses in California, there is a critical need to validate dispersion tools at distances within 50 meters.

ARB has responded to this need by sponsoring UCR to develop a new dispersion model that can be used to estimate the impact of urban sources at source-receptor distances of tens of meters. This report describes the development and the evaluation of the new dispersion model. The next section describes the technical approach used in developing the model.

2.2 PROJECT TASKS

The development of the dispersion model followed the following steps:

1. Formulate initial model.
2. Evaluate model with Prairie Grass data, and modify formulation.
3. Design and conduct field study in model urban area.
4. Evaluate model with data from field study.
5. Evaluate model with data from source in urban setting.
6. Develop user-friendly code for model.

The model developed in this project has been tested in real urban situations using data collected in a parallel project being sponsored at UCR by the Air Resources Board. The primary objective of this second project entitled "Development of short range dispersion models to estimate air toxics risk in urban environments" (ARB Contract NO., 00-720) is to evaluate dispersion models using tracer data collected at source-receptor distances ranging from tens of meters to kilometers in several urban areas in California.

The model has been designed to use on-site turbulence and wind data. The model code developed in this project will be incorporated into AERMOD (Lee et al., 1998).

2.3 MODEL EVALUATION FRAMEWORK

Because model evaluation plays a pivotal role in the development of a new model, we present the details of the framework that was used to compare model estimates to observations. A model prediction will always differ from the corresponding observation because the model cannot

include all the variables that affect the observation. So we have to assume that the best that the model can do is to provide an estimate of the average over the ensemble of all possible observations corresponding to the model inputs, α (Venkatram, 1982). Because observations respond to a set β not included in the model, we will have an infinite ensemble of observations associated with a given model input set α. Then, we can write

$$C_o(\alpha,\beta) = C_p(\alpha) + \varepsilon(\alpha,\beta) \qquad (2.1)$$

where C refers to the variable of interest, such as concentration, the subscript o refers to an observation, and p refers to the model prediction. The residual between model prediction and observation is $\varepsilon(\alpha,\beta)$. For a given value of the model input set α, we will have an infinite number of observations corresponding to different values of the unknown set β. By definition, the average of these observations for a given α is the model prediction,

$$\langle C_o(\alpha,\beta)\rangle^{\beta} = C_p(\alpha), \qquad (2.2)$$

which implies that

$$\langle \varepsilon(\alpha,\beta)\rangle^{\beta} = 0. \qquad (2.3)$$

We refer to $\varepsilon(\alpha,\beta)$ as inherent uncertainty because it is inherent to a model with a given input set α. Notice that, in principle, expanding the input set to include more of the unknown set can reduce inherent uncertainty β. Thus, the word "inherent" refers to a particular model and its input set, and does *not* refer to an error that is irreducible in principle. However, reducing inherent uncertainty can increase the error associated with imperfect knowledge of model inputs. The third type of error is related to the formulation of the model itself, which could also be in error. Then the actual measured residual is the sum of all three components of error.

As indicated earlier, expanding the model input set can reduce the inherent error α. But, both the model input as well as formulation error can increase as a result. Errors in model inputs are less of a problem if we are only interested in the distribution of predicted concentrations. If the model formulation is essentially correct, model input errors will not affect the predicted distribution of concentrations as long as the incorrect model inputs belong to the population of possible inputs. Ensuring this property becomes an increasingly difficult problem as we increase the model input set, because the model inputs have to be physically consistent with each other; in other words, model input errors become important as more relationships between inputs are inevitably introduced as the model input set expands. This would suggest a modeling strategy that would consist of formulating a model that uses inputs that are as independent of each other as possible. Unfortunately, this does not guarantee a small inherent error. Thus, we need to use trial and error to develop models that reach a compromise between the competing requirements of small inherent error and model input independence.

In the absence of model formulation errors, the major components of model uncertainty are those associated with model input error and variables not included in the model (inherent uncertainty). If we assume, as a working hypothesis, that inherent uncertainty is small, we can avoid accounting

explicitly for model input errors by comparing the distributions of model estimates and observations. Then, if the model can consistently generate distributions of concentrations that are similar to those of observations, we have to conclude that the model is a useful tool for examining air quality impacts.

Because concentrations are observed to be log-normally distributed about the model prediction (Csanady, 1973), the log-transformed equivalent of Equation (2.1) is

$$\ln(C_o) = \ln(C_p) + \varepsilon \ . \qquad (2.4)$$

This model evaluation framework leads to the following methods for comparing model estimates to corresponding observations:

1. Because we can have infinite set of observations for a given model estimate, the model estimate will be treated as the independent variable and plotted on the x-axis. The dependent variable, the corresponding observation will be plotted on the y-axis. In such a plot, points lying to the right of the one-to-one line will indicate model overprediction, and points lying to the left of the line will indicate underprediction.
2. In view of Equation (2.4), we will compare the logarithms of the model estimates with the logarithms of the observations.
3. If the deviations between model estimates and corresponding observations are too large to allow meaningful comparison of the performance of different models, we will assume that model input errors are dominant. Under these circumstances, we will compare the distributions of the model estimates and observations by plotting the ranked observations against ranked model estimates.

3. MODEL FORMULATION

The new generation of short-range dispersion models, such as AERMOD and ADMS, use Monin-Obhukov (M-O) similarity to describe the mean and turbulence structure in the surface boundary layer. The ground-level concentration is generally expressed in terms of the surface friction velocity, u_*, and the M-O length, L, variables that are not measured directly. These variables implicitly contain information on the turbulence and the mean wind that govern dispersion. However, this information is constrained by the relationships of M-O similarity theory, which is not likely to describe the surface meteorology at most locations where the model is applied. Specifically, models based on M-O similarity cannot be applied to dispersion within the urban canopy, below the top of buildings, where building effects can dominate turbulence production. A model designed to estimate concentrations in the vicinity of buildings needs to incorporate the effects of building induced turbulence on dispersion.

The dispersion model proposed in this project estimates concentrations using measured turbulence levels and winds in the vicinity of the source in the urban area. We assume that these measurements reflect the effects of buildings, and thus there is no need to explicitly account for buildings in the model formulation. This assumption implies that such measurements will be available, or it is possible to estimate turbulence levels from the morphology of the urban area. We believe that such a model would have more applicability than that based on M-O theory.

3.1 MODEL FORMULATION

We will first formulate the model for surface releases and then extend it to elevated releases. The model is based on the assumption that the vertical and horizontal spreads of the plume depend on the turbulent intensities at a constant fraction, α, of the vertical spread σ_z. We express the plume growth rates as:

$$\frac{d\sigma_z}{dx} = \frac{\sigma_{we}}{U_e}, \tag{3.1}$$

$$\frac{d\sigma_y}{dx} = \frac{\sigma_{ve}}{U_e}, \tag{3.2}$$

where the subscript 'e' refers to effective quantities evaluated at

$$z = \alpha\sigma_z. \tag{3.3}$$

The expression for vertical spread is consistent with gradient transport if we take the length scale in the eddy diffusivity expression to be the vertical spread, σ_z.

Equation (3.2) is based on Eckman's (1994) model for horizontal spread in the surface layer. Using M-O theory to evaluate U_e and Van Ulden's (1978) results on vertical plume spread, Eckman (1994) shows convincingly that the small time limit embodied in Equation (3.2) explains observations of σ_y drawn from several field experiments, including the Prairie Grass experiment (Barad, 1958). He reduces his numerical results to a simple parameterization:

$$\frac{\sigma_y}{z_0} = a\frac{\sigma_v}{u_*}\left(\frac{x}{z_0}\right)^p, \qquad (3.4)$$

where the parameters "a" and "p" are tabulated according to ranges of z_0/L. The appearance of the roughness length, z_0, and the surface friction velocity in the expressions betrays its origins in M-O theory. While the expression is relatively simple to use, it still requires input variables that are usually inferred from appropriate measurements through M-O theory. In keeping with the objective of this project, we will express σ_y in terms of variables that do not require this inference.

In formulating the model, we assume, for the time being, that in the surface layer turbulence levels vary less in the vertical than the mean does. So we will take σ_u and σ_v to be constant with height, and describe the mean wind and the vertical turbulent velocity using power laws,

$$U(z) = U_r\left(\frac{z}{z_r}\right)^p$$
$$\sigma_w = \sigma_{wr}\left(\frac{z}{z_r}\right)^m, \qquad (3.5)$$

where the subscript "r" refers to the reference height at which all meteorological inputs are measured, and p and m are parameters obtained from the observations. Although, σ_w might not increase or decrease monotonically, as implied by Equation (3.5), the turbulent intensity is generally a monotonically decreasing function with the largest values near the ground. Because the formulation of the model is based on turbulent intensity rather than the turbulent velocity, the coefficient 'm' is determined indirectly by fitting the turbulent intensity to data.

If we substitute Equations (3.5) into Equations (3.1) and (3.2), and integrate we obtain

$$\left(\frac{\sigma_z}{\sigma_{zr}}\right) = \alpha^{-q/(1+q)}(1+q)^{1/(1+q)}\left(\frac{\sigma_{zr}}{z_r}\right)^{-q/(1+q)}$$
and
$$\left(\frac{\sigma_y}{\sigma_{yr}}\right) = \alpha^{((1-m)/(1+q)-1)}\frac{(1+q)^{(1-m)/(1+q)}}{(1-m)}\left(\frac{\sigma_{zr}}{z_r}\right)^{-p/(1+q)}, \qquad (3.6)$$

where q=p-m, and the reference values for the horizontal and vertical plume spreads are calculated using the reference meteorology,

$$\sigma_{zr} = \frac{\sigma_{wr} x}{U_r}$$

and (3.7)

$$\sigma_{yr} = \frac{\sigma_v x}{U_r}$$

Note that the horizontal spread depends explicitly on the vertical spread, and the variation of the horizontal and vertical spreads as a function of distance from the source are given by

$$\sigma_z \sim x^{1/(1+q)}$$

and (3.8)

$$\sigma_y \sim x^{(1-m)/(1+q)}$$

In the equations, α is treated as an undetermined constant that will be estimated by comparing model estimates with observations.

3.2 DISPERSION FROM AN ELEVATED SOURCE

In treating dispersion from an elevated source, we need to account for the fact that plume spreads above and below the release height behave differently. The plume approaching the ground is likely to grow faster because the turbulent intensity becomes larger as the ground is approached. Conversely, the growth rate of the upper part of the plume slows down as turbulent intensity decreases with height. Figure 3.1 depicts this behavior of the elevated plume.

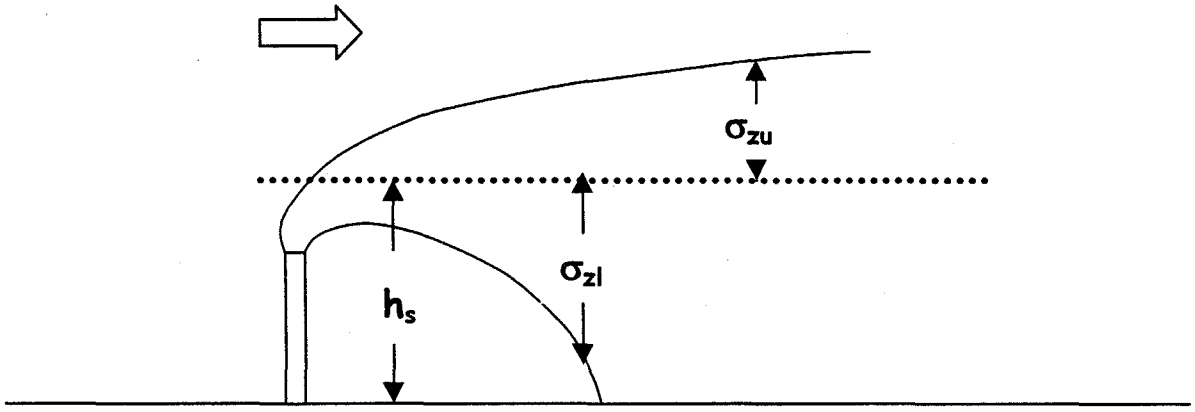

Figure 3.1: Schematic showing unequal plume spreads above and below the plume centerline.

We account for the different growth rates of the two parts of the plume by modeling them separately. The effective properties of the upper plume are evaluated at

$$\bar{z} = h_s + \alpha\sigma_z, \quad (3.9)$$

and the corresponding expression for the lower plume uses a negative α in the above equation.

Then, using a procedure similar to that used for the surface release, we can obtain

$$\bar{z} = \left[h_s^{(1+q)} + \alpha(1+q)z_r^q \sigma_{zr}\right]^{\frac{1}{(1+q)}}, \tag{3.10}$$

so that

$$\sigma_{zu} = (\bar{z} - h_s)/\alpha. \tag{3.11}$$

The letter 'u' in the subscript denotes the upper plume. Using Equation (3.10) in Equation (3.2), we obtain

$$\sigma_{yu} = \frac{\sigma_v}{\sigma_{wr}} \frac{z_r^m}{\alpha(1-m)} \left[\bar{z}^{(1-m)} - h_s^{(1-m)}\right]. \tag{3.12}$$

In treating the lower plume, we need to account for the fact that $\bar{z}$ decreases with distance and becomes zero at a "touchdown" distance given by

$$x_o = h_s^{(1+q)} \frac{u_r}{\sigma_{wr}} \frac{1}{\alpha(1+q)} \frac{1}{z_r^q}. \tag{3.13}$$

Then, the subsequent growth of σ_z is given by

$$\sigma_{zl} = \left(h_s + \bar{z}^{\frac{1}{(1+q)}}\right)/\alpha, \tag{3.14}$$

where the letter 'l' in the subscript denotes the lower plume, and

$$\bar{z} = \left[\alpha(1+q)z_r^q \frac{\sigma_{wr}}{U_r}(x - x_o)\right]^{\frac{1}{(1+q)}}. \tag{3.15}$$

The horizontal spread of the plume after touchdown is given by

$$\sigma_y(x) = \sigma_y(x_o) + \frac{(1+q)}{(1-m)}\left(\frac{z_r}{\bar{z}}\right)^p \frac{\sigma_v}{U_r}(x - x_o), \tag{3.16}$$

and

$$\sigma_y(x_o) = \frac{\sigma_v}{\sigma_{wr}} \frac{h_s}{\alpha(1-m)}\left(\frac{z_r}{h_s}\right)^m. \tag{3.17}$$

The preceding expressions for plume spread are used in the following expression for the concentration:

$$C(x,y,z) = \frac{Q}{U_{eff}} H(x,z).V(x,y). \tag{3.18}$$

where the horizontal concentration distribution is given by the Gaussian,

$$H(x,y) = \frac{1}{\sqrt{2\pi}\sigma_{yeff}} \exp\left(-\frac{y^2}{2\sigma_{yeff}^2}\right). \tag{3.19}$$

The vertical distribution accounts for reflection from the ground and the top of the mixed layer,

$$V(x,z) = \frac{1}{\sqrt{2\pi}\sigma_{zeff}} \left\{ \left[\exp\left(-\frac{(h_s - z)^2}{2\sigma_{zeff}^2}\right) + \exp\left(-\frac{(h_s + z)^2}{2\sigma_{zeff}^2}\right) \right] + \left[\exp\left(-\frac{(z_t - z)^2}{2\sigma_{zeff}^2}\right) + \exp\left(-\frac{(z_t + z)^2}{2\sigma_{zeff}^2}\right) \right] \right\} \tag{3.20}$$

where

$$z_t = 2z_i - h_s. \tag{3.21}$$

Here z_i is the mixed layer height. The effective mean velocity and plume spreads in the preceding concentration equations are taken to be vertical plume spread weighted values,

$$\beta_{eff} = (\beta_u \sigma_{zu} + \beta_l \sigma_{zl})/(\sigma_{zu} + \sigma_{zl}), \tag{3.22}$$

where β refers to any one of these variables. Equation (3.22) is designed to emphasize the contribution of the plume with the larger magnitude. If the upper and lower plume spreads are equal, the effective value is a simple average of the upper and lower quantities. Clearly, this is a tentative expression that needs to be evaluated with observations.

3.3 DISPERSION AT LOW WIND SPEEDS

In urban areas, the wind speeds can become comparable to the turbulent velocities. Under these circumstances, it is necessary to consider dispersion in the direction of the mean wind. To model this feature, we have chosen the formulation used in AERMOD. The horizontal concentration distribution is assumed to consist of a plume component, given by the equations in the previous section, and a random component, which assumes that the plume spreads equally in all directions. Then,

$$H(x,y) = f_{ran} H_{ran} + (1 - f_{ran}) H_p(x,y), \tag{3.23}$$

where the plume component is given by Equation (3.19), and the random component is

$$H_{ran} = \frac{1}{2\pi r}, \tag{3.24}$$

where 'r' is the radial distance between source and receptor. The weighting factor f_{ran} is taken to be

$$f_{ran} = \frac{2\sigma_y^2}{\left(x^2 + 2\sigma_y^2\right)}. \qquad (3.25)$$

The factor 2 in the equation is based on the assumption that the horizontal velocity components are equal. Thus, the random component of dispersion is emphasized when the turbulent velocities become comparable to the mean wind. Under these circumstances, the transport wind used in the random component of the concentration is taken to be

$$U_{trans} = (U_{eff}^2 + 2\sigma_v^2)^{1/2}, \qquad (3.26)$$

to ensure that the transporting wind corresponds to the vector wind along the line joining the source to the receptor.

The next section describes the application of the model to data from the Prairie Grass experiment.

4. EVALUATION WITH DATA FROM THE PRAIRIE GRASS EXPERIMENT

The model described in the previous section was evaluated with data from the Prairie Grass experiment (Barad, 1958). Even though the experiment was conducted as long ago as 1956, the data from the experiment still represent the most complete available for the analysis of surface layer dispersion. Evaluation with the data set represents a litmus test for models applicable to the surface boundary layer. Previous studies (Venkatram, 1982; Van Ulden, 1978) indicate that it is possible to obtain excellent agreement between model estimates and corresponding observations from this experiment, conducted under relatively idealized conditions. The relatively small scatter between model estimates and observations allows the estimation of the model parameters described in Chapter 3.

4.1 PROJECT PRAIRIE GRASS

Most of our current understanding of dispersion in the surface layer is derived from the Project Prairie Grass (PPG) experiment conducted in 1956 at O'Neill, Nebraska. The experiment involved more than 60 scientists drawn from MIT, Texas A&M, University of Wisconsin, University of Washington, Air Force Cambridge Research Center, and Air Weather Service. Planning for the experiment was initiated in 1953, and the experiment was conducted in July and August 1956. During this intervening period, the SO_2 sampling was developed and tested at experiments in Round Hill, Massachusetts. The careful planning and equipment testing led to the success of the experiment. Although several tracer experiments have been conducted since then, none of them has matched the scope and completeness of the Prairie Grass experiment.

In the PPG experiment, the tracer, SO_2, was released at a height of 0.46 m, for an interval of 10 minutes. The release was sampled with 5 semi-circular arcs at 50m, 100m, 200m, 500m, and 800m from the source. The samplers on these arcs were spaced at 2^o intervals on the first four arcs, and at 1^o on the 800m arc, for a total of 545 samplers. The PPG experiment provided limited information on vertical profiles of concentrations: 6 towers on the 100m arc measured concentrations at heights ranging from 0.5m to 17.5m.

The concentration measurements have allowed us to make accurate estimates of the horizontal distribution of the concentration field for 70 experiments, roughly half of which were conducted under stable conditions and the remaining under unstable conditions. The meteorological conditions covered a wide range from very stable to very unstable conditions.

The mean wind was measured at 8 levels ranging from 0.125 m to 16 m. The standard deviation of the horizontal direction and vertical velocity fluctuations were measured at a single height of 2 m. It is not clear that the bivanes used to make these measurements had the response times required to capture all the turbulent velocity frequencies at 2 m. However, this lack of adequate instrumentation for measuring turbulence was more than compensated by the sampler network's ability to resolve the ground-level plume. Lee and Irwin (1997) fitted Gaussian distributions to the concentrations along each arc and derived horizontal spreads and peak concentrations for each arc. This information was used to evaluate the proposed model.

4.2 MODEL EVALUATION

The model contains 3 parameters. The first is α, which is fraction of σ_z at which the effective properties are evaluated. We will also assume that the vertical and horizontal plume spreads calculated using the model equations require to be multiplied by factors α_z and α_y to bring them

into agreement with observations. Thus, the model contains 3 empirically derived parameters. The model is useful only if these parameters do not have to be adjusted for a range of observations. This will be evaluated by using the model to describe the observations made in the Dugway experiment, described in section 6.

We computed the value of the parameter p in the equations by fitting a power curve to the mean wind measurements at all 6 levels corresponding to the 68 tracer experiments; roughly half of them corresponded to unstable conditions. Because PPG did not measure vertical profiles of σ_w, we initially took m=0, which assumes little variation of the turbulent velocity. The parameter p varied from 0.16 to 0.48 for stable conditions, with an average value of 0.27. For unstable conditions, p varied from 0.08 to 0.48 with an average value of 0.2.

Figure 4.1 compares model estimates of C/Q of the peak ground-level concentrations (z =1.5 m) observed during stable conditions. The model parameters worked out to be α_z=0.55 and α_y=0.6, and α=0.5 to obtain the fit shown in the following figures. We see that the modeled concentrations are highly correlated with the observations (r^2>0.9), and most of the modeled values are well within a factor of two of the observations.

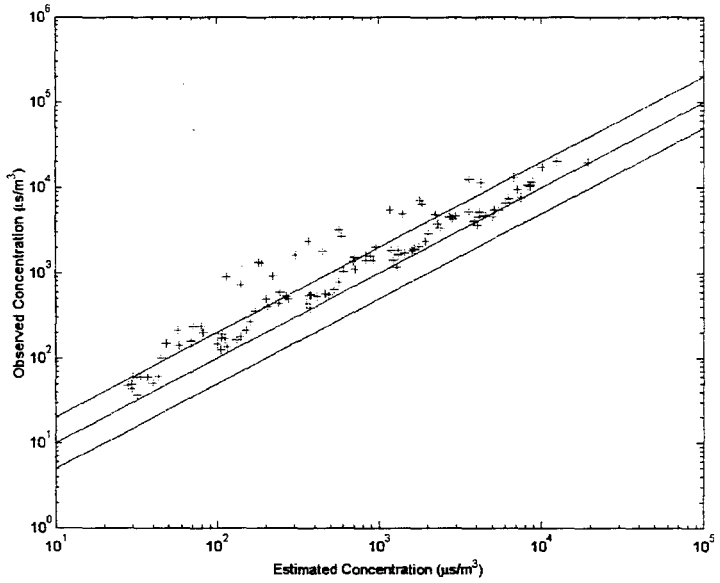

Figure 4.1: Comparison of observed to model estimated concentrations for stable conditions in Prairie Grass Experiment. No variation of turbulence with height.

However, the modeled values (See Figure 4.1) illustrate behavior that suggests the need to include other variables in the model. Figure 4.2, which shows a plot of the ratio of the observed to model concentrations shows that the model's tendency to underpredict increases as σ_z increases. This indicates the possibility that the model is overpredicting σ_z because it does not account for the decrease in the turbulent velocity fluctuations with height. To explore this possibility, we allowed σ_w to vary with height as follows

$$\sigma_w = \sigma_{wo} \exp\left(-\frac{z}{u_* \tau}\right), \qquad (4.1)$$

where the time constant τ was chosen to be 67 seconds. This is an entirely empirical equation that is used only to illustrate the possible effects of a decreasing σ_w on vertical plume spread; the scale height for this decrease is taken to be $u_*\tau$. The value of the coefficient m in the model equations was computed by evaluating Equation (4.1) at heights of 2m and 10m. The computed values of m varied from –0.82 to –0.16 with a median value of –0.27.

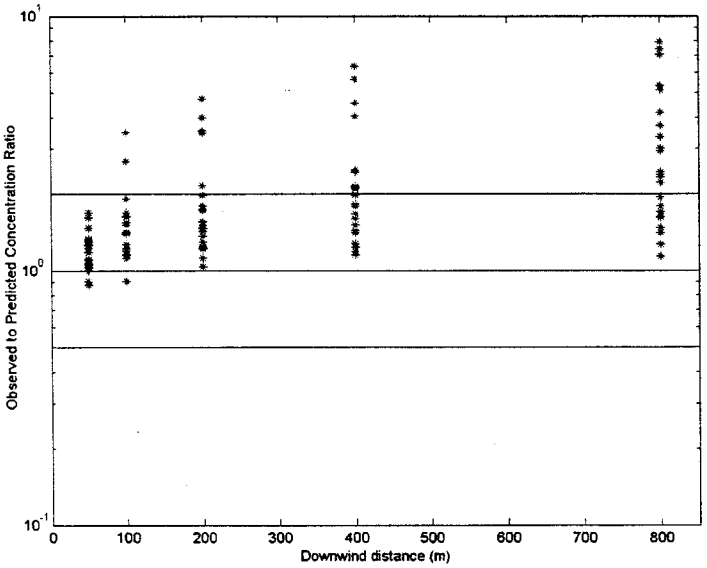

Figure 4.2: Ratio of observed to predicted concentration as function of downwind distance for stable conditions in Prairie Grass Experiment. No variation of turbulence with height.

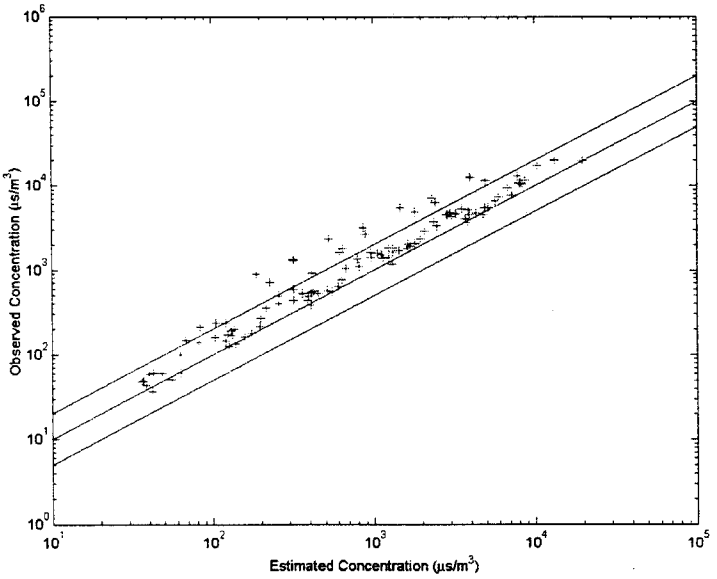

Figure 4.3: Comparison of observed to model estimated concentrations for stable conditions in Prairie Grass experiment. Turbulence varies with height.

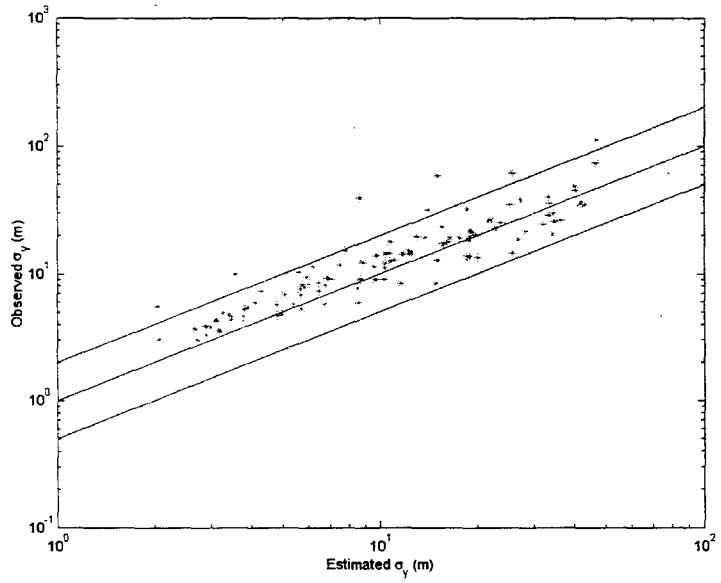

Figure 4.4: Comparison of observed to model estimated horizontal plume spreads under stable conditions in Prairie Grass experiment. Turbulence varies with height.

Figure 4.3 shows that this empirical correction makes a noticeable improvement in model performance; most of the points are close to the one-to-one line. Figure 4.4 shows the comparison of model estimates of horizontal spread with corresponding observations. It turns out that the estimates of horizontal spread are less sensitive to the variation of m than the centerline ground-level concentrations.

Figure 4.5 compares model estimates with observations of ground-level concentrations for the unstable boundary layer. In this case, we assume that σ_w does not increase with height, so that m=0.0. The fitted value of the power coefficient for the mean wind varies from 0.08 to 0.48 with a median value of 0.17.

Figure 4.6 shows the improvement in model performance when the increase of σ_w is taken to follow the similarity profile:

$$\sigma_w = 1.3u_*\left(1 - 3\frac{z}{L}\right)^{1/3}. \qquad (4.2)$$

The power law coefficient, m, obtained by evaluating Equation (4.2) at 2m and 10m ranges from 0.02 to 0.24 with a median value of 0.11; this relatively low value explains the small improvement in model performance compared to that for the stable boundary layer.

Figure 4.7 compares model estimates of horizontal spread with corresponding observations. As for the stable cases, the model explains close to 90% of the observed variance, although the model does underpredict the observations. Model estimates of horizontal spread are relatively insensitive to the use of Equation (4.2).

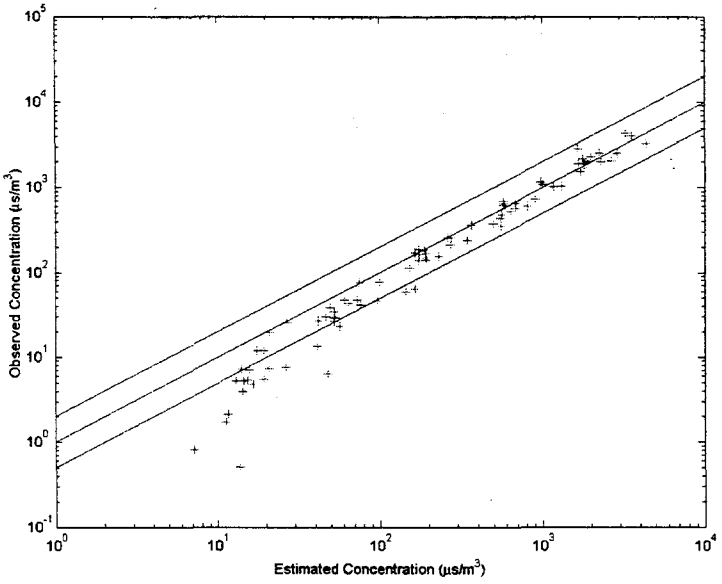

Figure 4.5: Comparison of observed to model estimated concentrations under unstable conditions in Prairie Grass experiment. Turbulence does not vary with height.

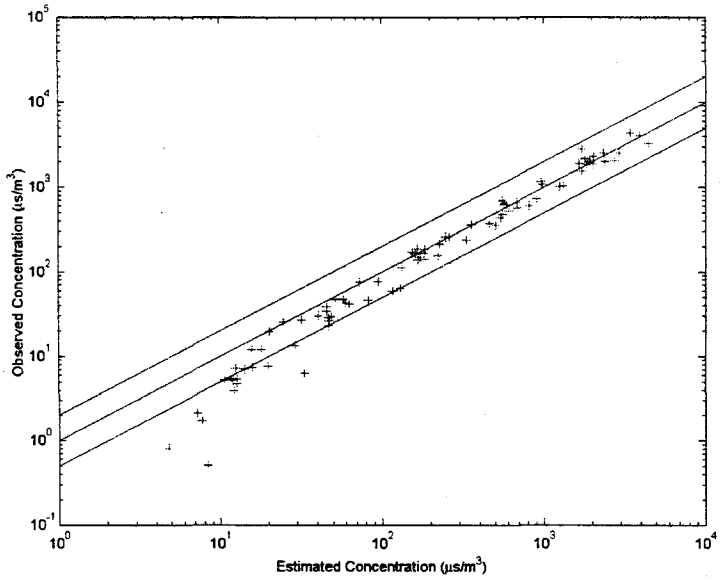

Figure 4.6: Comparison of observed to model estimated concentrations under unstable conditions in Prairie Grass experiment. Turbulence varies with height.

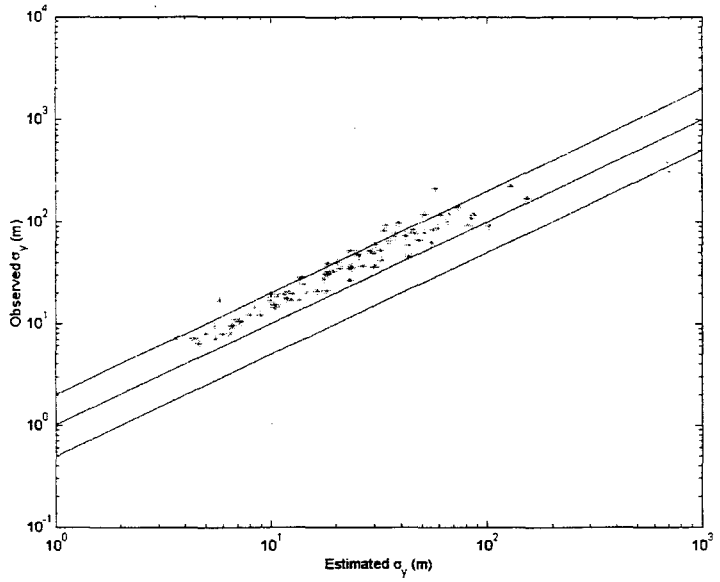

Figure 4.7: Comparison of observed to model estimated horizontal spreads for unstable conditions in Prairie Grass experiment. Turbulence varies with height.

4.3 CONCLUSIONS

We have developed a dispersion model that uses onsite measurements of turbulence and wind speed to estimate plume spread parameters. This obviates the need to compute micrometeorological parameters, such as the surface friction velocity and the Monin Obukhov, required by the current generation of dispersion models (van Ulden, 1978; Venkatram, 1992; Du and Venkatram, 1997). This is clearly an advantage especially in situations in which these micrometeorological variables are not well defined, such as in urban areas.

We have evaluated the model with data from the Prairie Grass experiment, and shown that it performs at least as well as similarity-based models. The proposed model also provides excellent estimates of the horizontal spread, which other models have some difficulty in doing. Note that the underpredictions of concentrations for the stable cases and horizontal spreads for the unstable cases can be improved by adjusting the model parameters as a function of stability. However, this is inconsistent with the concept of keeping these parameters constant over a range of stabilities. Thus, for the time being, we accepted the slight reduction in model performance in exchange for maintaining this concept.

This next chapter describes the application of the model to data from the Dugway experiment.

5. EVALUATION OF MODEL USING THE DUGWAY EXPERIMENTS

The overall objective of the field study at Dugway Proving Ground, Utah, was to collect data that would allow the development and evaluation of air quality models at spatial scales less than 100 meters in an urban setting. Existing models, such as ISC and AERMOD, have not been evaluated in an urban area at these spatial scales.

The experiment at Dugway was designed to simulate a source in an urban area modeled at a scale of roughly 1:5. The distances in the model corresponded to scales of less than 100 meters in the real world. The experiment was designed to examine the relative roles of turbulence levels in the immediate vicinity of the source and average turbulence levels in the urban canopy in controlling dispersion close to the source. The data collected in the experiment were used to evaluate the model described in chapters 3 and 4.

5.1 EXPERIMENTAL DESIGN

The experiment was based on the assumption that the horizontal and vertical scales of turbulence that govern dispersion within the urban canopy are proportional to the dimensions of the building (Macdonald et al., 1998). This allowed us to use obstacles to simulate buildings, and conduct dispersion experiments whose results can be scaled up to full-scale urban areas. In the experiment, 55-gallon drums were used as obstacles. These drums were 0.91 m high, and had a diameter of 0.57 m. If we assume that typical urban buildings are about 5 meters high, the experiment corresponded roughly to a length scale ratio of 1:5. A cylindrical obstacle is not representative of a typical urban building. However, because it is symmetric relative to wind direction, we can avoid the complexity associated with wake characteristics changing substantially with wind direction. Thus, average turbulence levels in the canopy are not likely to be sensitive to wind direction. At the same time, we can vary the turbulence levels close to the source by varying the source configuration as described later.

The urban canopy was constructed with 45 drums laid out in a 5 by 9 array, as shown in Figure 5.1. The longer side of the array, with 9 drums, was aligned with the prevailing northerly wind direction at Dugway. The drums were separated by a distance of 1.8 m, which translates into a ratio of obstacle frontal area to plan area of about 16%. This ratio is typical of urban areas where there is interaction among wakes of different buildings (Britter and Hanna, 2003).

Propylene (C_3H_6) was used as a tracer, which was released from the location of the 4th drum. At this downwind distance, we expect the flow field to come into equilibrium with the obstacle array. The source configuration was varied using 6 drums. These configurations were designed to simulate releases from different types of buildings in urban areas. For example, we could change the aspect ratio of the source by placing two drums, side by side. Another possible arrangement consisted of two drums stacked on top of each other.

The tracer was sampled using a fast response (50 Hz) photo-ionization detectors (PID). The concentration time series was averaged over 5 minutes; this averaging time corresponds to 25 minutes if we assume a length scale ratio of 1:5. Although we were primarily interested in these time averaged concentrations, the high-resolution concentrations from the PIDs can be used to gain insight into the physics of dispersion in the building wakes.

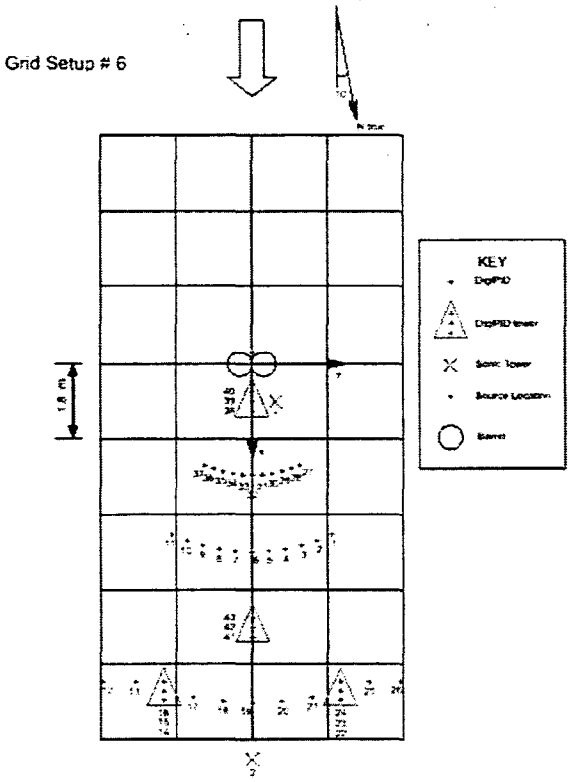

Figure 5.1: Schematic of experimental setup at Dugway Proving Grounds.

The ideal receptor network should have the density to sample the tracer plume, and at the same time resolve the concentration gradients in the plume. With a limited number of samplers, it was difficult to achieve both objectives simultaneously. The minimum spacing between samplers was determined by assuming that we can resolve the plume by placing samplers at one sigma-y and two sigma-y from the plume centerline. If we take the time-averaged sigma-y to be approximately 0.1 times the downwind distance from the source (Macdonald et al., 1998), one sigma-y corresponds to roughly 6^{o} from the plume centerline. The wind direction was not expected to change by more than 50^{o} during the course of the planned one-hour sampling period when the mean wind direction is normal to the upwind edge of the urban canopy. This means that we needed approximately 8 samplers at each sampling arc to ensure sampling of the plume. During the course of the daily 8-hour sampling period, we expected several hours during which the plume would miss the sampling arc entirely. However, during this time, we expected enough hours with measurable concentrations to allow us to describe the dispersion patterns in the obstacle array.

The experiment at Dugway was designed to

1. Provide data that will allow the development of a simple model that uses on-site wind and turbulence data.
2. Collect data under controlled conditions that allow separation of governing variables, and thus avoid confounding effects.
3. Simulate the essential features of dispersion in the urban area. We wanted to describe the processes that govern dispersion both near the source as well as that several building heights from the source.

The next section describes the actual experiment.

5.2 THE DUGWAY EXPERIMENT

The experiments was conducted at the Surface Layer Turbulence and Environmental Sciences Test (SLTEST) site, located at 40° 8.5' N, 113° 26' W, 1297 m above mean sea level. The SLTEST site is 8 km west of the north end of Granite Mountain along Goodyear Road on the U.S. Army Dugway Proving Ground, Utah. This site, on the north side of Goodyear Road, was established with National Science Foundation funding to serve as a test bed for atmospheric boundary layer experiments and dispersion studies. Because of the extended fetch over low roughness terrain, free of large-scale obstructions, flow over the SLTEST site is often remarkably steady from the northerly direction. Thus, it was often possible to perform dispersion testing over periods up to 1 hour with variations in wind direction contained within a 40° arc.

The small-scale experiment was conducted at Dugway Proving Ground, Utah from 17th July 2001 to 26th July 2001. Figure 5.2 shows a photograph of the experimental setup.

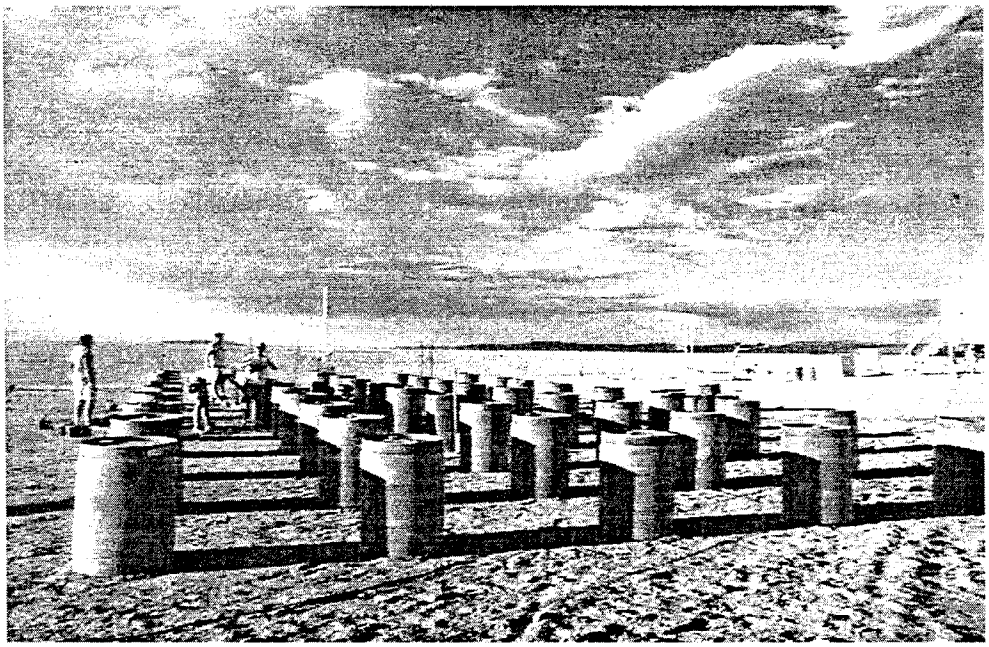

Figure 5.2: Photograph of experimental setup at Dugway Proving Grounds, Utah.

Propylene (C_2H_6), a tracer, was released through a 25.4 mm diameter pipe, both upstream and within the barrel array. The dissemination rate was fixed at 15 liters/minute using a mass flow controller. The tracer was sampled on receptor arcs at 1.5S, 2.5S, and 4.5S from the source, where S (=1.8m) is the spacing between the drums. Each arc contained 11 photo-ionization detectors (PIDs), 5^{o} apart at 0.23 H. The furthest distance of 4.5S scales up to approximately 40 meters in a real urban area. Three PID were placed at 0.5S to sample the cavity region of the obstacle where the source was located. At 4.5S, two PIDs were placed at 0.5H and 1.5H, where H is the height of the obstacle. The vertical array of three PIDs at 4.5S provided information to construct the vertical profile of concentrations.

Turbulence, velocity, and temperature measurements were made with sonic anemometers at three locations. Three sonics at 0.5H, 1.0H, and 2.0H on an upwind tower provided information on the approach flow. One sonic at 0.5H, behind the source obstacle, provided flow and turbulence

information in the cavity region of the source. Two sonics at 0.5H and 1.5H located at 4.5S from the source provided information on the fully developed flow in the urban canopy.

The tracer source was located at either ground-level or at 1H. For each source location, four different barrel configurations were arranged near the source. The effects of the source on dispersion were examined by releasing the tracer from drum configurations of increasing complexity:

1. the top and bottom of a single barrel,
2. the top and bottom of a pair of barrels placed side-by-side,
3. the top of a set of four barrels, and
4. from the top of a "tall" structure consisting of two barrels placed on top of each other.

Details of the grid and source configurations are described in Appendix A. We next describe the performance of the model in explaining the Dugway data.

5.3 MODEL EVALUATION

The experiment yielded 13.5 hours of data covering a wide variety of meteorological conditions. Figure 5.3 shows the variation of the stability parameter, z/L (equal to the Richardson number in a constant stress layer), during the course of the experiments conducted on July 19, 2001 analyzed in 15-second blocks. The parameter was derived from observations at tower 2 (See Figure 5.2).

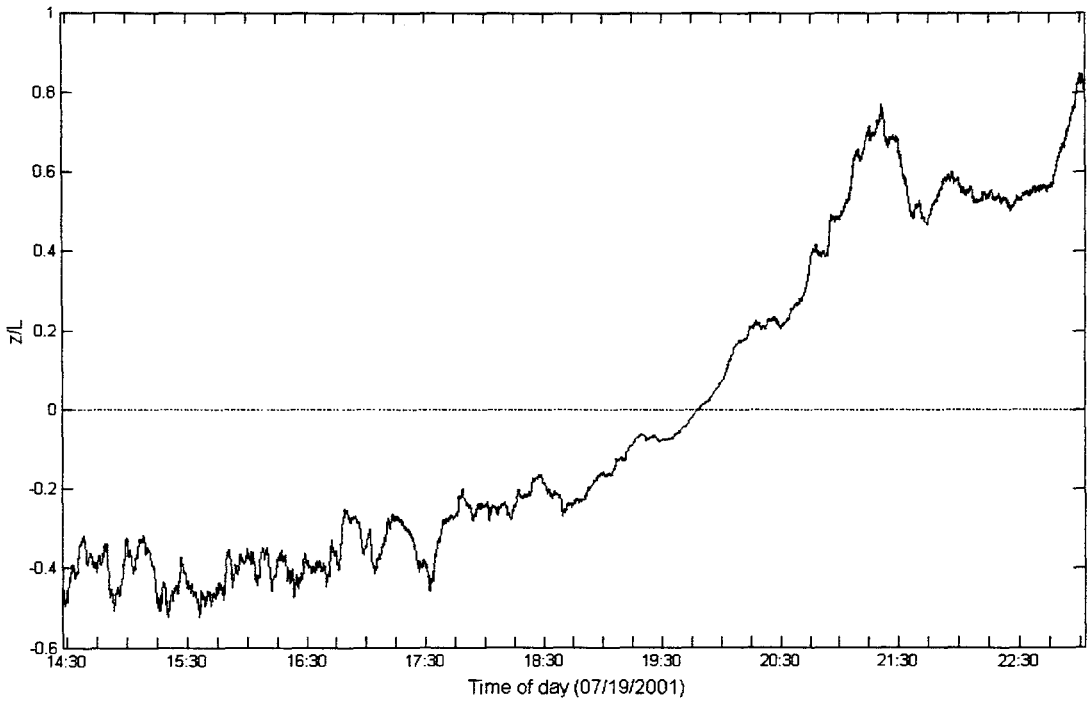

Figure 5.3: Variation of the stability parameter, z/L, at July 19, 2001. (Data collected from sonics on tower 2 at z = 3.185m)

We see that, as expected, the surface layer is unstable during the daytime, and becomes stable around 20:00 hours. The absolute magnitude of Monin-Obukhov length, L, is greater than 5 m, suggesting that the model canopy is generally embedded in a shear dominated, neutral boundary layer.

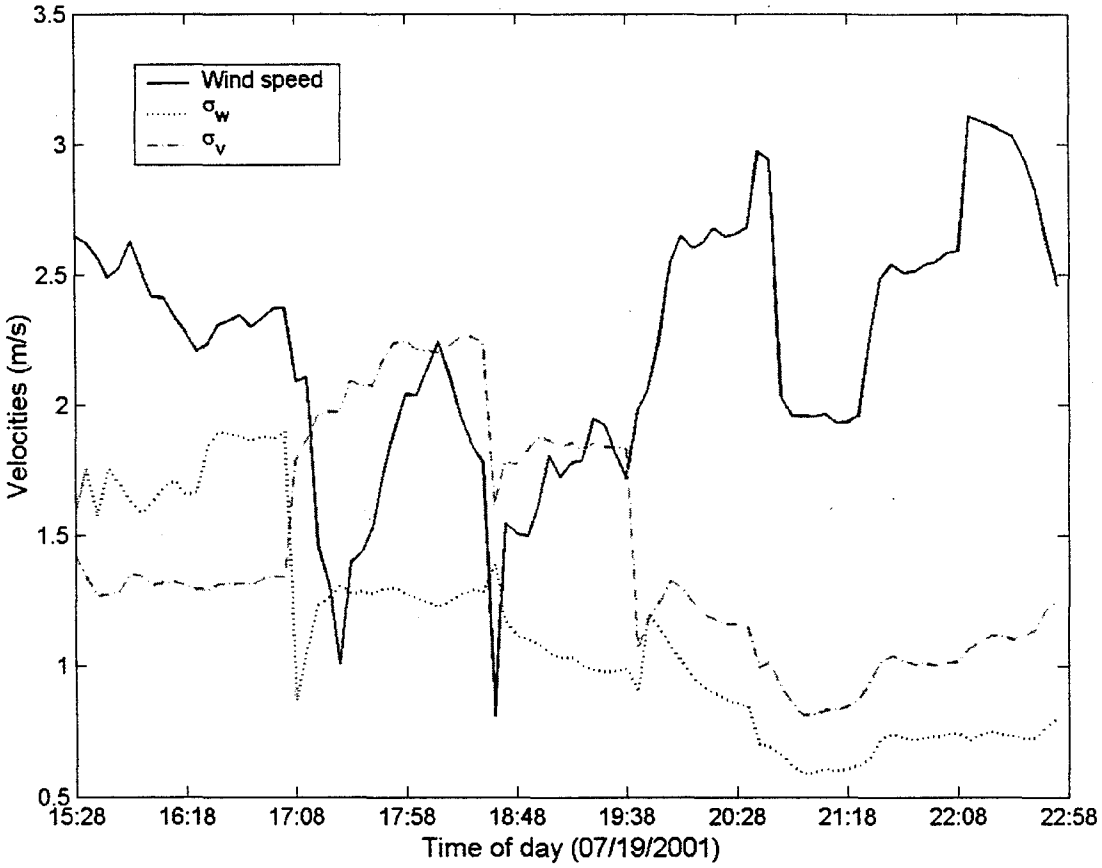

Figure 5.4: Variation of wind speed, σ_v, and σ_w, at July 19, 2001.
(Data collected from sonics on tower 1 at z = 0.50m)

Figure 5.4 shows the variation of the mean wind, U, σ_v, and σ_w measured within the canopy at 0.5H during the experiment at tower 1 (See Figure 5.1); these measurements, which constituted the model inputs, are 5-minute averages. The mean wind within the canopy varies between 1 m/s and 3 m/s, showing substantial variations over 5 minutes periods. The vertical component of turbulent velocity, σ_w, is above 1 m/s during the day, attaining its maximum value close to 2 m/s around 17:00 hours, and decreases to around 0.7 m/s in the evening. The horizontal turbulent velocity is larger than 1.3 m/s through the day, and then decreases to about 1 m/s in the evening hours.

Effects of Obstacles on Concentrations and Flow

The first set of experiments was conducted without any obstacles to provide baseline data that could be compared with that in the presence of the obstacle array. Note that the three receptor arcs

range from about 4 m to 16 m from the source. Thus, the experiment evaluates the model at distances that are much smaller than the closest receptor at 50 m in the Prairie Grass experiment.

Figure 5.5 shows the overall effects of the obstacle array on the variation of the maximum concentration on each arc as a function of downwind distance averaged over all meteorological cases. The top panel shows that the presence of obstacles reduces the concentrations by about a factor of five for ground-level releases. For an elevated release, from the top of the barrel, the reduction is about a factor of 2.5. These reductions in ground-level concentrations are consistent with data from the Kit Fox field experiments reported by Hanna and Chang (2001).

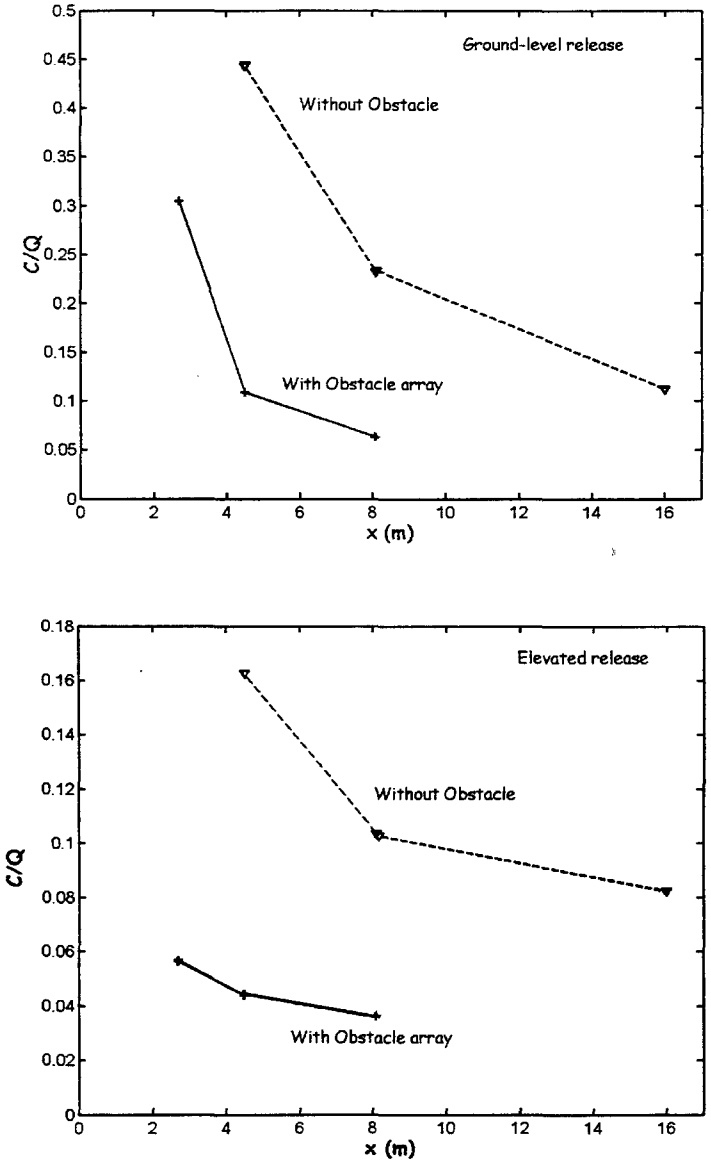

Figure 5.5: Variation of observed normalized concentrations with distance (x): (a) ground-level release and (b) elevated release at 1H.

Model evaluation

In all the model runs, the meteorological data were obtained from the 0.5H level of the sonic next to the source. It was not physically possible to locate another sonic anemometer at a different height within the canopy on the same tower. Thus, it was difficult to estimate the gradients of velocity and turbulence within the model canopy. We have used p=0.23 and m= 0.0, implying a velocity gradient in the model canopy, but no turbulence gradient. Figure 5.6 shows model estimates compared with observations for a ground-level release for all meteorological cases. The large scatter is related to the effects of inevitable errors in the wind direction on model performance. Figure 5.7 shows that although the model provides adequate estimates of the cross-wind distribution, the mismatch between concentrations at any crosswind receptor can be large. This effect is reduced substantially in the Q-Q plot of Figure 5.8, which shows that the model provides an adequate description of the distribution of observed concentrations.

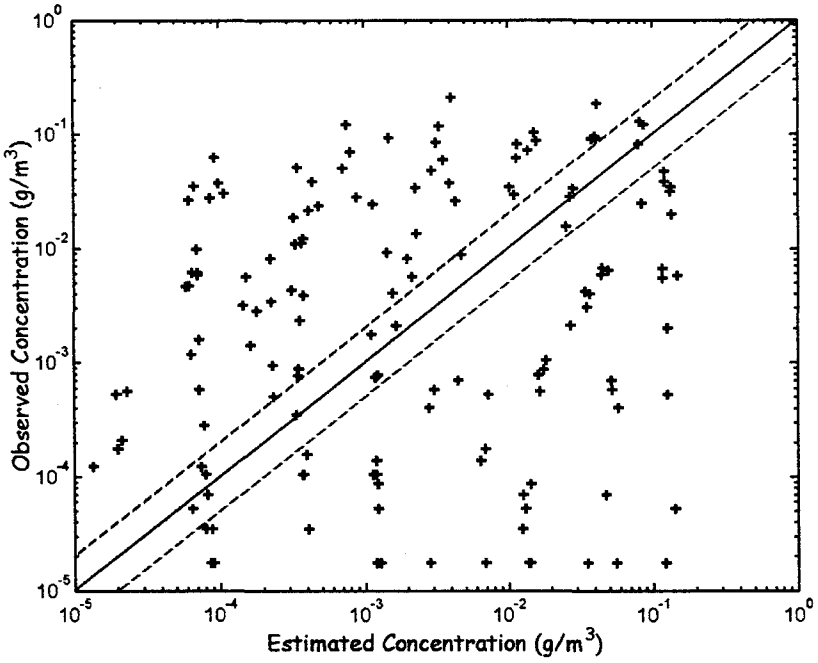

Figure 5.6: Comparison of observed and estimated concentrations for ground-level release for all meteorological cases in without obstacle configuration.

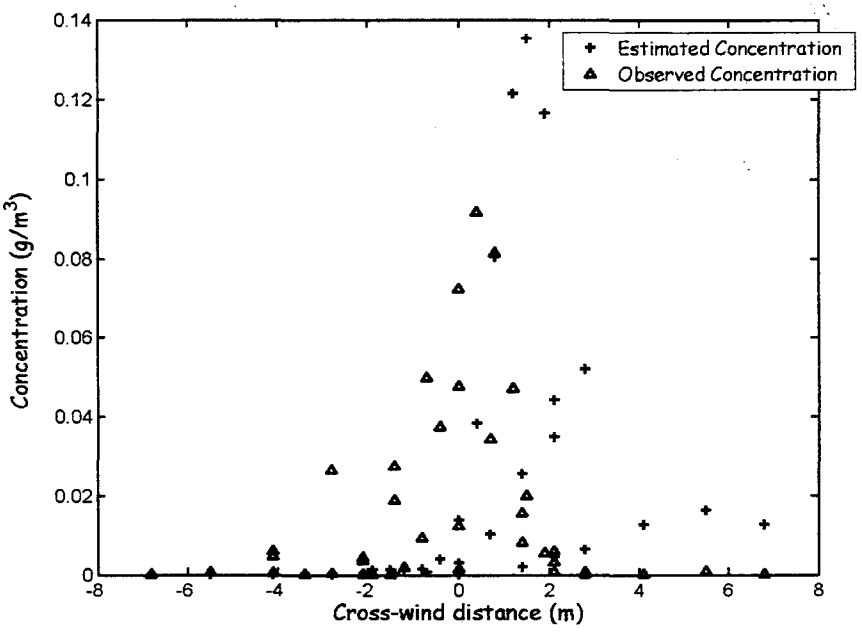

Figure 5.7: Averaged observed and estimated concentrations along cross-wind direction for ground-level release in without obstacle configuration.

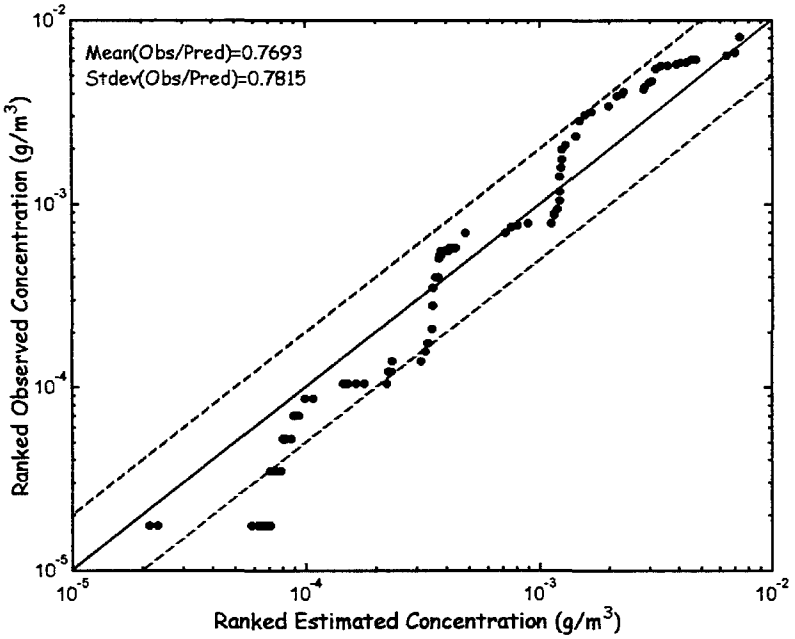

Figure 5.8: Q-Q Plot for ground-level release for all meteorological cases in without obstacle configuration.

Figures 5.9 to 5.10 show the scatter and the Q-Q plots for a ground-level release within the obstacle array. Although the scatter between observed and estimated concentrations is large, as seen in Figure 5.9, Figure 5.10 shows that the model reproduces the distribution of observed concentrations.

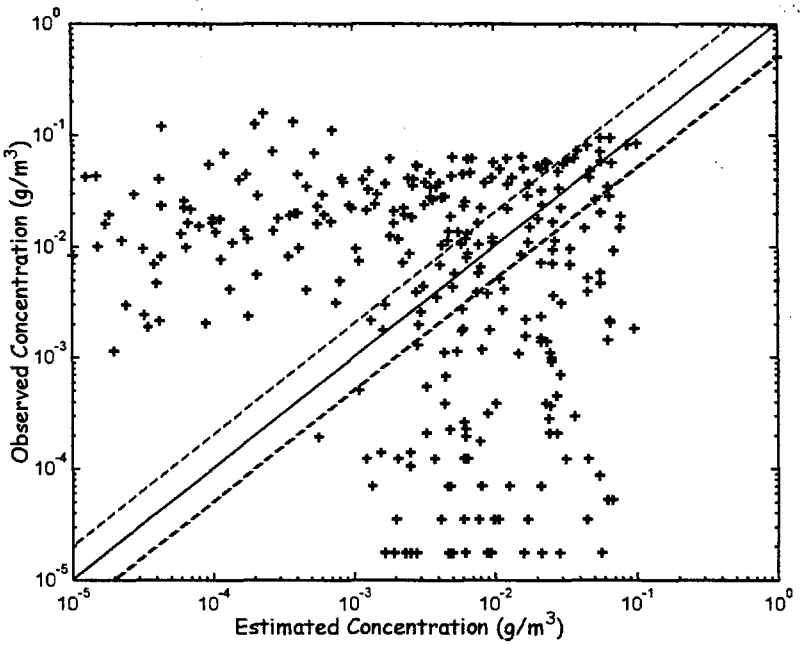

Figure 5.9: Comparison of observed and estimated concentrations for ground-level release for all meteorological cases in array of obstacles configuration.

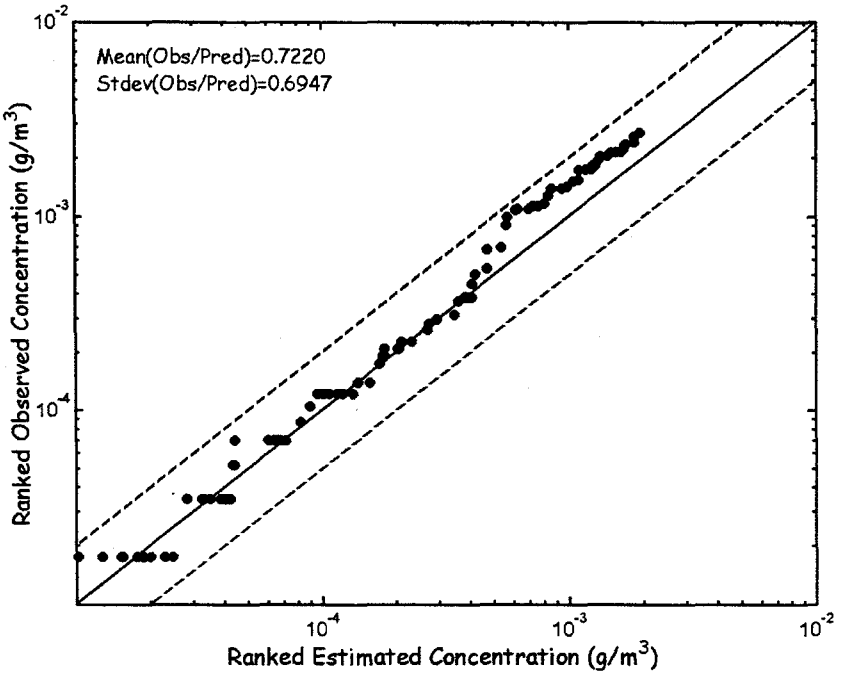

Figure 5.10: Q-Q Plot for ground-level release for all meteorological cases in array of obstacles configuration.

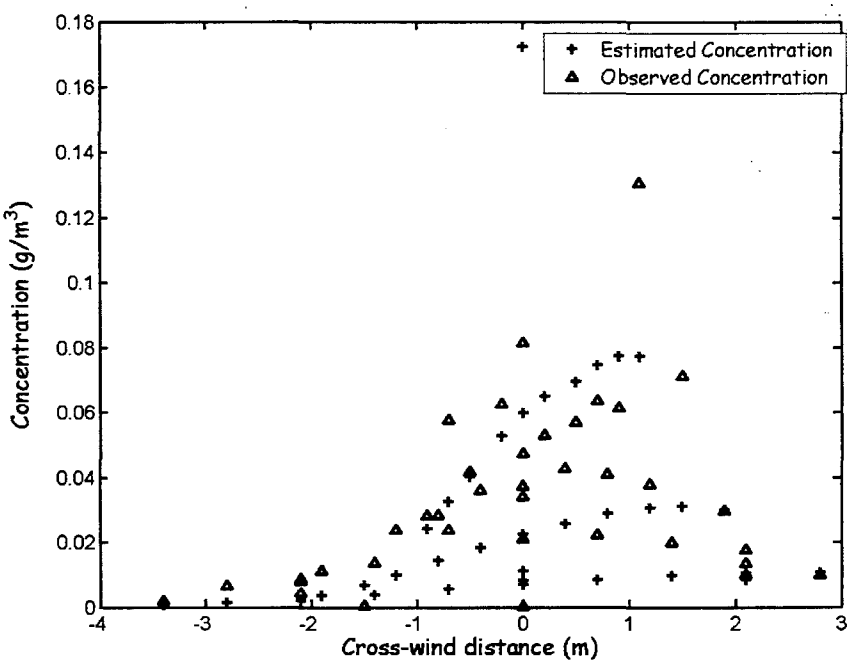

Figure 5.11: Averaged observed and estimated concentrations along cross-wind direction for ground-level release for all meteorological cases in array of obstacles configuration.

Effects of Source Configuration on Dispersion

In the comparison of this section, we have averaged the concentrations over all the hours for a particular grid-setup; the scatter is reduced only to facilitate comparison between different cases. Figure 5.12 shows the scatter and Q-Q plots for a ground-level release behind obstacles (Grid 6). We see that the placing two barrels in front of the source does not appear to affect model performance for the receptors being considered in the experimental setup.

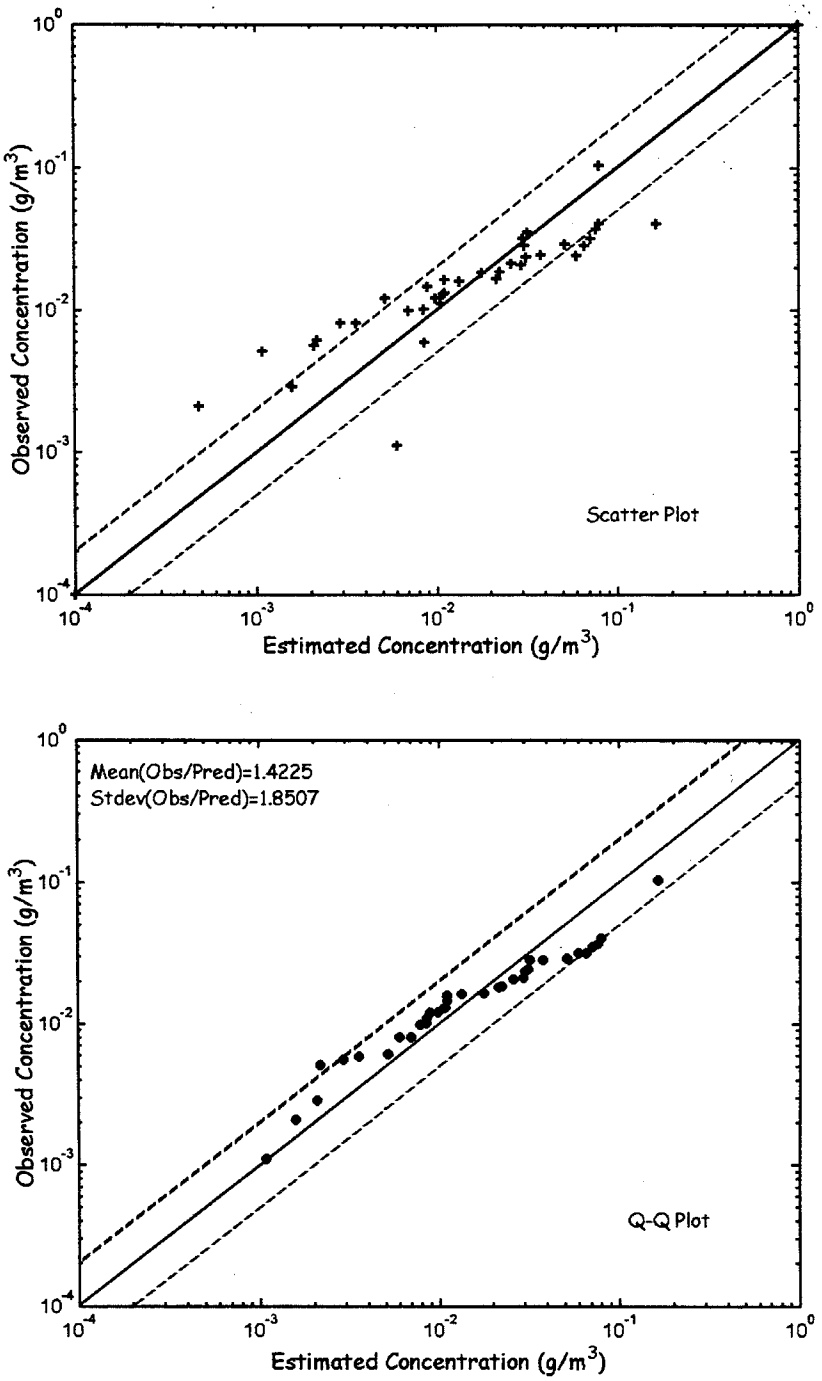

Figure 5.12: Ground-level release behind two barrels in Grid No. 6.

Figure 5.13 indicates that placing an obstruction consisting of a barrel on top of two barrels between the second and third arcs appears to have little effect on model performance. We see similar robustness in model performance for elevated releases with different source configurations 5.14 and 5.15 (Grid No. 5 and Grid No. 7). The effect of source displacement is illustrated in Figure 5.16. However, Figure 5.17 shows that the model underestimates concentrations in the immediate vicinity of the source at 0.9 m.

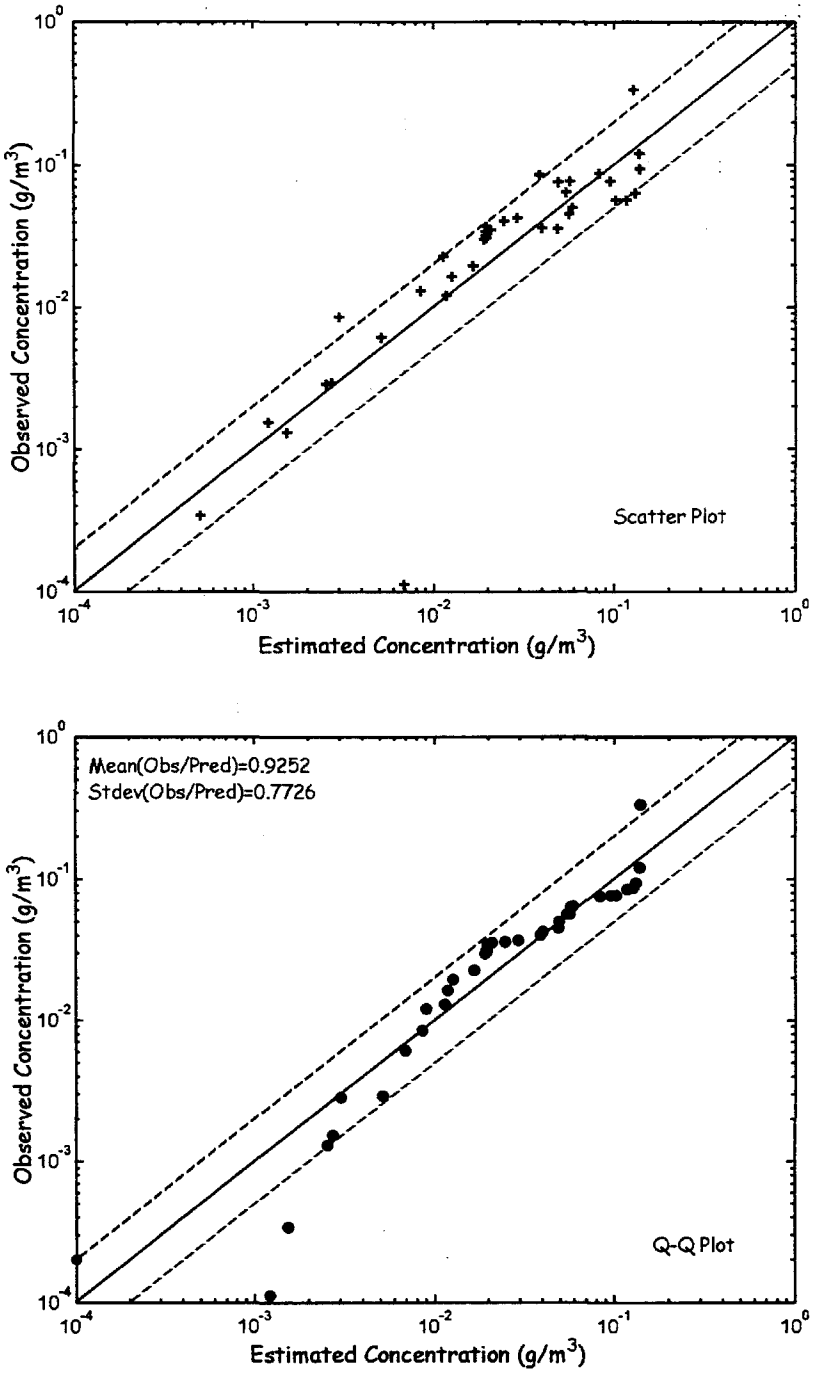

Figure 5.13: Ground-level release behind one barrel. Three-barrel obstacle downwind of source-Grid No. 8.

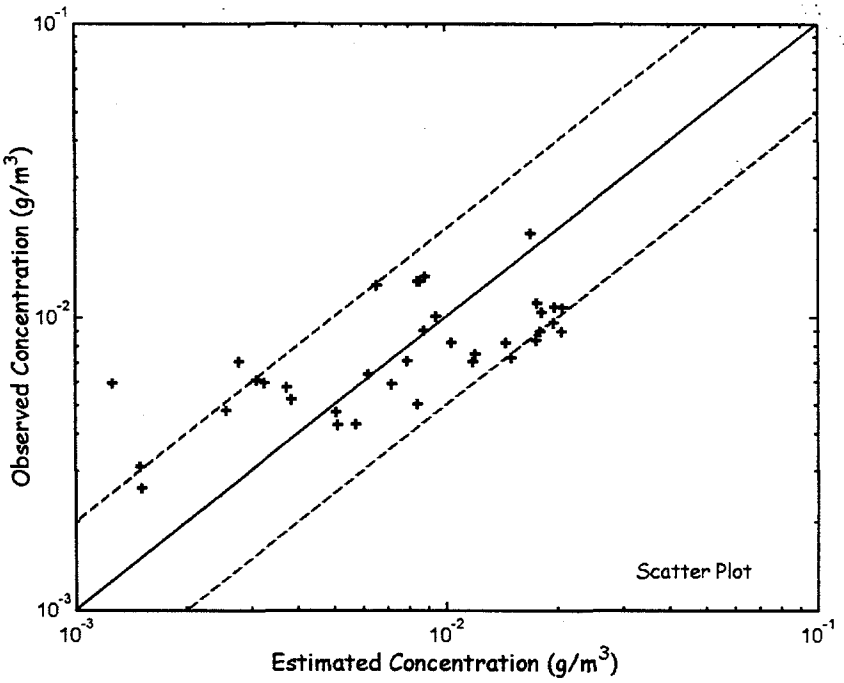

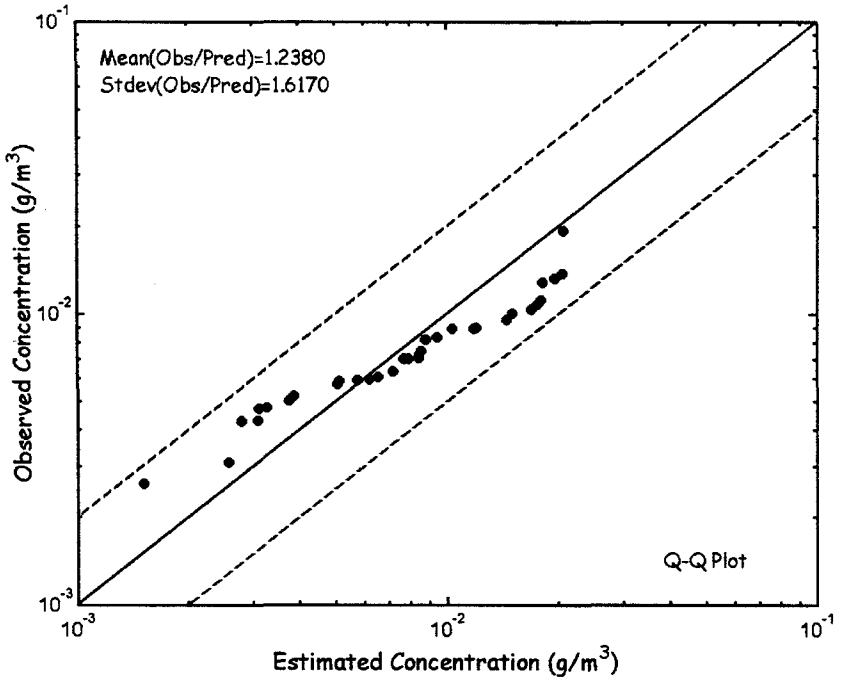

Figure 5.14: Elevated release behind one barrel in Grid No. 5.

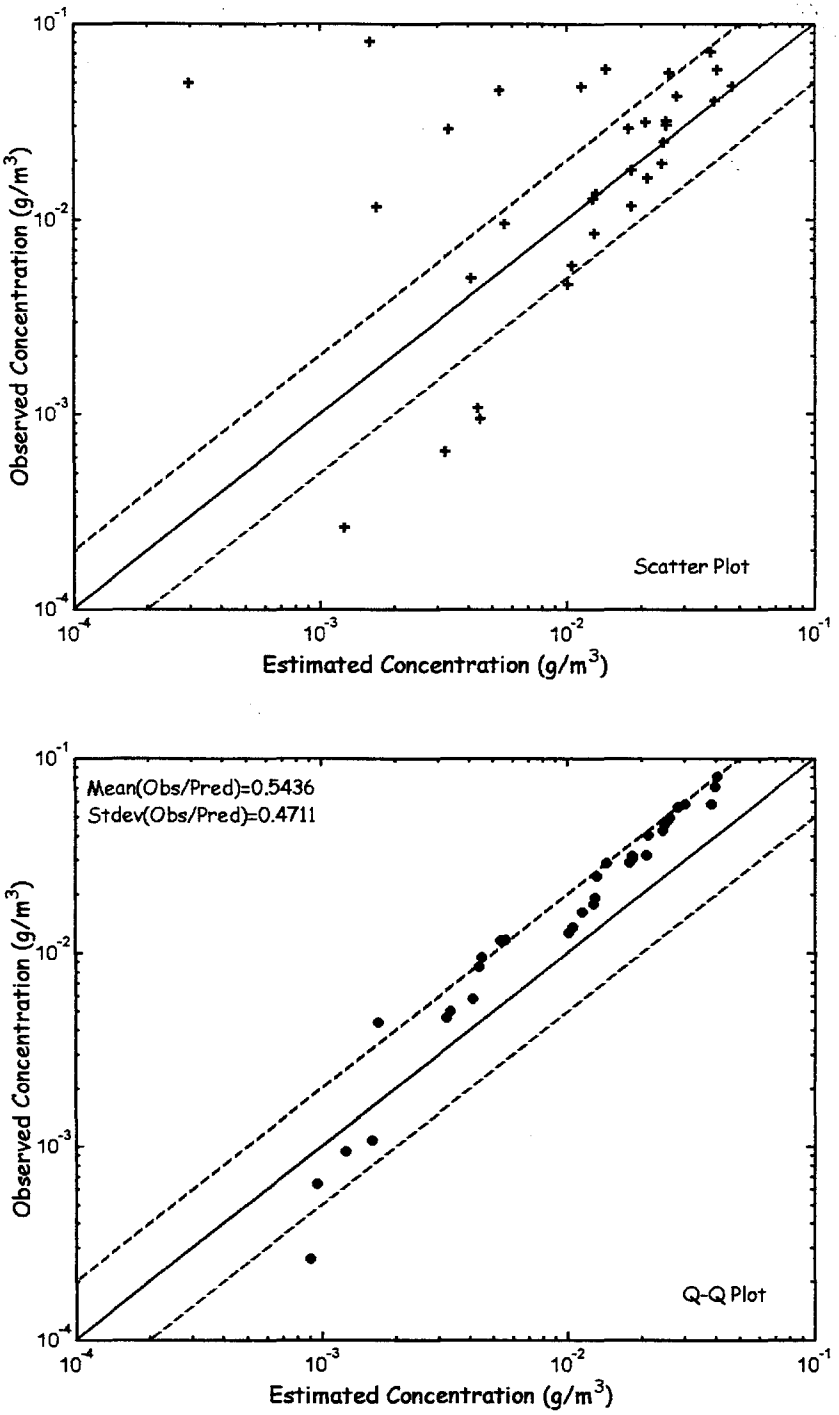

Figure 5.15: Elevated release with source surrounded by four barrels in Grid No. 7.

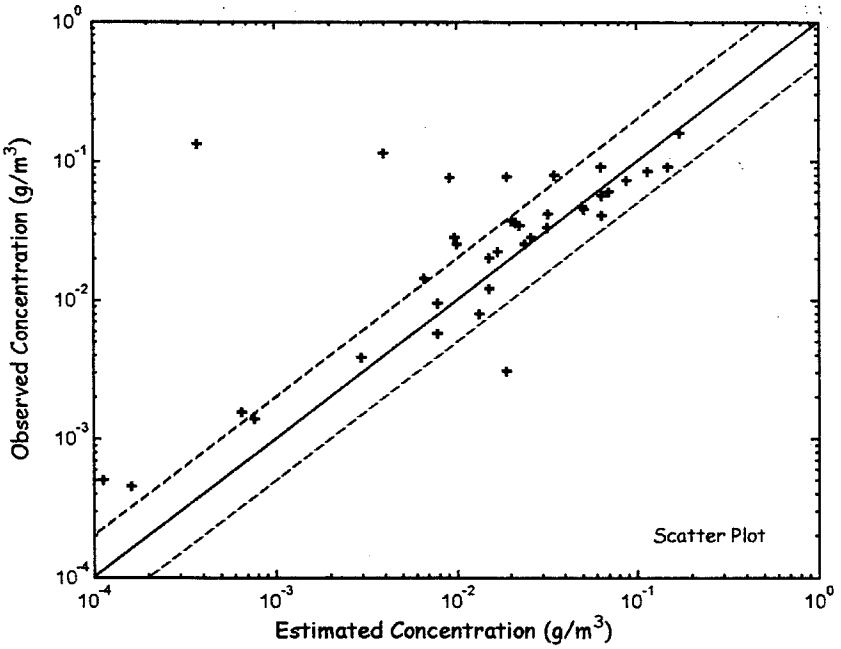

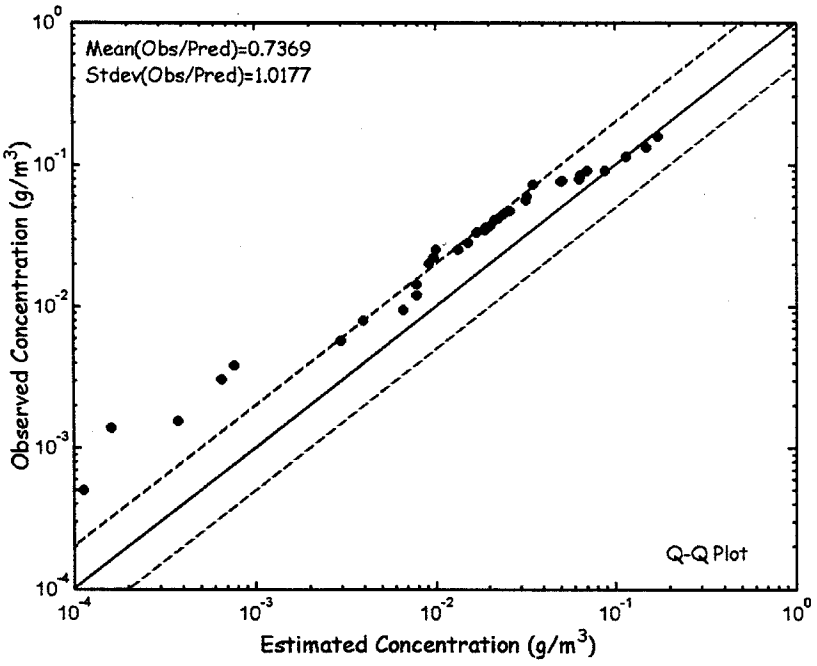

Figure 5.16: Ground-level release behind one barrel with source position displaced in Grid No. 9.

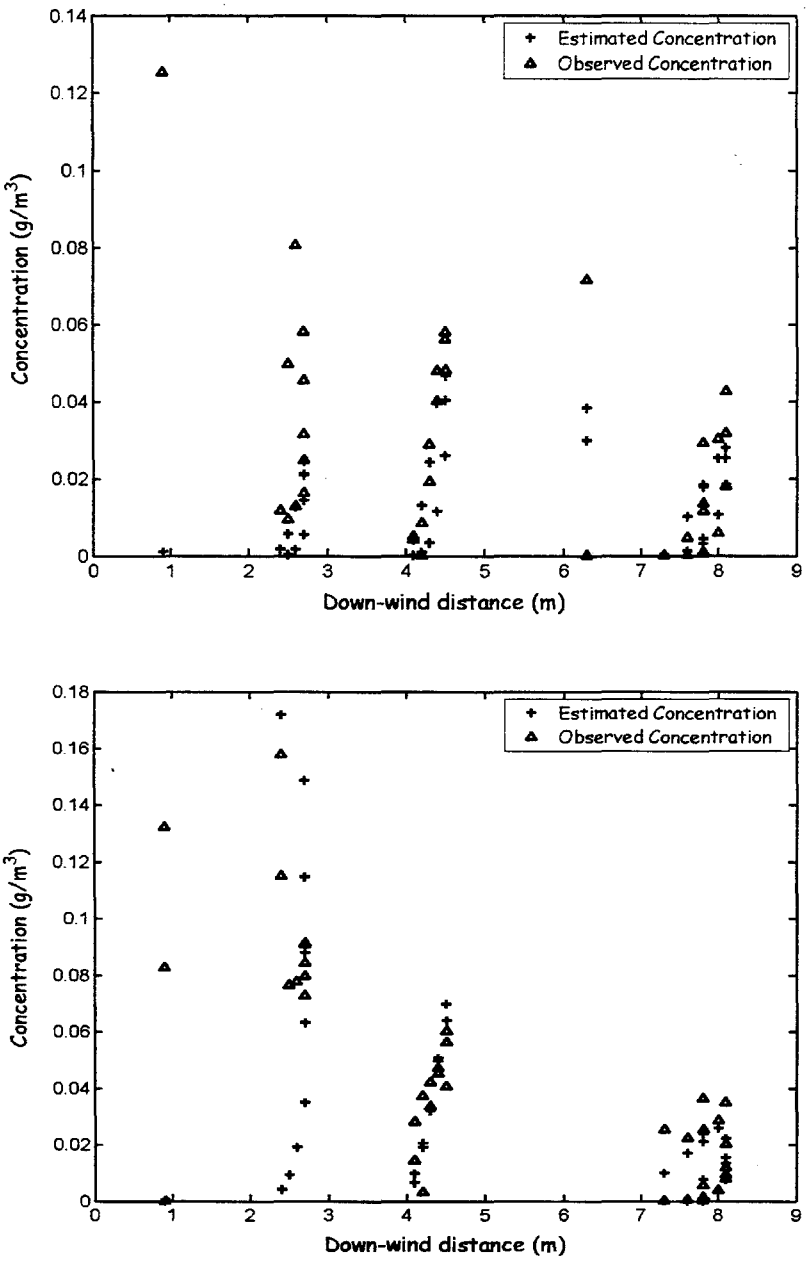

Figure 5.17: Variation of concentration along the down-wind direction in Grid No. 7 (Top) and Grid No. 9 (Bottom).

5.4 CONCLUSIONS

The results from the evaluation of the model with data from a variety of source and grid configurations of the model urban canopy indicates that the basic premise of the model is essentially correct: a relatively simple model can be used to estimate concentrations at small distances from the source if the model inputs correspond to measurements in the vicinity of the source. However, the underestimation of concentrations at receptors within 1H of the source indicates that the model might have to be modified to account for rapid mixing that is not reflected in the measured turbulence levels.

6. CE-CERT SHORT DISTANCE DISPERSION EXPERIMENTS

The performance of the proposed model was evaluated in the near-field of an urban source by conducting a tracer experiment (sponsored by the California Air Resources Board , ARB contract #00-720) at a parking lot of the College of Engineering's Center for Environmental Research and Technology. SF_6 was released from a line source from the top of a trailer situated in a parking lot surrounded by buildings. This arrangement mimics a small source on the top of a building in an urban area. Figure 6.1 shows a photograph of the source, and the experimental instrumentation.

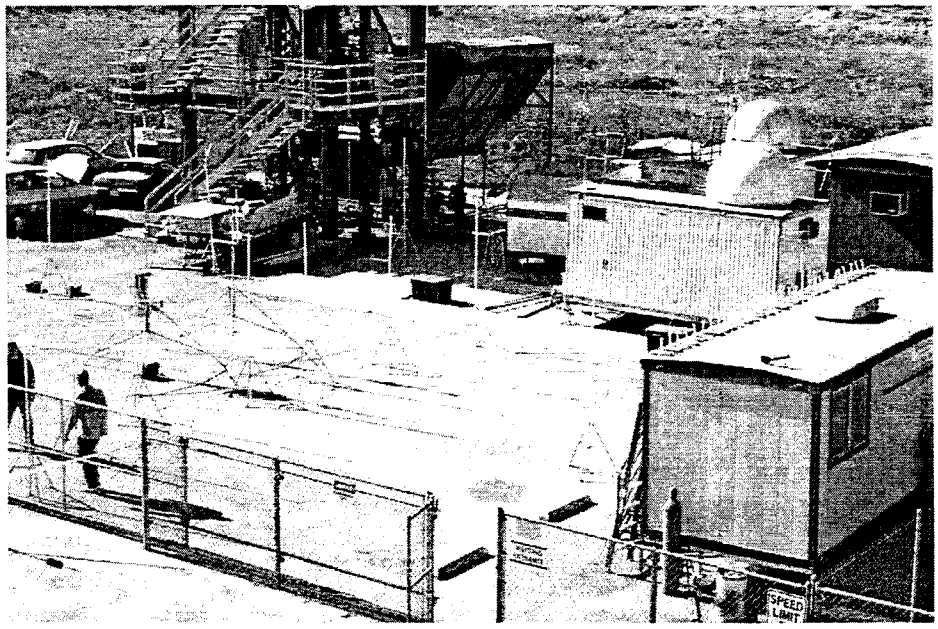

Figure 6.1: Urban tracer experiment at CE-CERT parking lot.

6.1 EXPERIMENTAL ARRANGEMENT

Data were collected continuously during the last three weeks of June 2001. An automated sampling system was used that measured the concentrations at twenty-four receptor points with 30-minute sample integration times. Samples from different locations were sampled with plastic tubing to fill plastic bags in a central analysis unit where one set of bags was analyzed for SF_6 while another was being filled. This system resulted in minimal turn-around-times because it avoids manual collection of samples and subsequent analysis in a laboratory.

Figure 6.2 shows a schematic of the experimental arrangement. A line source was located on the roof of a modular building. The line source consisted of ¼ inch OD tubing with a total of fifty 'T's with capillaries attached. The SF_6 flow was regulated between 1.4 to 5.6 g/hr and diluted with 10 L/min of ambient air prior to dispersal through the line source. Sampling receptors were placed near the trailer and in two arcs, one at 10 m from the trailer center and the other at 20 m as shown in Figure 6.2. In addition, we continuously measured SF_6 at six locations on all sides of the trailer, each at a distance of approximately 1m from the source. At each sampling location, SF_6 was drawn at a height of 1 m and transferred through polyethylene tubes to a trailer where

concentrations were continuously analyzed. All sampling lines were of the same length and sampled at the same rate so that all samples corresponded to the same time.

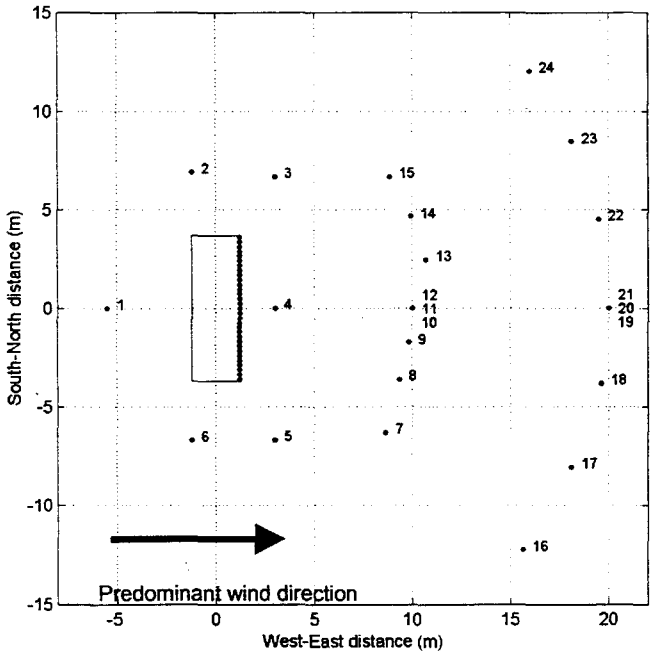

Figure 6.2: Locations of SF6 sampling sites, CE-CERT Tracer Experiment 06/11-28/2001.

6.2 METEOROLOGICAL MEASUREMENTS

Meteorological observations were made at 3 m using a sonic anemometer located on the 20 m arc. Meteorological observations included mean and turbulent velocities, wind speed, direction, and temperature. SF_6 was released continuously over the two-week period between June 11th and June 28th 2001, to ensure that measurements could be collected over a wide range of atmospheric conditions. For analysis, we averaged concentrations and meteorological measurements over 30 minute periods.

Figures 6.3 to 6.5 show the variation of the meteorological measurements relevant to dispersion as a function of the time of day. Figure 6.3 shows that the wind speeds were lower than 1 m/s during most of the nighttime hours. The wind speeds generally started to increase around 10:00 hours and reached a maximum of about 2.5 m/s around 15:00 hours.

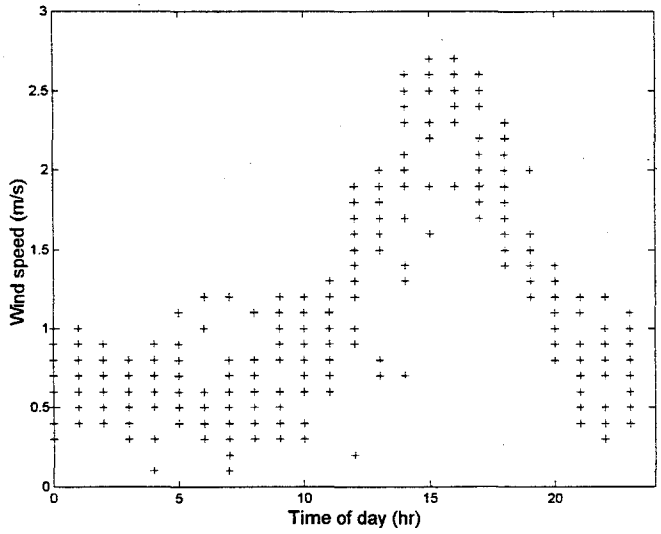

Figure 6.3: Variation of wind speed with time of day.

The diurnal behavior of σ_w and σ_v was similar to that of the wind speed with the lower values occurring during the night and the higher values occurring during the day. The turbulent intensity, σ_w/U, shown in Figure 6.4, varied from 0.03 to 0.3 during the course of the day, with large values, exceeding 0.5 occurring between 5:00 and 10:00 hours. The majority of the horizontal turbulent intensities, σ_v/U, were between 0.2 and 1.0. However, there were several large values going up to 5 during the night and early morning hours. The relatively large values of σ_v/U suggest the possible importance of meandering on dispersion. This is addressed in the next section.

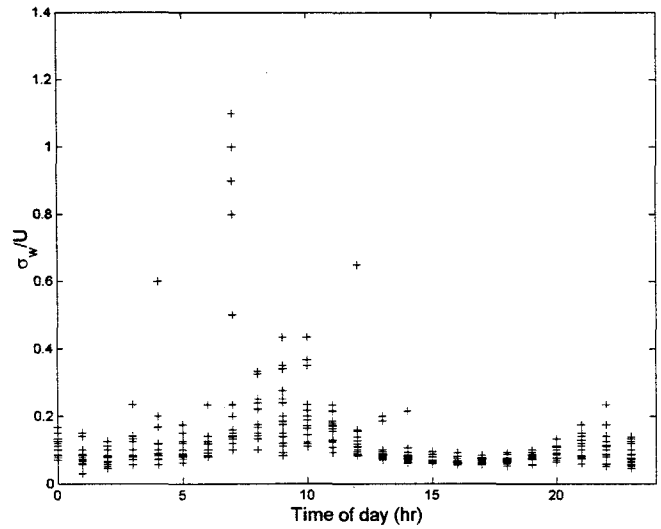

Figure 6.4: Variation of vertical turbulent intensity with time of day.

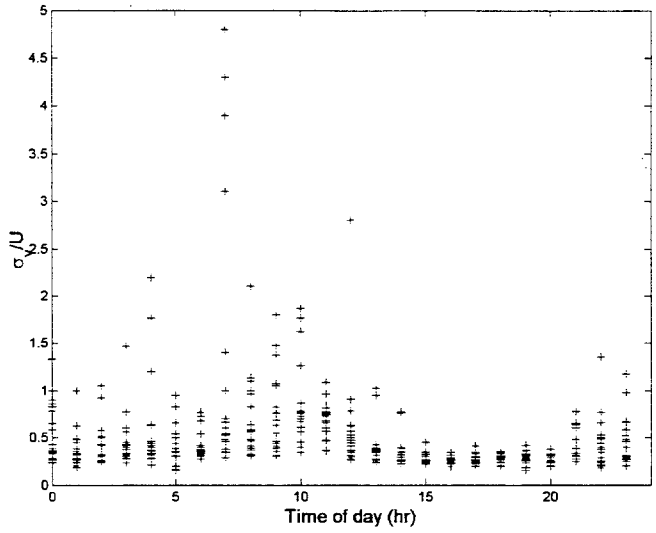

Figure 6.5: Variation of horizontal turbulent intensity with time of day.

6.3 EVALUATION OF THE EFFECTS OF WIND MEANDERING

Figure 6.6 shows concentrations as a function of the deviation of the direction from the line joining the center of the source to the receptor. Observed concentrations are shown in the upper panel of this figure. Although, the highest concentrations occurred directly downwind of emission sources, levels close to half the maximum value occurred at almost all angles. There is a peak concentration at 50°, which we cannot explain at this point in our analysis. The observations clearly show the effects of building-induced turbulence in randomizing the wind direction, especially at low wind speeds. For convenience, we will refer to this as the upwind dispersion effect.

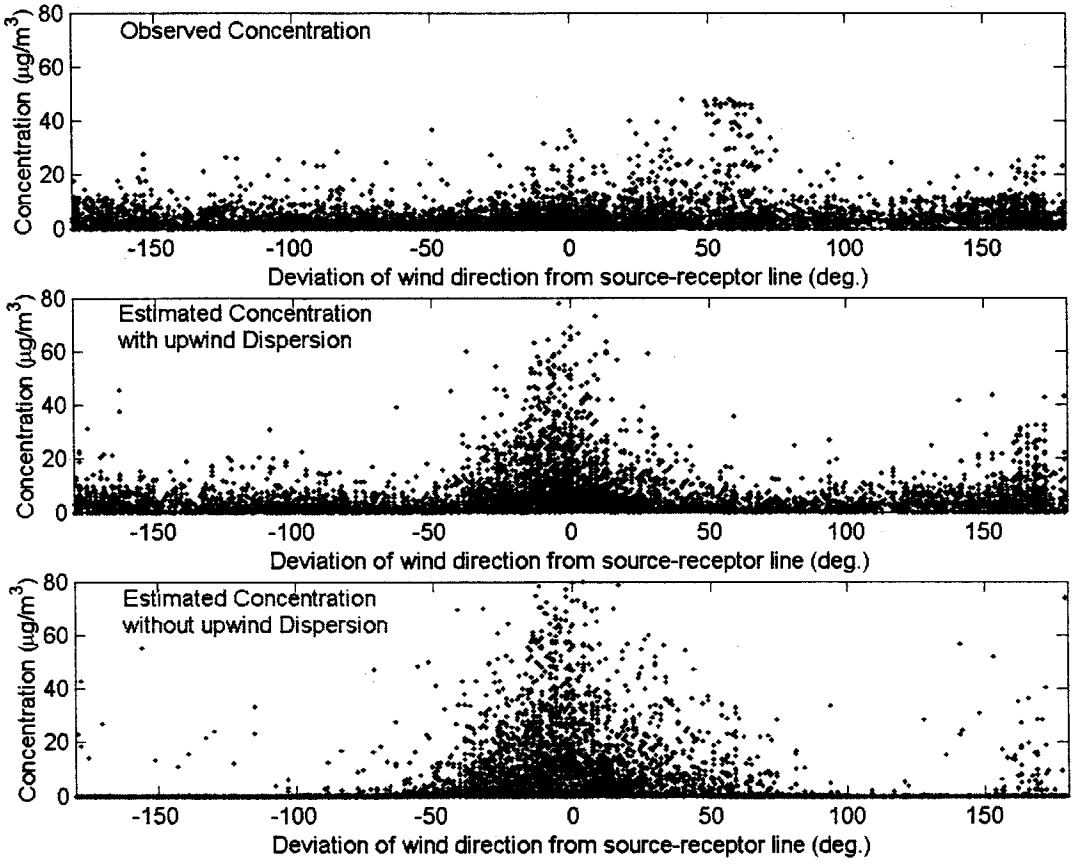

Figure 6.6: Variation of observed and estimated concentrations as a function of deviation of wind direction from source-receptor line.

In running the model, the emissions were treated as 30 equally spaced point sources located at 1.6 m, which is one-half the height of the trailer. Sensitivity studies with the model indicated that this was the simplest method to account for downwash effects in the vicinity of the source.

Because we had a single level of meteorological measurements, we used p=0.23 and m=0.0, which imply a gradient in mean wind but none in the turbulence. These are tentative values based on the Dugway experiment. The model estimates, shown in the middle panel of Figure 6.6, illustrate the randomizing effects embodied in Equations (3.23) to (3.25). Relatively high concentrations are estimated at all angles, although there is a definite peak at 0° degrees that is more distinct than in the observations (See top panel of Figure 6.6).

The bottom panel of Figure 6.6 shows the estimated concentrations from the new model, when the background effect is neglected. We see the expected peak at 0°, but the background concentration disappears. The relatively high concentrations at + and – 150° occurs at receptors 2 and 6, shown in Figure 6.2.

In air pollution modeling involving complicated real situations, the deviations between model estimates and corresponding observations are typically very large because of unavoidable uncertainties in model inputs. Thus, it is common practice to compared ranked observations with

ranked model estimates, which is equivalent to comparing the distributions of the concentrations. From a regulatory point of view, the performance of a model in estimating the observed concentration distribution is relevant because one is generally interested in estimating the highest concentrations. It is possible to distinguish between a correct and deliberately falsified model using a comparison of concentration distributions (Venkatram, 1999). In the subsequent comparisons, we will only compare distributions using plots referred to as Quantile-Quantile (Q-Q) plots.

The importance of including the upwind dispersion effect is more clearly seen in the Q-Q plot of Figure 6.7. We see that with upwind dispersion, the model performs well with the Q-Q line lying within the factor of two limits. Without upwind dispersion, the model underestimates the concentrations below observed levels of 10 $\mu g/m^3$, which is roughly the magnitude of the upwind dispersion effect.

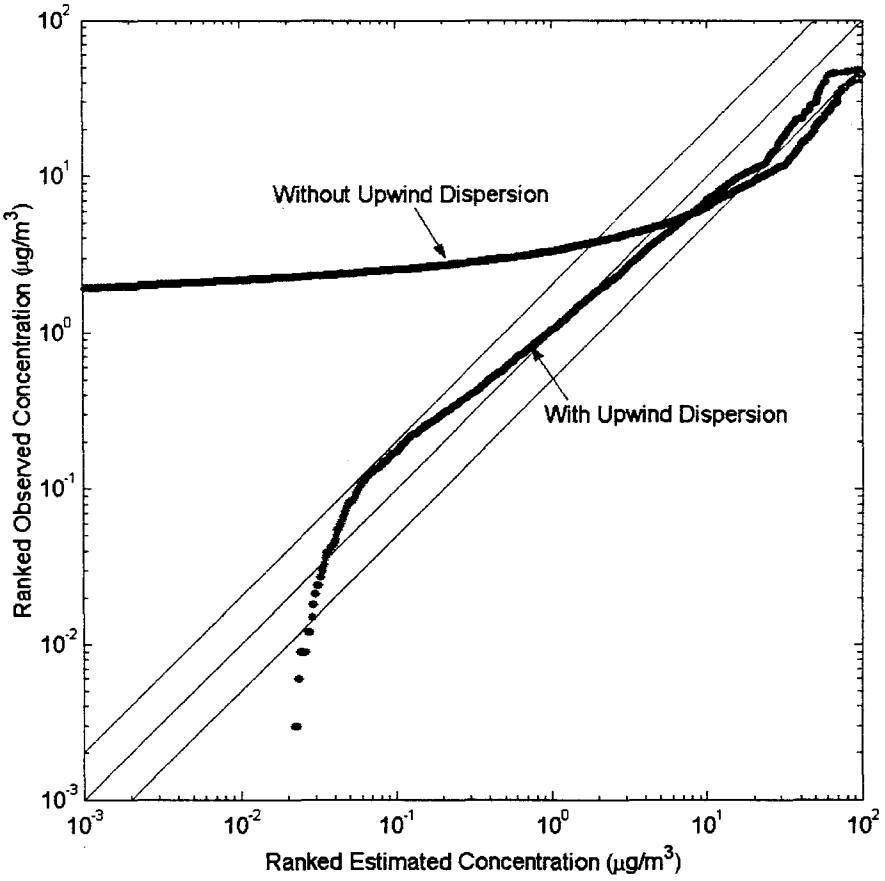

Figure 6.7: Q-Q plot showing the effect of including the upwind dispersion on model estimates for the CE-CERT experiment.

6.4 COMPARISON OF MODEL PERFORMANCE

We evaluated the performance of three currently available models and that of the new model with observations from the CE-CERT experiment. Two of the models are used in regulatory applications-ISC (Industrial Source Complex) and ISC-PRIME (PRIME, which stands for Plume Rise Model Enhancements, refers to a new treatment of the effects of buildings on dispersion and plume rise). The third model is AERMOD-PRIME, which has been proposed by the USEPA as a replacement for ISC. Dr. Vlad Isakov of ARB generated the model results for ISCST, ISCST-PRIME and AERMOD-PRIME. The meteorological inputs were generated from the data from the 3-meter sonic anemometer.

Figure 6.8a and 6.8b compare the performance of the three models with that of the new model proposed here at receptors 1, 2, and 6, which were located upwind and beside the source (See Figure 6.2). Concentrations below the detectable limit of 0.06 $\mu g/m^3$ were not included in the analysis. Daytime is defined as the 12 hours between 6:00 and 18:00 hours, which corresponds roughly to the period when the wind speed showed its greatest diurnal variation, and the turbulent velocities were relatively high (See Figures 6.3 and 6.4). Nighttime is taken to be the period between 18:00 and 6:00 hours. This division between night and day roughly corresponds to unstable conditions during the day when the surface heat flux is positive, and stable conditions during the night when the heat flux is negative.

ISC and ISC-PRIME predict essentially zero concentrations (within machine precision) for a range of observed concentrations that are above 0.06 $\mu g/m^3$. Because these zero concentrations cannot be plotted on the logarithmic scales of the Q-Q plots, the observed concentrations corresponding to the model estimated zeros do not appear in the plots. Thus, the ranges of observed concentrations for ISC and ISC-PRIME in the figure are not exactly the same as that for AERMOD-PRIME and the new model, which do not yield zero concentrations because of the upwind dispersion effect.

We see from Figure 6.8a that ISC-PRIME, AERMOD-PRIME, and the new model overpredict concentrations at the high end of the distribution during the day; the proposed model shows the largest overestimation. All the models, except the new model, underestimate concentrations at the lower end of the distribution. However, AERMOD-PRIME's Q-Q plot is within a factor of two of the one-to-one line for most of the range of observed concentrations. ISC underestimates concentrations for the entire range of observed concentrations. During nighttime, from Figure 6.8b, the distribution of concentrations estimated from the new model is within a factor of two of the observed distribution over most of the range of observed concentrations. On the other hand, both AERMOD-PRIME and ISC-PRIME overestimate the high concentrations by well over a factor of two. At the same time, these models underestimate concentrations for estimated concentrations below 8 $\mu g/m^3$. ISC again underestimates concentrations over the entire range of concentrations.

The subsequent figures will use a minimum concentration of 10^{-3} $\mu g/m^3$ to better illustrate the performance of the models. The resulting truncation of the observed concentration ranges for ISC and ISC-PRIME does not alter any conclusions on their performance.

Figure 6.9a and 6.9b compare model performance for receptors 3, 4, and 5 (See Figure 6.2) located around 3 meters downwind of the source. The behavior of the models is similar to that seen in Figure 6.8. Model estimates from the new model are within a factor of two of the

observations over most of the range of observations. ISC-PRIME overpredicts the high concentrations and underestimates the lower range of concentrations. AERMOD-PRIME shows similar tendencies, but is much closer to the performance of the proposed model.

Figure 6.10a and 6.10b compare performance for receptors 7-15 located 10 m from the source. For daytime conditions, the new model has a slight tendency to overestimate concentrations in the upper end of the distribution, but the model estimated distribution is within a factor of two of the observed concentration distribution. AERMOD-PRIME and ISC-PRIME overestimate the upper end of the observed distribution, but underestimate the lower concentrations. ISC explains the upper end of the distribution, but underestimates most of the range of observed concentrations. During nighttime conditions, the concentration distribution from the new model is within a factor of two of the observed concentration distribution. The behavior of ISC-PRIME and AERMOD-PRIME performances is similar to that of daytime, which overestimates the high end of the distribution and underestimate the lower concentrations. ISC underestimates through the entire range of observations.

Figure 6.11a and 6.11b correspond to receptors 16 to 24 located about 20 meters from the source. The new model well explains most of the distribution, but has a small tendency to underestimate concentrations in the lower end of the distribution. The behavior of ISC and ISC-PRIME estimates are similar to those observed at receptors 7-15. The AERMOD-PRIME performs well during daytime except for overestimating the upper end of the distribution. While for nighttime, it overestimates the high end of the distribution and underestimates the lower concentrations.

Evaluation of the relative performance of the models in estimating longer term concentrations such as annual averages will require a longer time series than that available. However, we can obtain some indication of model performance through 24-hour averaged concentrations shown in Figure 6.12. Here the distributions estimated by ISC-PRIME and AERMOD-PRIME are within a factor of two of the observed distribution over half of the range of observations, but the lower range is underestimated. ISC underestimates the concentrations, while the proposed model is within a factor of two of the observations.

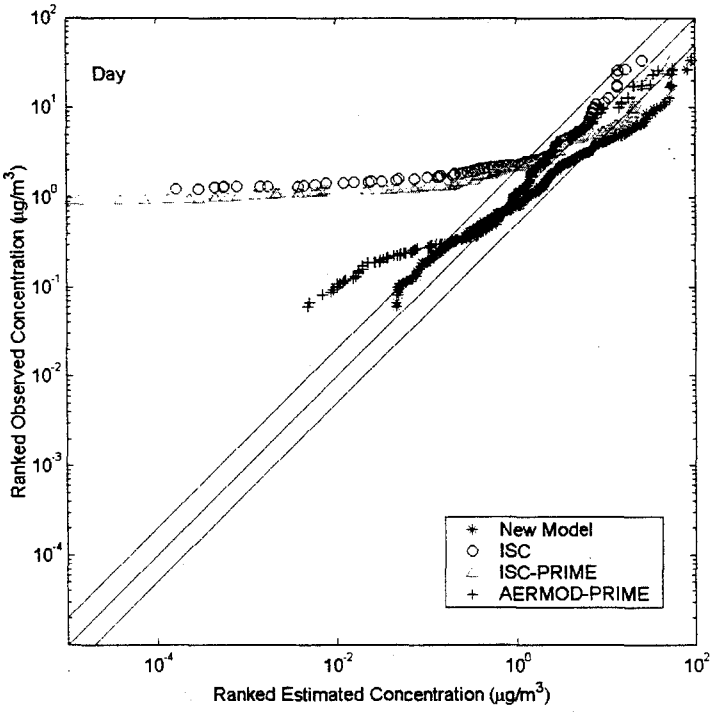

Figure 6.8a: Daytime performance of models for concentrations measured at receptors 1, 2, and 6 behind and beside the release line.

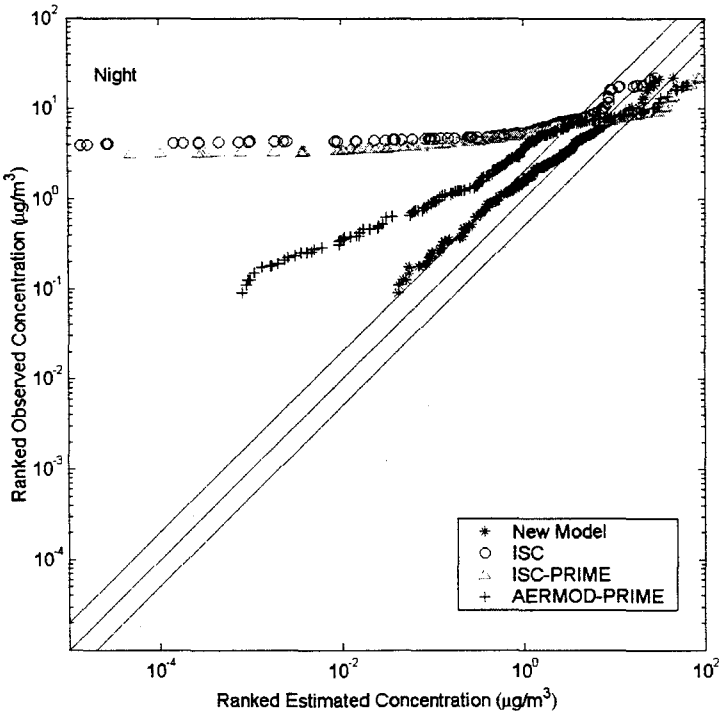

Figure 6.8b: Nighttime performance of models for concentrations measured at receptors 1, 2, and 6 behind and beside the release line.

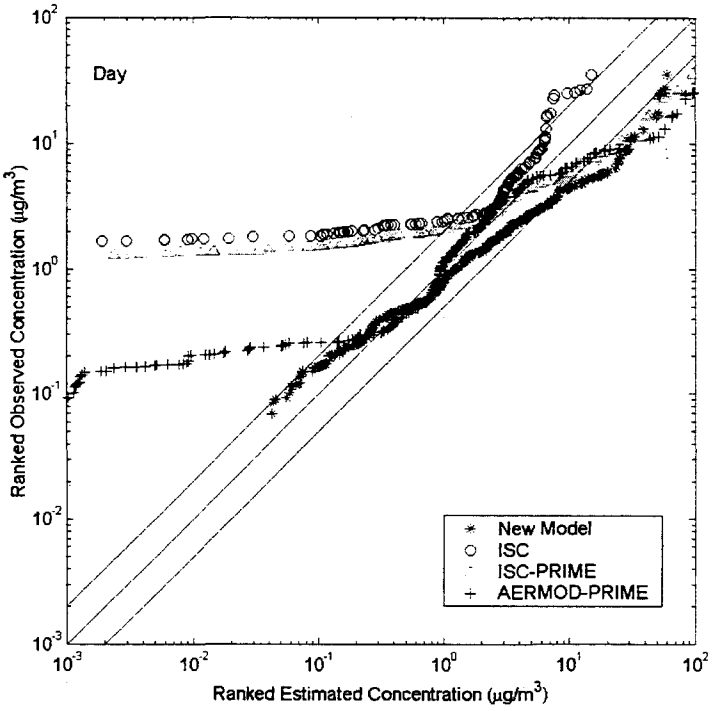

Figure 6.9a: Daytime performance of models for concentrations measured at receptors 3, 4, and 5 at 3 meters.

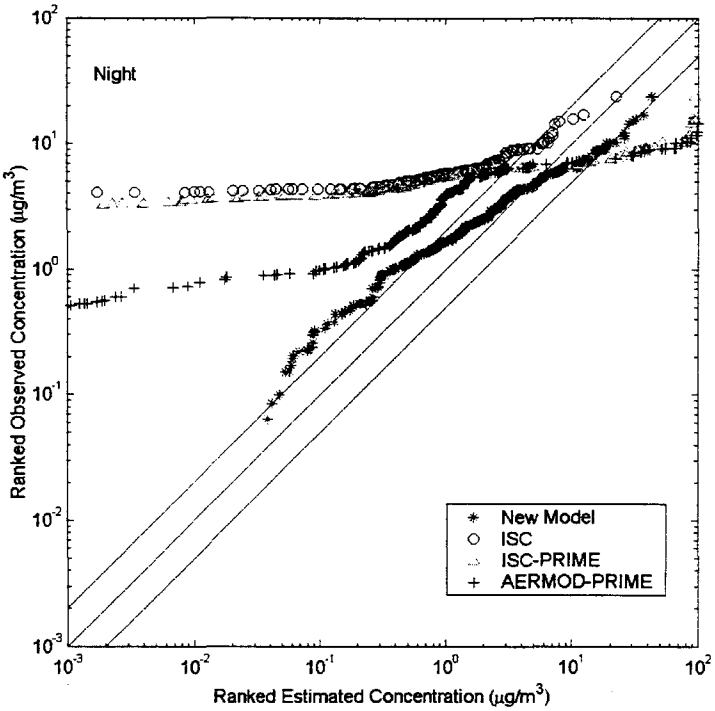

Figure 6.9b: Nighttime performance of models for concentrations measured at receptors 3, 4, and 5 at 3 meters.

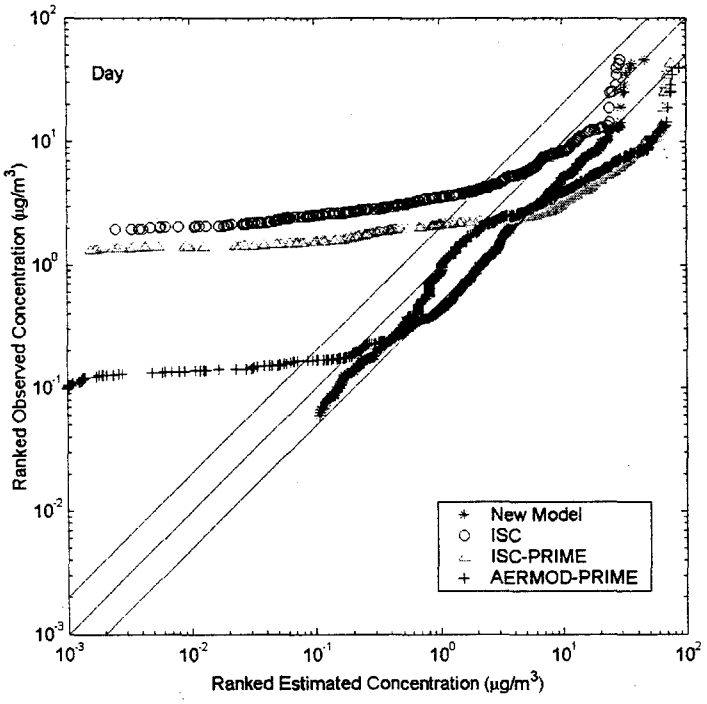

Figure 6.10a: Daytime performance of models for concentrations measured at receptors 7-15 at 10 meters.

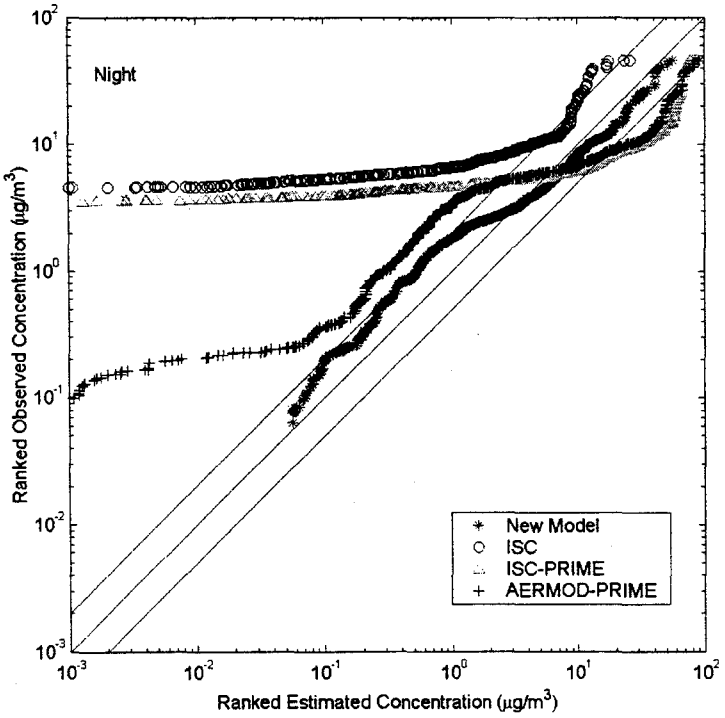

Figure 6.10b: Nighttime performance of models for concentrations measured at receptors 7-15 at 10 meters.

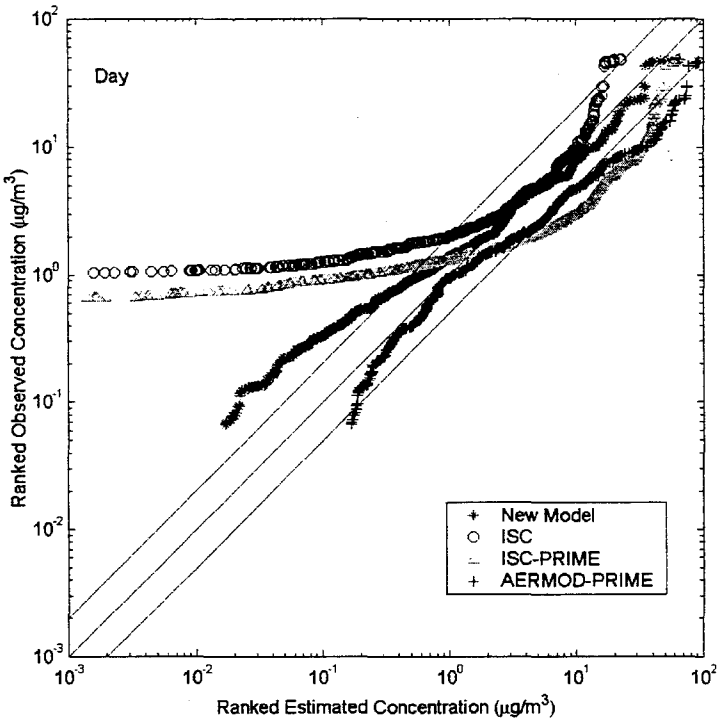

Figure 6.11a: Daytime performance of models for concentrations measured at receptors 16-24 at 20 meters.

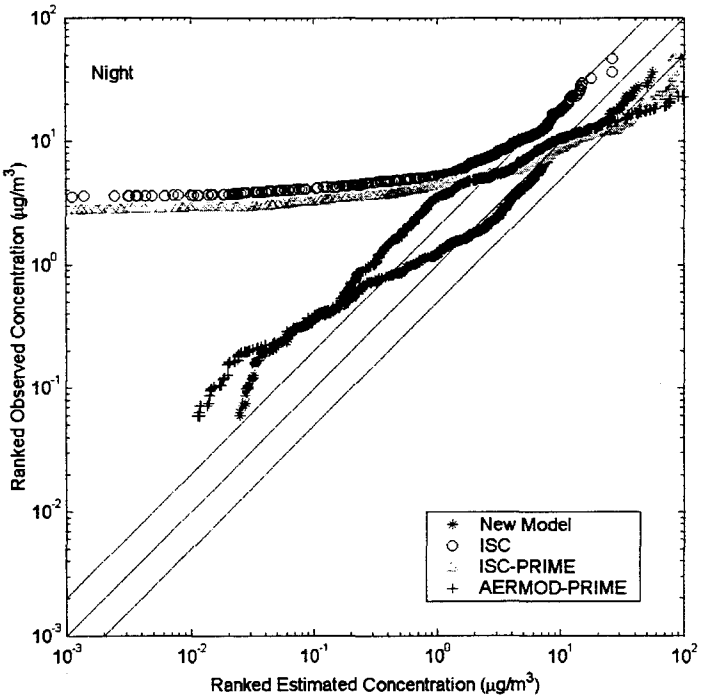

Figure 6.11b: Nighttime performance of models for concentrations measured at receptors 16-24 at 20 meters.

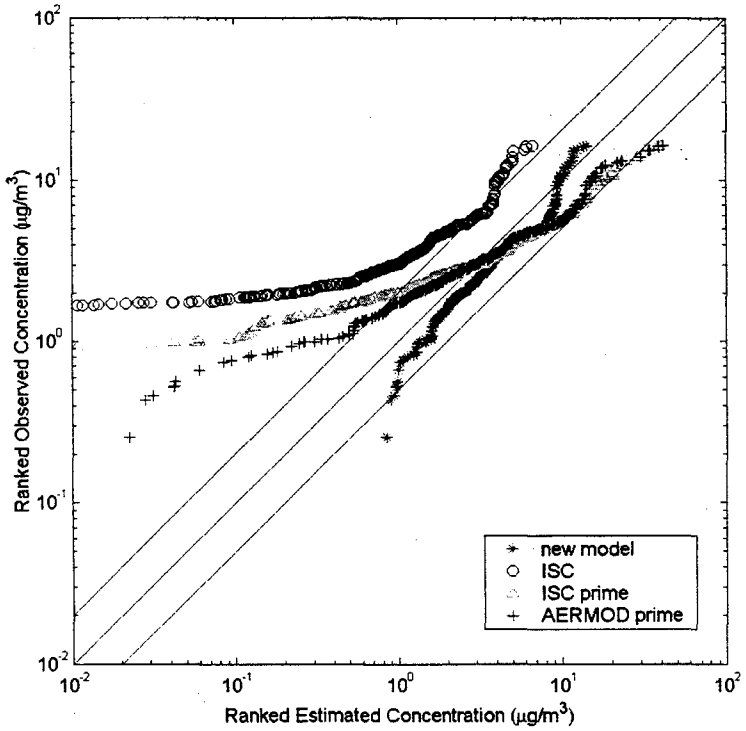

Figure 6.12: Model performance for 24-hour averaged concentrations measured at all receptors.

6.5 PERFORMANCE STATISTICS

Table 6.1 summarizes the Q-Q plots shown in the previous section in terms of model performance statistics. The distributions are characterized in terms of the median, the lowest quartile to provide information on estimating the lower range of concentrations, and the 95th percentile to indicate the model's performance in estimating the highest concentrations. These statistics are compared with the observed values using the metric:

$$\text{Bias in statistic} = \frac{(C_p - C_o)}{(C_p + C_o)/2} \times 100, \qquad (6.1)$$

where C represents a statistic, and p and o refer to model estimates and observations respectively. Normalizing the difference between the observed and estimated values by the average of the two values rather than either the observed or the estimated value avoids exaggerating the bias when the denominator is close to zero. The bias is positive when the model overestimates the statistic, and negative when it underestimates. The maximum value of the bias is 200% when the modeled statistic is much larger than the observed value, and attains its minimum value of –200% when the modeled statistic is zero.

When the modeled statistic is within a factor of two of the observed value, the bias ranges from 67% to –67%. If we assume that the model is acceptable if this factor of two criterion is met, the model is given a score of 1 and 0 otherwise. Table 6.1 confirms the observations made using the Q-Q plots presented earlier. The new model, AERMOD-PRIME, and ISC-PRIME overestimate

the 95th percentile as indicated by the positive bias; the new model does not overestimate as much. ISC has a negative bias for most of the statistics.

The summary scores indicate the percentage of "correct" scores out of the maximum possible of 24 possible choices between 0 and 1. We see that this scheme results in the following ranking: New Model (75%), AERMOD-PRIME (46%), ISC (8%), and ISC-PRIME (4%). Note that ISC-PRIME is marginally worse than ISC because it consistently overestimates the 95th percentile.

6.6 CONCLUSIONS

The model evaluation clearly indicates the importance of including the randomizing effect of buildings on wind directions; although the mean wind direction might be well defined above the urban canopy, the winds within the canopy vary over large angles. This effect has been incorporated in the proposed model through a simple formulation. AERMOD-PRIME also incorporates the same formulation, which is responsible for its relatively good performance at the lower end of the observed concentration distribution.

We point out that in recent study conducted by CARB (Isakov et al., 2003), it was necessary to include the upwind dispersion formulation to explain the observed levels of Chromium VI measured in the vicinity of a metal plating facility in Barrio Logan, San Diego. AERMOD, which includes this effect, was used in this study.

The fact that ISC-PRIME overestimates the 95th percentile at all distances while ISC underestimates these concentrations suggests that the PRIME (downwash and wake effects) component of the model might be responsible for the overestimation. PRIME might be less of a problem in AERMOD because of the inclusion of the upwind dispersion component. The relative performance of the proposed model suggests that downwash effects can be simply modeled by reducing the source height by a factor, which is 0.5 in our case.

Table 6.1: Model Performance Statistics. Concentrations are expressed in $\mu g/m^3$.

Receptors	Time	Model Name	Median	95th Percentile	Lower Quartile	Bias in Median	Bias in 95th Percentile	Bias in Lower Quartile	Score
1,2,6	Day N=499	Observations	1.09	7.54	0.42	0	0	0	
		New Model	1.40	28.02	0.32	**25**	115	**-25**	2
		AERMOD-PRIME	0.95	7.34	0.41	**-14**	**-3**	**-1**	3
		ISC-PRIME	0.00	20.00	0.00	-199	90	-200	0
		ISC	0.00	6.54	0.00	-200	-14	-200	0
	Night N=537	Observations	3.31	9.17	1.76	0	0	0	
		New Model	3.01	14.54	1.13	**-10**	**45**	**-43**	3
		AERMOD-PRIME	0.94	20.98	0.37	-112	78	-131	0
		ISC-PRIME	0.00	29.58	0.00	-200	105	-200	0
		ISC	0.00	6.70	0.00	-200	-31	-200	0
3,4,5	Day N=507	Observations	1.26	8.83	0.45	0	0	0	
		New Model	1.61	28.43	0.41	**25**	105	**-7**	2
		AERMOD-PRIME	1.08	19.00	0.53	**-15**	73	**17**	3
		ISC-PRIME	0.00	22.98	0.00	-200	89	-200	0
		ISC	0.00	5.70	0.00	-200	**-43**	-200	1
	Night N=542	Observations	3.10	8.91	1.62	0	0	0	
		New Model	2.62	15.71	0.91	**-16**	**55**	**-56**	3
		AERMOD-PRIME	0.89	40.30	0.38	-111	128	-124	0
		ISC-PRIME	0.00	34.27	0.00	-200	117	-200	0
		ISC	0.00	3.34	0.00	-200	-91	-200	0
7 to 15	Day N=1472	Observations	1.06	7.64	0.37	0	0	0	
		New Model	2.32	16.33	0.80	74	73	74	0
		AERMOD-PRIME	1.08	33.90	0.55	1	126	**38**	2
		ISC-PRIME	0.00	37.20	0.00	-200	132	-200	0
		ISC	0.00	7.69	0.00	-200	1	-200	0
	Night N=1537	Observations	3.49	12.54	2.00	0	0	0	
		New Model	3.68	18.62	1.17	**5**	**39**	**-53**	3
		AERMOD-PRIME	1.03	38.87	0.56	-109	102	-113	0
		ISC-PRIME	0.00	45.47	0.00	-200	114	-200	0
		ISC	0.00	7.47	0.00	-200	-51	-200	0
		Observations	1.38	11.12	0.53	0	0	0	

	New Model	0.99	15.90	0.20	-32	35	-91	2
Day	AERMOD-PRIME	1.81	40.57	0.66	27	114	22	2
N=1365	ISC-PRIME	1.24	35.28	0.00	-11	104	-200	1
16 to 24	ISC	0.18	10.99	0.00	-155	-1	-200	1
	Observations	3.77	13.32	1.66	0	0	0	
	New Model	4.42	19.84	1.78	16	39	7	3
Night	AERMOD-PRIME	1.19	20.71	0.48	-104	43	-110	1
N=1566	ISC-PRIME	0.44	30.10	0.00	-158	77	-200	0
	ISC	0.02	7.83	0.00	-198	-52	-200	0

	New Model	75
Summary Scores	AERMOD-PRIME	46
% of maximum possible	ISC-PRIME	4
	ISC	8

N refers to the number of observations used to compute the statistics. Its value depends on the number of samplers in the particular arc. The number 0.00 in the table corresponds to values less than 5×10^{-3} $\mu g/m^3$.

7. REFERENCES

Barad, M.L. 1958: *Project Prairie Grass, a Field Program in Diffusion.* Vol. 1, Geophysics Research Paper No. 59, Air Force Cambridge Research Center, Bedford, MA.

Britter, R. E., and Hanna, S. R., 2003: Flow and dispersion in urban areas. Annual Review of Fluid Mechanics **35**, 469-496

Csanady, G. T. 1973: *Turbulence Diffusion in the Environment.* D. Reidel Publishing Co.

Cimorelli A. J. *et al.* 1996: Current progress in the AERMIC model development program. Proceedings of the 89th Annual Meeting of the Air and Waste Management Association, 96-TP24B.04, AWMA, Pittsburgh, PA.

Cimorelli, A. J. *et al.* 1998: AERMOD Description of Model Formulation. USEPA, QAQPS, Research Triangle Park, NC .

Du, S., and Venkatram, A. 1997: A Parameterization of Vertical Dispersion of Ground-level Releases. *J. Appl. Met.* **36**, 1004-1015.

Eckman, R. M. 1994: Re-examination of empirically derived formulas for horizontal diffusion from surface sources. *Atmos. Environ.* **28**, 265-272

Hanna, S. R., and Chang, J. C., 2001: Use of the Kit Fox field data to analyze dense gas dispersion modeling issues. *Atmos. Environ.* **35**, 2231-2241,

Hanna, S.R., Britter R.E., and Franzese P., 2000: The effect of roughness obstacles on flow and dispersion at industrial facilities. Prepared for American Institute of Chemical Engineers.

Isakov, V. *et al.* 2003: Near Field Dispersion Modeling for Regulatory Applications. *J. Air & Waste Manage. Assoc.* (submitted).

Lee, R. F. and Irwin, J. S. 1997: Improving concentration measures used for evaluating air quality models, *J. Appl. Met.* **36**, 1107-1112.

Lee, R.F.; Paine, R.J.; Perry, S.G.; Cimorelli, A.J.; Weil., J.C.; Venkatram, A.; and Wilson, R.B. 1998: Developmental Evaluation of the AERMOD Dispersion Model. Tenth Joint AMS/AWMA Conference on Applications of Air Pollution Meteorology, January 11-16, 1998, Phoenix, AZ, American Meteorological Society, Boston.

Macdonald, R.W., R.F. Griffiths, and D.J. Hall, 1998: A comparison of results from scaled field and wind tunnel modelling of dispersion in arrays of obstacles. *Atmos. Environ.* **32**, 3845-3862.

McElroy, J. L., and Pooler, F., 1968: The St. Louis dispersion study-volume II-analysis. National Air Pollution Control Administration, Pub. No. AP-53, US DHEW Arlington, 50 pages.

Van Ulden, A. P. 1978: Simple estimates for vertical dispersion from sources near the ground. *Atmos. Environ.* **12**, 2125-2129.

Venkatram, A. 1982: A framework for evaluating air quality models. *Boundary-Layer Meteorology* **24**, 372-385.

Venkatram, A. 1992: Vertical dispersion of ground-level releases in the surface boundary layer. *Atmos. Environ.* **26A**, 947-949.

Venkatram, A. 1999: Applying a framework for evaluating the performance of air quality models. Sixth International Conference on Harmonisation within Atmospheric Dispersion Modeling for Regulatory Applications, October 11-14, 1999, Rouen, France.

APPENDIX A

Close-Range Dispersion within a Roughened Sublayer: Road Map to Experimental Data Acquired at SLTEST

Prepared for:

A. Venkatram
Department of Mechanical Engineering
University of California
Riverside, CA 92521

Prepared by:

H. Miner and M. Metzger
Physical Fluid Dynamics Laboratory
Department of Mechanical Engineering
University of Utah
Salt Lake City, Utah 84112

November 30, 2001

Contents

1 Introduction

Field trials to study close-range atmospheric dispersion in the presence of surface mounted obstacles were conducted at the SLTEST site (113° 16′W, 40° 8.5′N) in Utah's Western Desert. The surface at the site was artificially roughened using a 5 × 9 rectangular array of 45 barrels, height $H = 0.91$ m and diameter $d = 0.57$ m, with a barrel spacing of 1.8 m, center to center. A photograph of the setup is displayed in figure 1. Propylene (C_3H_6) tracer gas was released through a 25.4 mm diameter pipe, both upstream and within the barrel array. The dissemination rate was fixed at 15 slm using a mass flow controller. The tracer source was located at both ground level and $1H$. At each of the two source heights, five different barrel configurations were arranged near the source. In the first configuration, the source was located directly upwind of a single barrel. In the second configuration, the source was located directly upwind of two barrels placed side by side. In the third configuration, the source was surrounded by four barrels. In the fourth and fifth configurations, the source was located directly upwind and at a distance of $3H$ upwind, respectively, of a three barrel pyramid. Instantaneous concentration measurements were simultaneously acquired within the array from 43 photoionization detectors (digiPIDs) arranged in three, 50 degree arcs. Turbulence data in the roughness sub layer and near the source were also measured using 6 sonic anemometers.

Figure 1: Photograph of the barrel array at the SLTEST site, July 2001.

A total of 13.5 hours of turbulence and concentration data were acquired spanning four days (July 17, 18, 19, and 26) in the summer of 2001. The purpose of this report is to document the experiments performed and to provide a road map for accessing the experimental data on the attached CD-ROM. Appendix I lists the directory structure on the CD-ROM. Data are stored in binary format as a single column of 4 byte, floating point numbers. Individual data files, thus, represent a single time series of either concentration, velocity, or sonic temperature. Appendix II provides a sample code for reading the data into Matlab. Specific details regarding the experimental conditions associated with each data file are provided in the following sections.

2 Experimental Setup

Schematics of the experimental setup are provided in Appendix III (figures 4–14). Eleven different experimental grids were used in the study; each grid schematic is labeled sequentially starting with Grid #1 (figure4). The schematics show the relative locations of the barrels in the array (as intersections of a uniform, rectangular grid), the location of the source and the barrel configuration near the source, as well as the locations of the digiPID concentration sensors and sonics. For clarity, a new grid schematic was created each time the experimental configuration changed. All of the schematics are drawn to scale and include a legend.

Also shown is the (x, y, z) coordinate system of the grid used to reference the positions of the sensors. In addition, the orientation of the barrel array relative to true North is given in the upper right hand corner of the grid. The large arrow at the top of the grid indicates the mean wind direction; however, over the course of any give run, the mean wind direction may have shifted by upto $\pm 30°$. The actual mean wind direction may be obtained from the sonic anemometer data.

Three, 50 degree arcs each containing 11 digiPIDs (in 5° increments) were setup downwind of the source. The digiPIDs along these arcs were located at a height $z = 0.23$ m above the surface. Four 2 m towers were also used to mount additional digiPIDs within the barrel array. Two 3 m towers and one 5 m tower were used to mount the sonic anemometers. Sonic towers were located both within the barrel array and upwind/downwind of the array. The positions of the sensor towers varied from run to run and are shown explicitly in the grid schematics.

3 Sonic Anemometer Data

A total of 6, three dimensional sonic anemometers (CSAT3, Campbell Scientific) were used in the study to measure wind turbulence within and directly above the roughness sublayer

created by the barrel array. On July 17, 18, and 19 only 3 sonics were active. A drawing of one sonic is shown in figure2. Each sonic measures two horizontal velocity components (U, V), the vertical velocity component (W), and the sonic temperature (T). The U, V, and W components correspond to the velocity along the positive X, Y, and Z axes of the sonic, respectively, as shown in figure 2. In some cases, the (X, Y) axes of the sonic do not correspond to the (x, y) axes of the grid. For these cases, an offset is given in terms of the degree deviation from x. For example, an offset of 20° indicates that the X axis of the sonic must be rotated 20° CW to align with the x axis of the grid (a negative offset corresponds to a CCW rotation).

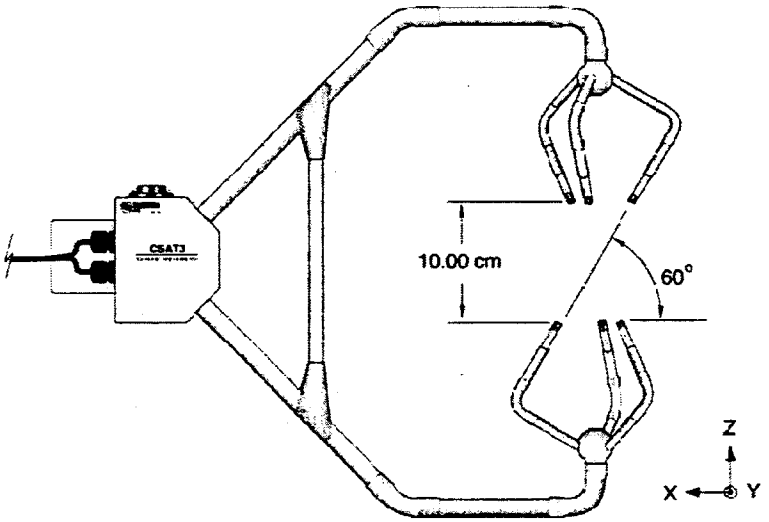

Figure 2: Schematic of the CSAT3 sonic anemometer showing the sonic coordinates.

All of the sonic data is summarized in tables 1–4 in Appendix IV. One table is provided for each of the four days that data was acquired. Each table lists the data file name (without the extension), the start and end time referenced to Mountain Standard Time (MST), the tower on which the sonic was mounted, the grid number (see Appendix III), the x, y, z location of the sonic in the grid, and the offset of the sonic X axis relative to the grid x axis, as described above. In all cases, the sampling frequency was 20 Hz. Note, the filename extension indicates the appropriate measured quantity: '.U', velocity along the sonic X axis in m/s; '.V', velocity along the sonic Y axis in m/s; '.W', vertical velocity in m/s; '.T', sonic temperature in °C. A sample file name is 'z0_5H.U' where 'z0_5H' indicates that the sonic height is $z = 0.5H$ and the extension '.U' indicates the velocity along the X axis of the sonic.

4 DigiPID Data

A total of 43 digital photoionization detectors (digiPID, Aurora Scientific) were used to measure tracer concentration within the barrel array. A schematic of the digiPID sensor is shown in figure 3. Due to communication problems with some of the sensors, only approximately 40 sensors were active during any particular run. All of the digiPID sensors were sampled simultaneously at 50 Hz. Post processing of the raw digiPID data files included removing the baseline trend, applying the calibration, and thresholding the resultant time series, such that any negative concentration was set to zero. Note, the post processed digiPID data files use the file extension '.pid' and contain concentration data in ppm. A sample file name is 'dpid01_sn29.pid', where 'dpid01' is the base file name and 'sn29' is the sensor serial number.

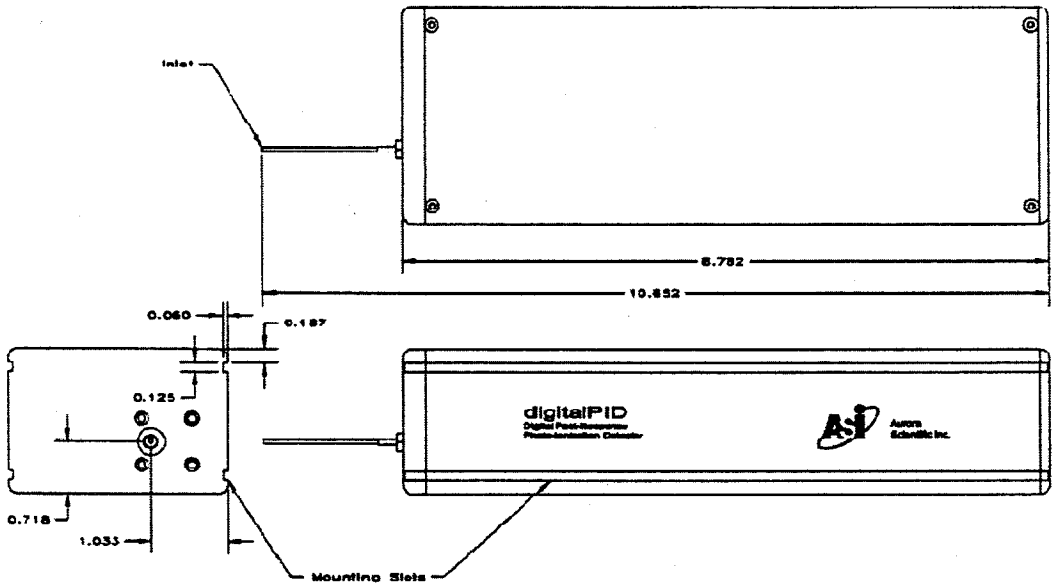

Figure 3: Schematic of the DigiPID concentration sensor. All dimensions are in inches.

All of the digiPID data is summarized in tables 5–12 in Appendix V. Two tables are provided for each of the four days that data was acquired. Tables 5–8 list each digiPID data file name along with the corresponding start and end time in MST and the grid number (see Appendix III). Tables 9–10 list the sensor position number as drawn on the grid schematic, the sensor serial number, and the x, y, z location of the sensor relative to the grid origin.

Appendix I: Directory Structure on CD-ROM

The directory structure on the attached CD-ROM is shown below.

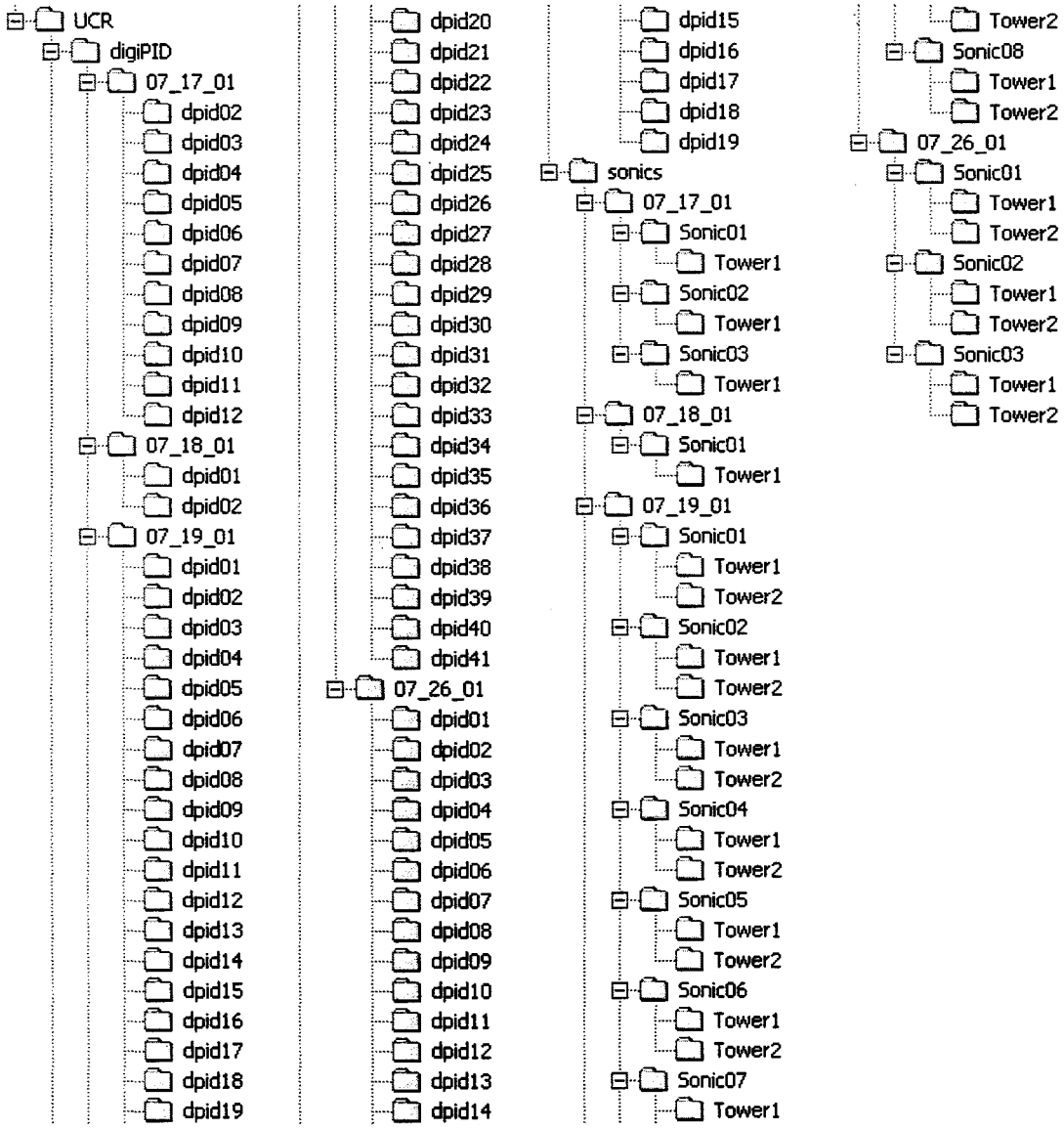

Appendix II: Reading Binary Data Files in Matlab

The following code may be used in a Windows environment to read the binary data files into Matlab and, for example, compute the mean and standard deviation. In order to read the files on a Unix based system, one will have to modify the line using "fopen" (see Matlab help documentation for more details).

```
%-------------------------------------------------
% Matlab sample code to read binary SLTEST data
%-------------------------------------------------

% change directory to CD-ROM
cd('e:\');

% data file name of interest
file='MyFileName';

% open data file
fid=fopen(file,'rb');

% read in entire data file
data=fread(fid,inf,'float32');

% close data file
fclose(fid);

% compute mean
MeanData=mean(data);

% compute standard deviation
StdData=std(data);

% plot out time series
plot(data);
```

Appendix III: Experimental Grid Schematics

Figures 4–14 contain schematics of the experimental grids used in the present study. The large arrow at the top of the grid indicates the approximate mean wind direction. During some runs, the mean wind direction did deviate by as much as $\pm 30°$. Also shown in the upper right hand corner is the direction of true North relative to the x axis of the grid.

In the experiments associated with grid #1 – #4, there were no barrels present. For all of the other grids, the barrel array is drawn as a uniform rectangular grid with the barrels located at the grid intersections. In some configurations, additional barrels were added near the source. For these cases, the barrel arrangement is shown explicitly.

In grid #1, the sonic anemometer tower location is not drawn to scale. The tower was positioned upwind and to the west of the source; however, the exact position was not measured. In grids #9, #10, and #11, sonic anemometer tower #2 was located upwind and to the west of the barrel array. The placement of the tower on the grid corresponds roughly to the actual location at the site; however, exact measurements were not taken. In all other aspects, the schematics are drawn to scale.

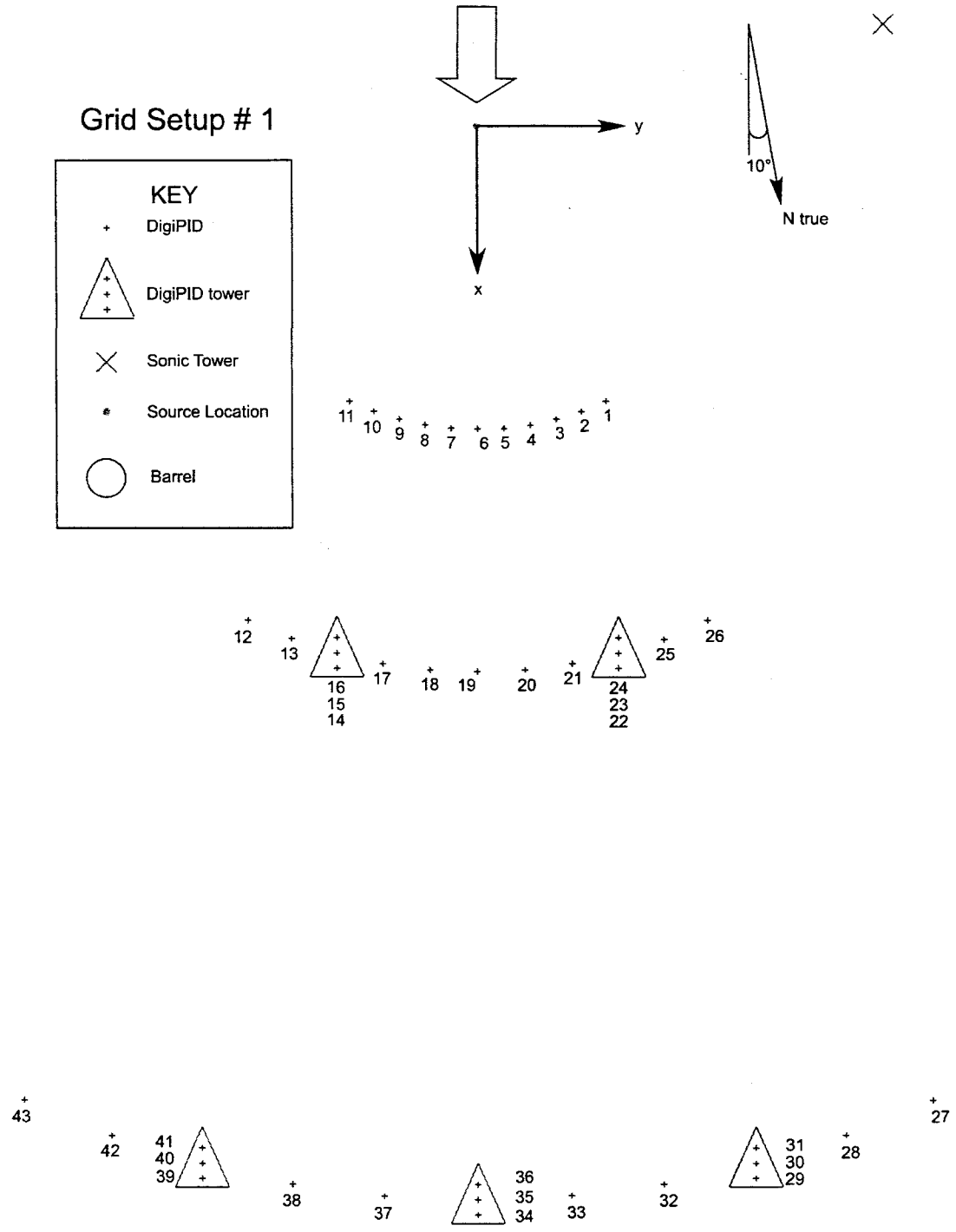

Figure 4: Experimental Grid #1.

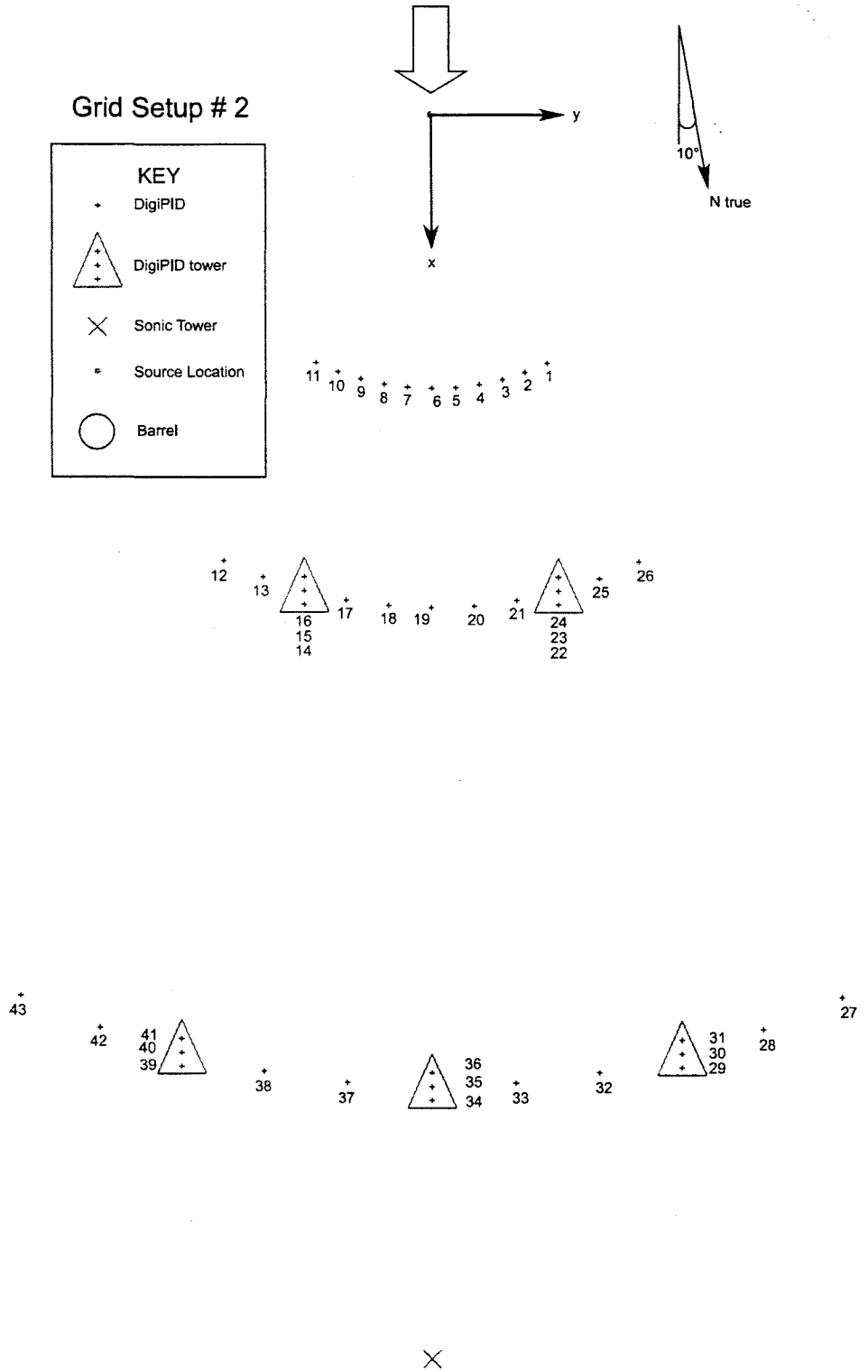

Figure 5: Experimental Grid #2.

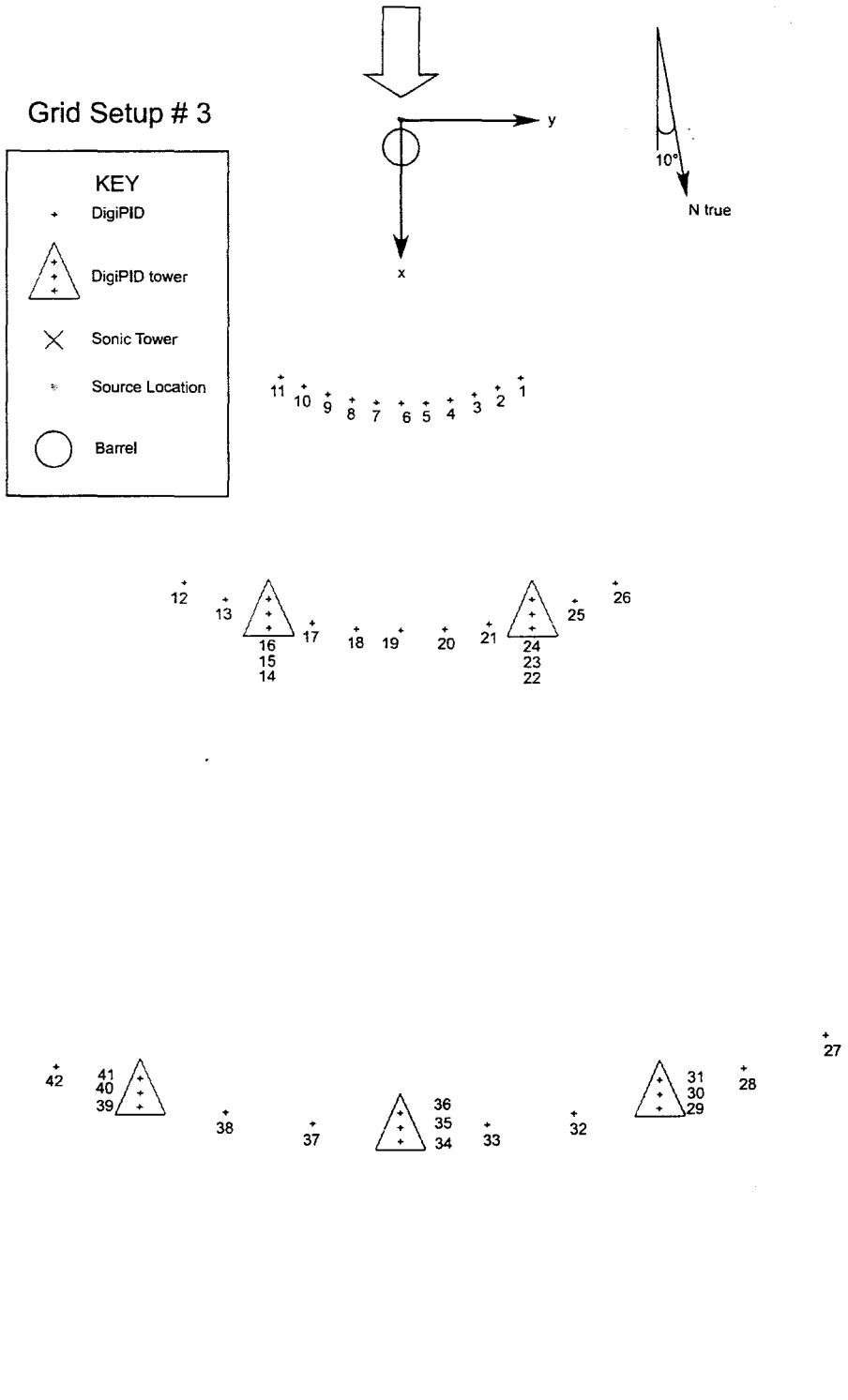

Figure 6: Experimental Grid #3.

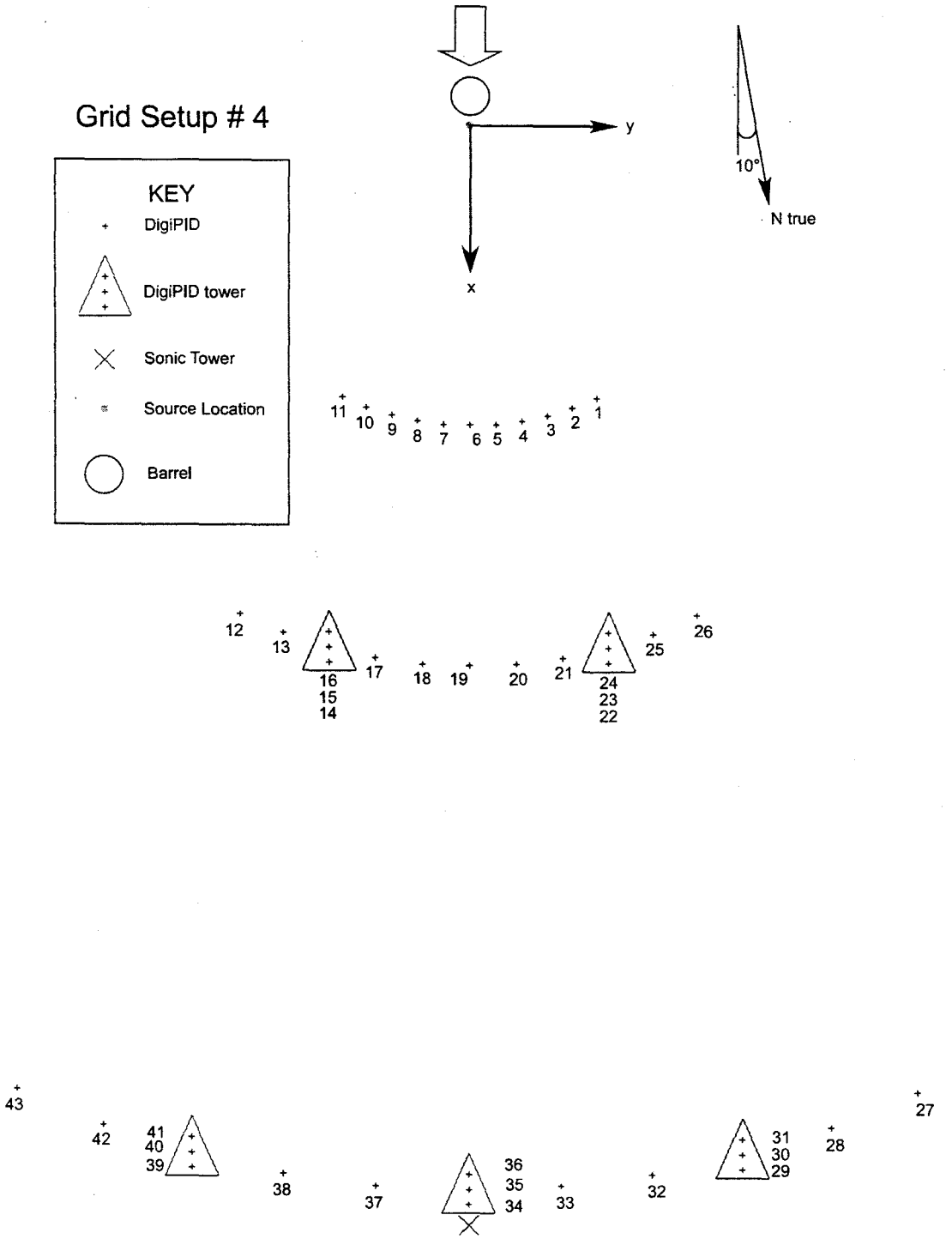

Figure 7: Experimental Grid #4.

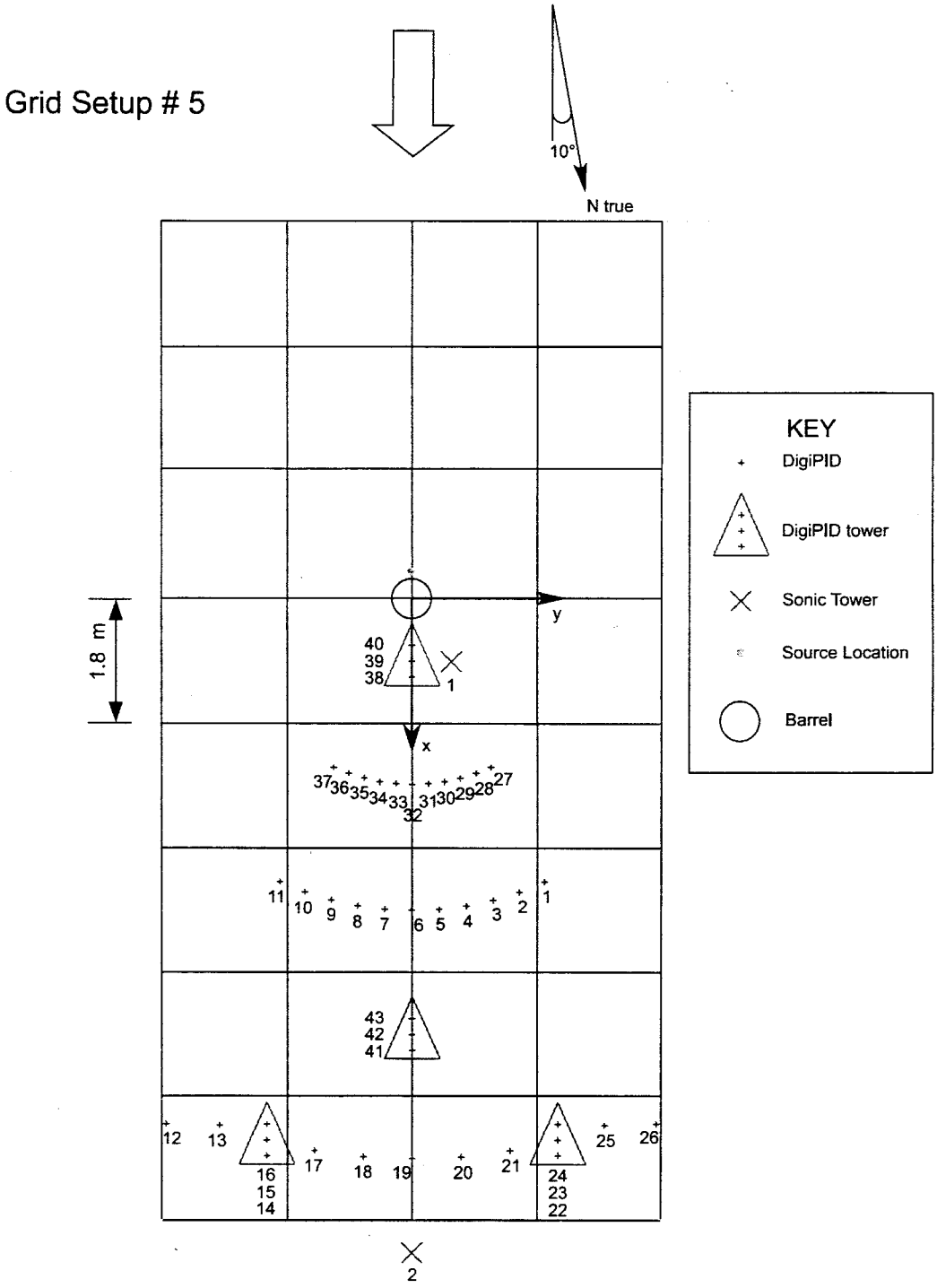

Figure 8: Experimental Grid #5.

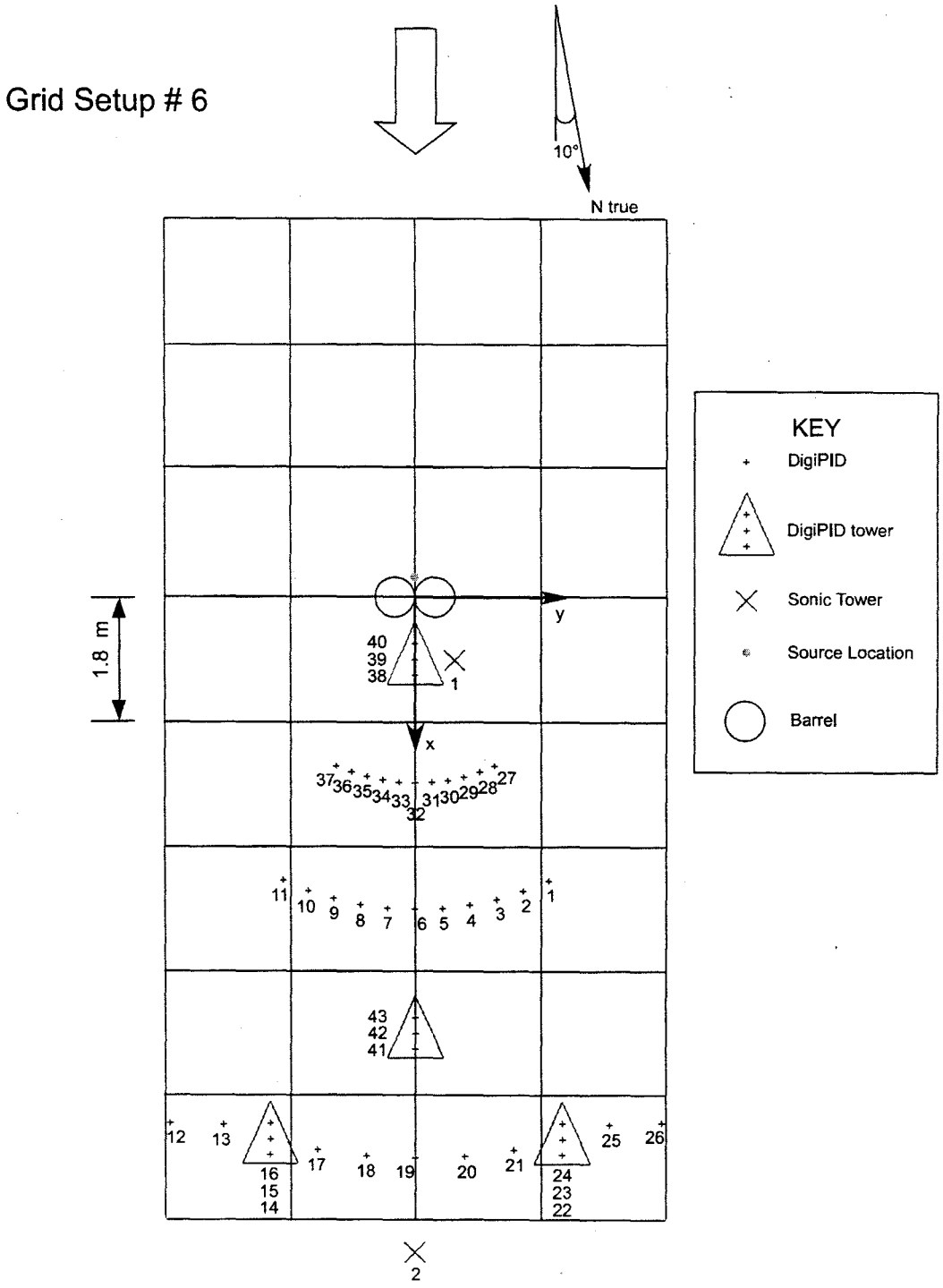

Figure 9: Experimental Grid #6.

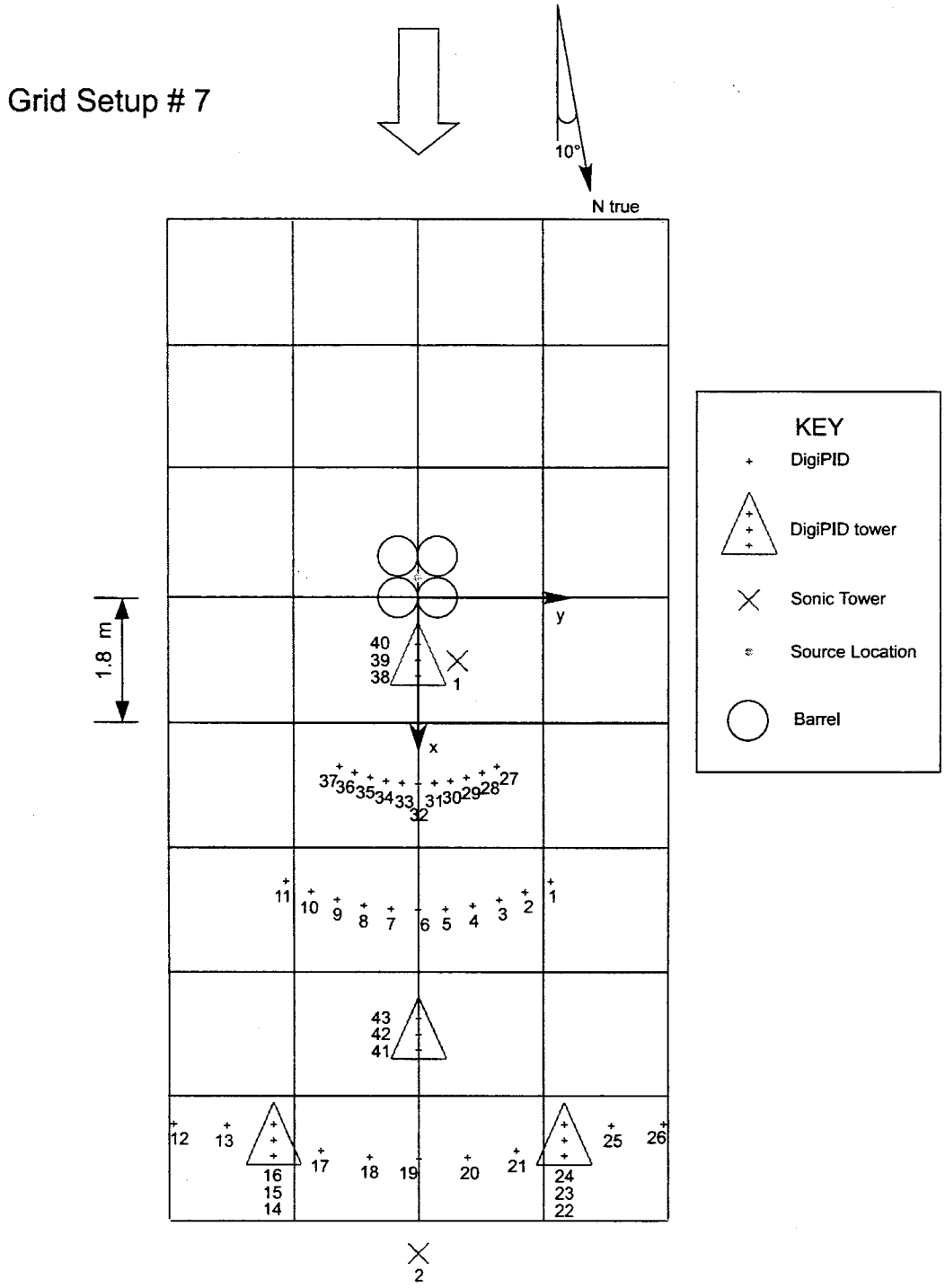

Figure 10: Experimental Grid #7.

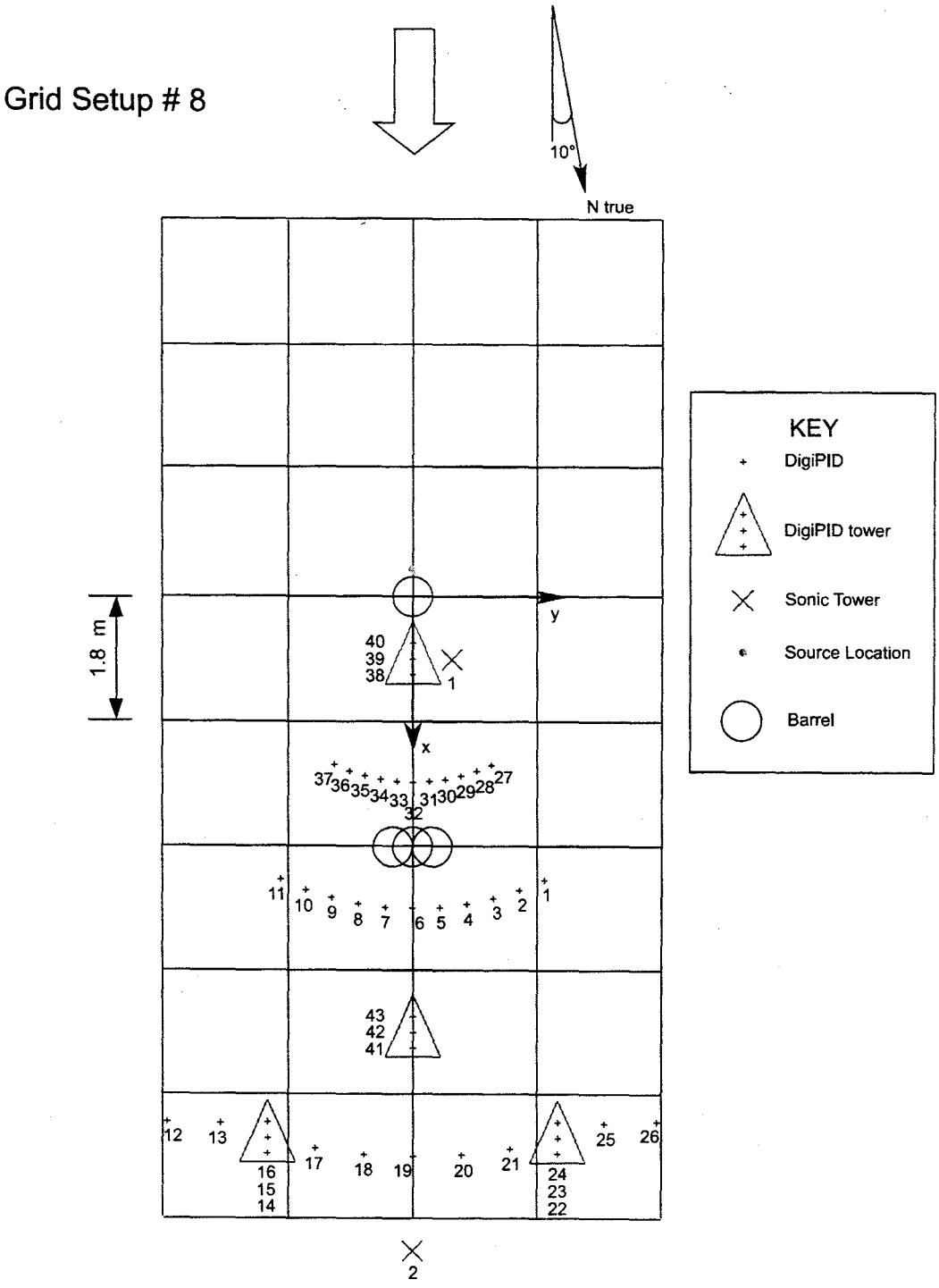

Figure 11: Experimental Grid #8.

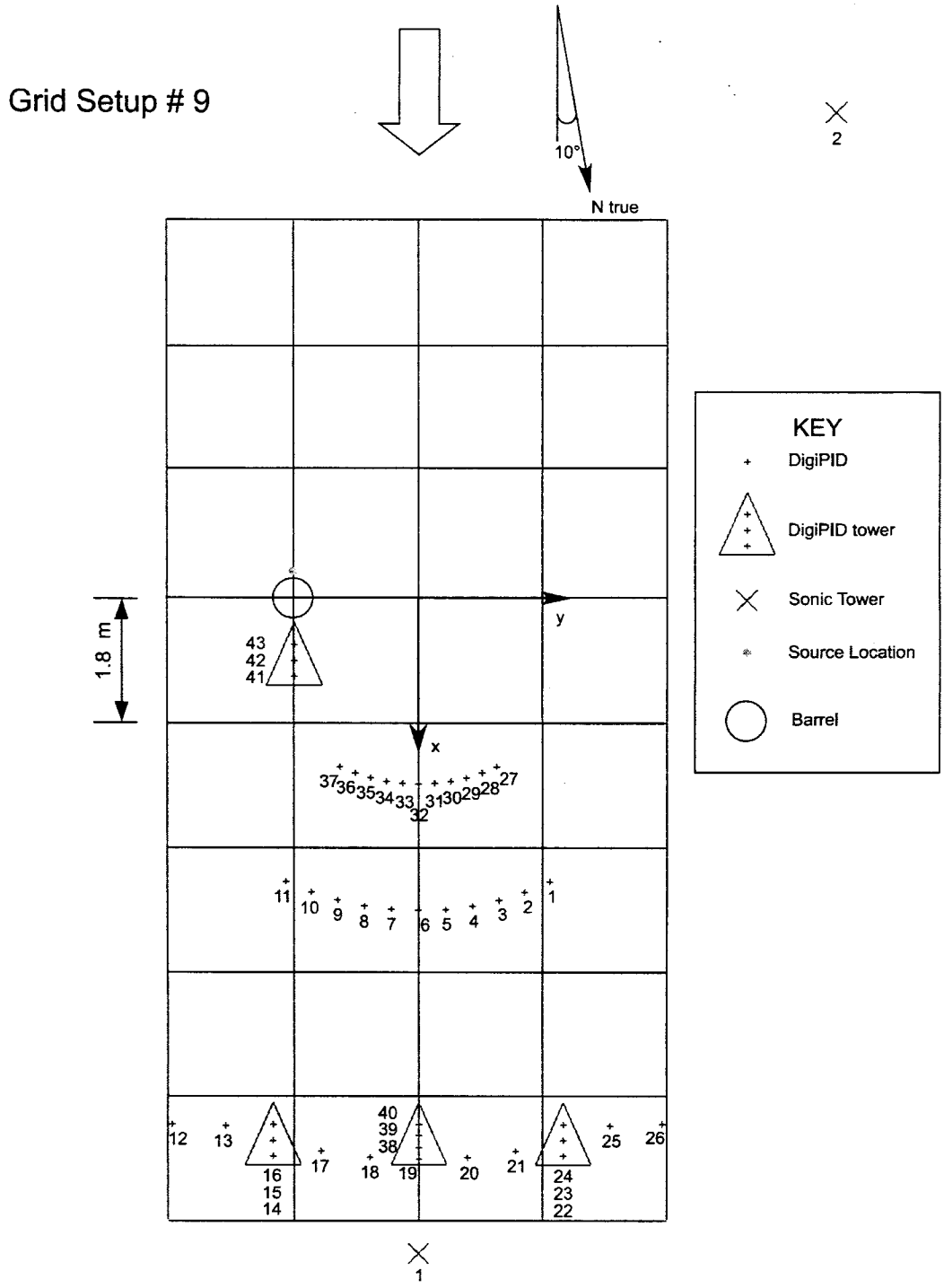

Figure 12: Experimental Grid #9.

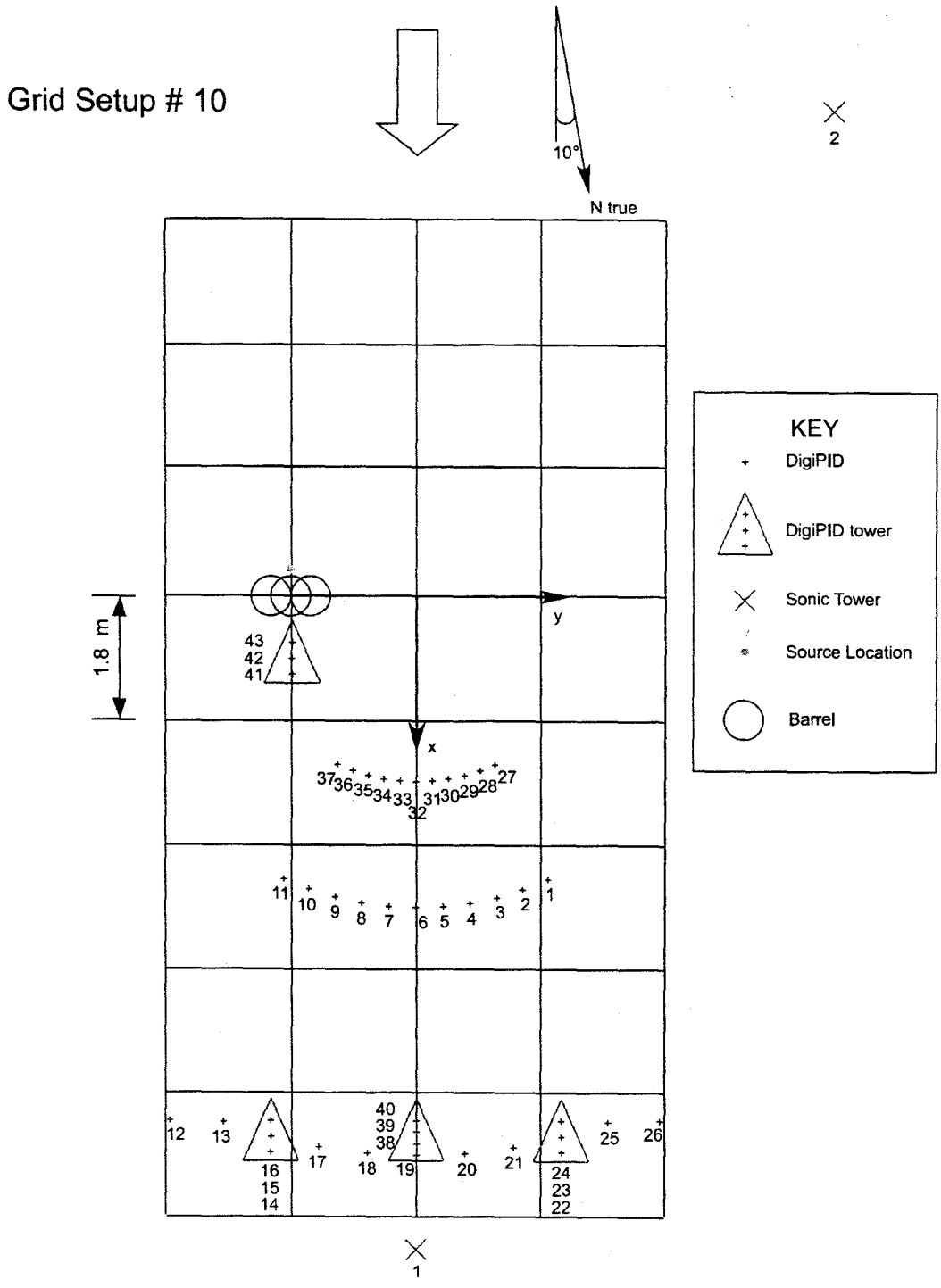

Figure 13: Experimental Grid #10.

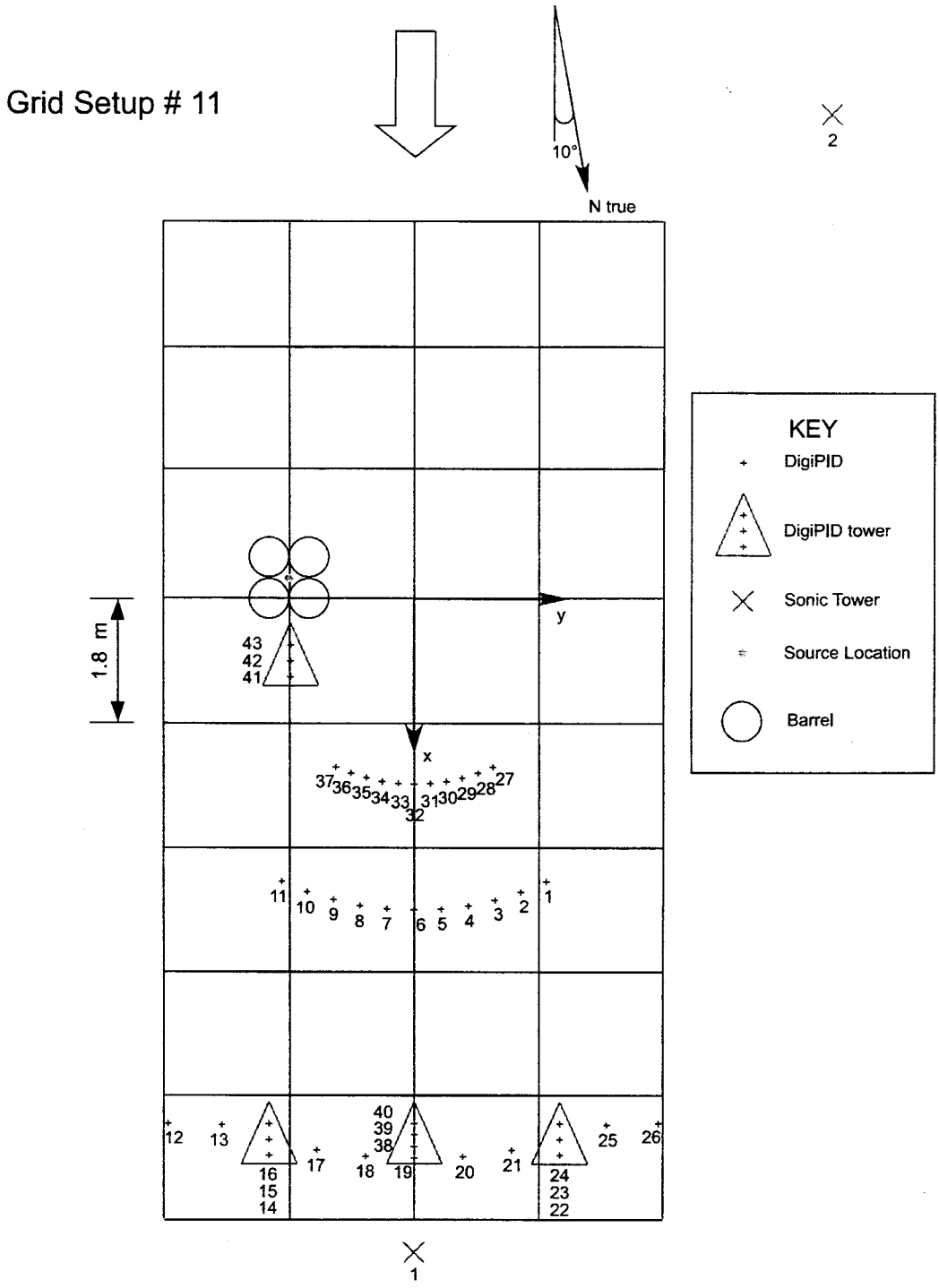

Figure 14: Experimental Grid #11.

Appendix IV: Sonic Anemometer Data Files

Tables 1–4 list all of the sonic anemometer data files collected (without the file name extension), the start and end time in MST, the tower on which the sonic was mounted, the corresponding grid number, the x, y, z position of the sonic relative to the grid coordinate system, and the sonic axis offset (see section 3 for details). One table is provided for each of the data acquisition days.

Table 1: SLTEST Sonic Anemometer Data, July 17, 2001

File	Start	End	Tower #	Grid #	x (m)	y (m)	z (m)	z/H	Offset
z0_5H	18:45	19:05	1	1	upwind	west	0.5	0.5	10°
z1_5H	18:45	19:05	1	1	upwind	west	1.4	1.5	10°
z3_5H	18:45	19:05	1	1	upwind	west	3.2	3.5	10°
z0_5H	19:19	20:34	1	2	20.5	0.0	0.5	0.5	10°
z1_5H	19:19	20:34	1	2	20.5	0.0	1.4	1.5	10°
z3_5H	19:19	20:34	1	2	20.5	0.0	3.2	3.5	10°
z0_5H	20:34	20:56	1	3	20.5	0.0	0.5	0.5	10°
z1_5H	20:34	20:56	1	3	20.5	0.0	1.4	1.5	10°
z3_5H	20:34	20:56	1	3	20.5	0.0	3.2	3.5	10°

Table 2: SLTEST Sonic Anemometer Data, July 18, 2001

File	Start	End	Tower #	Grid #	x (m)	y (m)	z (m)	z/H	Offset
z0_5H	19:06	19:30	1	4	16.5	0.0	0.5	0.5	10°
z1_5H	19:06	19:30	1	4	16.5	0.0	1.4	1.5	10°
z3_5H	19:06	19:30	1	4	16.5	0.0	3.2	3.5	10°

Table 3: SLTEST Sonic Anemometer Data, July 19, 2001

File	Start	End	Tower #	Grid #	x (m)	y (m)	z (m)	z/H	Offset
z0_5H	15:28	17:11	1	5	0.9	0.0	0.5	0.5	0°
z0_5H	15:28	17:11	2	5	9.5	0.0	0.5	0.5	0°
z3_5H	15:28	17:11	2	5	9.5	0.0	3.2	3.5	0°
z0_5H	17:11	18:42	1	6	0.9	0.0	0.5	0.5	0°
z0_5H	17:11	18:42	2	6	9.5	0.0	0.5	0.5	0°
z3_5H	17:11	18:42	2	6	9.5	0.0	3.2	3.5	0°
z0_5H	18:42	19:48	1	7	0.9	0.0	0.5	0.5	0°
z0_5H	18:42	19:48	2	7	9.5	0.0	0.5	0.5	0°
z3_5H	18:42	19:48	2	7	9.5	0.0	3.2	3.5	0°
z0_5H	19:48	20:43	1	8	0.9	0.0	0.5	0.5	0°
z0_5H	19:48	20:43	2	8	9.5	0.0	0.5	0.5	0°
z3_5H	19:48	20:43	2	8	9.5	0.0	3.2	3.5	0°
z0_5H	20:43	20:55	1	5	0.9	0.0	0.5	0.5	0°
z0_5H	20:43	20:55	2	5	9.5	0.0	0.5	0.5	0°
z3_5H	20:43	20:55	2	5	9.5	0.0	3.2	3.5	0°
z0_5H	20:55	21:37	1	7	0.9	0.0	0.5	0.5	0°
z0_5H	20:55	21:37	2	7	9.5	0.0	0.5	0.5	0°
z3_5H	20:55	21:37	2	7	9.5	0.0	3.2	3.5	0°
z0_5H	21:37	22:23	1	6	0.9	0.0	0.5	0.5	0°
z0_5H	21:37	22:23	2	6	9.5	0.0	0.5	0.5	0°
z3_5H	21:37	22:23	2	6	9.5	0.0	3.2	3.5	0°
z0_5H	22:23	23:11	1	8	0.9	0.0	0.5	0.5	0°
z0_5H	22:23	23:11	2	8	9.5	0.0	0.5	0.5	0°
z3_5H	22:23	23:11	2	8	9.5	0.0	3.2	3.5	0°

Table 4: SLTEST Sonic Anemometer Data, July 26, 2001

File	Start	End	Tower #	Grid #	x (m)	y (m)	z (m)	z/H	Offset
z0_5H	15:59	16:43	1	9	9.5	0.0	0.5	0.5	0°
z1_1H	15:59	16:43	1	9	9.5	0.0	1.0	1.1	0°
z2_2H	15:59	16:43	1	9	9.5	0.0	2.0	2.2	0°
z5_5H	15:59	16:43	1	9	9.5	0.0	5.0	5.5	0°
z1_5H	15:59	16:43	2	9	upwind	west	1.4	1.5	0°
z3_5H	15:59	16:43	2	9	upwind	west	3.2	3.5	0°
z0_5H	16:43	18:31	1	10	9.5	0.0	0.5	0.5	0°
z1_1H	16:43	18:31	1	10	9.5	0.0	1.0	1.1	0°
z2_2H	16:43	18:31	1	10	9.5	0.0	2.0	2.2	0°
z5_5H	16:43	18:31	1	10	9.5	0.0	5.0	5.5	0°
z1_5H	16:43	18:31	2	10	upwind	west	1.4	1.5	0°
z3_5H	16:43	18:31	2	10	upwind	west	3.2	3.5	0°
z0_5H	18:31	19:21	1	11	9.5	0.0	0.5	0.5	0°
z1_1H	18:31	19:21	1	11	9.5	0.0	1.0	1.1	0°
z2_2H	18:31	19:21	1	11	9.5	0.0	2.0	2.2	0°
z5_5H	18:31	19:21	1	11	9.5	0.0	5.0	5.5	0°
z1_5H	18:31	19:21	2	11	upwind	west	1.4	1.5	0°
z3_5H	18:31	19:21	2	11	upwind	west	3.2	3.5	0°

Appendix V: DigiPID Data Files

Two tables are provided for each of the four days that digiPID data was acquired. Tables 5–8 list all of the digiPID data files collected (without the corresponding serial number identification or file name extension), the start and end time in MST, and the corresponding grid number (see Appendix III). The asterisk in table 5 denotes that there were no sonic anemometers active during that particular digiPID run. Tables 9–12 list the sensor position number as shown on the grid schematic, the sensor serial number, and the x, y, z position of the sensor in terms of the grid coordinate system.

Table 5: SLTEST DigiPID Data, July 17, 2001

Filename	Start Time	End Time	Grid #
dpid02	18:45	18:55	1
dpid03	18:57:48	19:07:48	1
dpid04	19:08:13	19:18:13	1*
dpid05	19:22:51	19:32:51	2
dpid06	19:35:31	19:45:31	2
dpid07	19:45:54	19:55:54	2
dpid08	19:57:36	20:07:36	2
dpid09	20:07:56	20:17:56	2
dpid10	20:21:48	20:31:48	2
dpid11	20:34:11	20:44:11	3
dpid12	20:45:02	20:55:02	3

Table 6: SLTEST DigiPID Data, July 18, 2001

Filename	Start Time	End Time	Grid #
dpid01	19:06:33	19:16:33	4
dpid02	19:17:47	19:27:47	4

Table 7: SLTEST DigiPID Data, July 19, 2001

Filename	Start Time	End Time	Grid #
dpid01	15:28:37	15:38:37	5
dpid02	15:39:58	15:49:58	5
dpid03	15:50:35	16:00:35	5
dpid04	16:02:04	16:12:04	5
dpid05	16:17:47	16:27:47	5
dpid06	16:31:53	16:41:53	5
dpid07	16:42:39	16:49:28	5
dpid08	16:50:40	16:57:29	5
dpid09	16:58:06	17:08:06	5
dpid10	17:11:28	17:12:20	6
dpid11	17:13:18	17:14:10	6
dpid12	17:14:31	17:24:31	6
dpid13	17:24:53	17:34:53	6
dpid14	17:35:52	17:45:52	6
dpid15	17:46:10	17:56:10	6
dpid16	17:58:17	18:08:17	6
dpid17	18:08:30	18:18:30	6
dpid18	18:18:48	18:28:48	6
dpid19	18:29:13	18:39:13	6
dpid20	18:42:23	18:52:23	7
dpid21	18:52:39	19:02:39	7
dpid22	19:02:50	19:12:50	7
dpid23	19:13:26	19:23:26	7
dpid24	19:23:41	19:33:41	7
dpid25	19:34:40	19:44:40	7
dpid26	19:48:01	19:58:01	8
dpid27	19:58:10	20:08:10	8
dpid28	20:08:22	20:18:22	8
dpid29	20:18:34	20:28:34	8
dpid30	20:29:11	20:39:11	8
dpid31	20:43:00	20:53:00	5
dpid32	20:55:43	21:05:43	7
dpid33	21:05:53	21:15:53	7
dpid34	21:16:02	21:26:02	7
dpid35	21:26:18	21:36:18	7
dpid36	21:37:39	21:47:39	6
dpid37	21:47:52	21:57:52	6
dpid38	22:00:08	22:10:08	6
dpid39	22:10:28	22:20:28	6
dpid40	22:23:21	22:33:21	8
dpid41	22:33:39	22:43:39	8

Table 8: SLTEST DigiPID Data, July 26, 2001

Filename	Start Time	End Time	Grid #
dpid01	15:59:31	16:09:31	9
dpid02	16:09:57	16:19:57	9
dpid03	16:20:11	16:30:11	9
dpid04	16:30:27	16:40:27	9
dpid05	16:43:04	16:53:04	10
dpid06	16:53:15	17:03:15	10
dpid07	17:03:26	17:13:26	10
dpid08	17:13:40	17:23:40	10
dpid09	17:23:54	17:24:08	10
dpid10	17:27:54	17:34:30	10
dpid11	17:37:44	17:47:44	10
dpid12	17:48:22	17:58:22	10
dpid13	17:58:49	18:08:49	10
dpid14	18:09:07	18:19:07	10
dpid15	18:19:19	18:29:19	10
dpid16	18:31:36	18:41:36	11
dpid17	18:41:48	17:51:48	11
dpid18	18:55:04	19:05:04	11
dpid19	19:05:41	19:15:41	11

Table 9: SLTEST DigiPID Positions, July 17, 2001

Position	Serial Number	x (m)	y (m)	z (m)	z/H
1	29	4.1	1.9	0.2	0.25
2	30	4.2	1.5	0.2	0.25
3	31	4.3	1.2	0.2	0.25
4	32	4.4	0.8	0.2	0.25
5	33	4.5	0.4	0.2	0.25
6	34	4.5	0.0	0.2	0.25
7	35	4.5	-0.4	0.2	0.25
8	36	4.4	-0.8	0.2	0.25
9	38	4.3	-1.2	0.2	0.25
10	39	4.2	-1.5	0.2	0.25
11	40	4.1	-1.9	0.2	0.25
12	76	7.3	-3.4	0.2	0.25
13	42	7.6	-2.8	0.2	0.25
14	43	7.8	-2.1	0.2	0.25
15	44	7.8	-2.1	0.5	0.5
16	45	7.8	-2.1	1.4	1.5
17	46	8.0	-1.4	0.2	0.25
18	53	8.1	-0.7	0.2	0.25
19	54	8.1	0.0	0.2	0.25
20	56	8.1	0.7	0.2	0.25
21	57	8.0	1.4	0.2	0.25
22	58	7.8	2.1	0.2	0.25
23	47	7.8	2.1	0.5	0.5
24	--	7.8	2.1	1.4	1.5
25	49	7.6	2.8	0.2	0.25
26	50	7.3	3.4	0.2	0.25
27	55	14.5	6.8	0.2	0.25
28	51	15.0	5.5	0.2	0.25
29	52	15.5	4.1	0.2	0.25
30	59	15.5	4.1	0.5	0.5
31	61	15.5	4.1	1.4	1.5
32	--	15.8	2.8	0.2	0.25
33	63	15.9	1.4	0.2	0.25
34	64	16.0	0.0	0.2	0.25
35	--	16.0	0.0	0.5	0.5
36	66	16.0	0.0	1.4	1.5
37	67	15.9	-1.4	0.2	0.25
38	68	15.8	-2.8	0.2	0.25
39	69	15.5	-4.1	0.2	0.25
40	70	15.5	-4.1	0.5	0.5
41	71	15.5	-4.1	1.4	1.5
42	72	15.0	-5.5	0.2	0.25
43	74	14.5	-6.8	0.2	0.25

Table 10: SLTEST DigiPID Positions, July 18, 2001

Position	Serial Number	x (m)	y (m)	z (m)	z/H
1	29	4.1	1.9	0.2	0.25
2	30	4.2	1.5	0.2	0.25
3	31	4.3	1.2	0.2	0.25
4	32	4.4	0.8	0.2	0.25
5	33	4.5	0.4	0.2	0.25
6	34	4.5	0.0	0.2	0.25
7	35	4.5	-0.4	0.2	0.25
8	36	4.4	-0.8	0.2	0.25
9	38	4.3	-1.2	0.2	0.25
10	39	4.2	-1.5	0.2	0.25
11	40	4.1	-1.9	0.2	0.25
12	76	7.3	-3.4	0.2	0.25
13	42	7.6	-2.8	0.2	0.25
14	43	7.8	-2.1	0.2	0.25
15	44	7.8	-2.1	0.5	0.5
16	45	7.8	-2.1	1.4	1.5
17	46	8.0	-1.4	0.2	0.25
18	53	8.1	-0.7	0.2	0.25
19	54	8.1	0.0	0.2	0.25
20	56	8.1	0.7	0.2	0.25
21	57	8.0	1.4	0.2	0.25
22	58	7.8	2.1	0.2	0.25
23	47	7.8	2.1	0.5	0.5
24	48	7.8	2.1	1.4	1.5
25	49	7.6	2.8	0.2	0.25
26	--	7.3	3.4	0.2	0.25
27	--	14.5	6.8	0.2	0.25
28	51	15.0	5.5	0.2	0.25
29	52	15.5	4.1	0.2	0.25
30	59	15.5	4.1	0.5	0.5
31	61	15.5	4.1	1.4	1.5
32	62	15.8	2.8	0.2	0.25
33	63	15.9	1.4	0.2	0.25
34	64	16.0	0.0	0.2	0.25
35	65	16.0	0.0	0.5	0.5
36	66	16.0	0.0	1.4	1.5
37	67	15.9	-1.4	0.2	0.25
38	68	15.8	-2.8	0.2	0.25
39	69	15.5	-4.1	0.2	0.25
40	--	15.5	-4.1	0.5	0.5
41	71	15.5	-4.1	1.4	1.5
42	72	15.0	-5.5	0.2	0.25
43	--	14.5	-6.8	0.2	0.25

Table 11: SLTEST DigiPID Positions, July 19, 2001

Position	Serial Number	x (m)	y (m)	z (m)	z/H
1	29	4.1	1.9	0.2	0.25
2	30	4.2	1.5	0.2	0.25
3	31	4.3	1.2	0.2	0.25
4	32	4.4	0.8	0.2	0.25
5	33	4.5	0.4	0.2	0.25
6	34	4.5	0.0	0.2	0.25
7	35	4.5	-0.4	0.2	0.25
8	36	4.4	-0.8	0.2	0.25
9	38	4.3	-1.2	0.2	0.25
10	39	4.2	-1.5	0.2	0.25
11	40	4.1	-1.9	0.2	0.25
12	76	7.3	-3.4	0.2	0.25
13	42	7.6	-2.8	0.2	0.25
14	43	7.8	-2.1	0.2	0.25
15	44	7.8	-2.1	0.5	0.5
16	45	7.8	-2.1	1.4	1.5
17	46	8.0	-1.4	0.2	0.25
18	53	8.1	-0.7	0.2	0.25
19	54	8.1	0.0	0.2	0.25
20	56	8.1	0.7	0.2	0.25
21	--	8.0	1.4	0.2	0.25
22	58	7.8	2.1	0.2	0.25
23	47	7.8	2.1	0.5	0.5
24	48	7.8	2.1	1.4	1.5
25	49	7.6	2.8	0.2	0.25
26	50	7.3	3.4	0.2	0.25
27	55	2.4	1.1	0.2	0.25
28	51	2.5	0.9	0.2	0.25
29	52	2.6	0.7	0.2	0.25
30	59	2.7	0.5	0.2	0.25
31	61	2.7	0.2	0.2	0.25
32	62	2.7	0.0	0.2	0.25
33	63	2.7	-0.2	0.2	0.25
34	64	2.7	-0.5	0.2	0.25
35	65	2.6	-0.7	0.2	0.25
36	66	2.5	-0.9	0.2	0.25
37	--	2.4	-1.1	0.2	0.25
38	69	0.9	0.0	0.2	0.25
39	70	0.9	0.0	0.5	0.5
40	71	0.9	0.0	1.4	1.5
41	68	6.3	0.0	0.2	0.25
42	72	6.3	0.0	0.5	0.5
43	--	6.3	0.0	1.4	1.5

Table 12: SLTEST DigiPID Positions, July 26, 2001

Position	Serial Number	x (m)	y (m)	z (m)	z/H
1	29	4.1	1.9	0.2	0.25
2	30	4.2	1.5	0.2	0.25
3	31	4.3	1.2	0.2	0.25
4	32	4.4	0.8	0.2	0.25
5	33	4.5	0.4	0.2	0.25
6	34	4.5	0.0	0.2	0.25
7	35	4.5	-0.4	0.2	0.25
8	36	4.4	-0.8	0.2	0.25
9	38	4.3	-1.2	0.2	0.25
10	39	4.2	-1.5	0.2	0.25
11	40	4.1	-1.9	0.2	0.25
12	76	7.3	-3.4	0.2	0.25
13	42	7.6	-2.8	0.2	0.25
14	43	7.8	-2.1	0.2	0.25
15	44	7.8	-2.1	0.5	0.5
16	45	7.8	-2.1	1.4	1.5
17	46	8.0	-1.4	0.2	0.25
18	53	8.1	-0.7	0.2	0.25
19	54	8.1	0.0	0.2	0.25
20	56	8.1	0.7	0.2	0.25
21	57	8.0	1.4	0.2	0.25
22	58	7.8	2.1	0.2	0.25
23	47	7.8	2.1	0.5	0.5
24	48	7.8	2.1	1.4	1.5
25	49	7.6	2.8	0.2	0.25
26	50	7.3	3.4	0.2	0.25
27	55	2.4	1.1	0.2	0.25
28	51	2.5	0.9	0.2	0.25
29	52	2.6	0.7	0.2	0.25
30	59	2.7	0.5	0.2	0.25
31	61	2.7	0.2	0.2	0.25
32	62	2.7	0.0	0.2	0.25
33	63	2.7	-0.2	0.2	0.25
34	64	2.7	-0.5	0.2	0.25
35	65	2.6	-0.7	0.2	0.25
36	66	2.5	-0.9	0.2	0.25
37	67	2.4	-1.1	0.2	0.25
38	68	8.1	0.0	0.5	0.5
39	72	8.1	0.0	0.9	1
40	69	8.1	0.0	1.4	1.5
41	41	0.9	0.0	0.2	0.25
42	70	0.9	0.0	0.5	0.5
43	71	0.9	0.0	1.4	1.5

Appendix VI: Wind and Turbulence Data

Wind and turbulence during the experiments at Dugway are reported in tables 1-4 based on processing of the observations from sonic anemometer #1 on tower #1 using five-minute averaging. Some sampling periods were not integral multiples of five minutes; conditions are not reported for residual periods of less than five minutes.

It is important to note the definitions of wind components used here necessarily differ from the files described in Appendix IV. In both Appendix IV and VI the wind component w is defined as the vertical velocity. However, definitions of the horizontal components u and v differ between the two appendices. In Appendix IV, observations are described with a fixed coordinate system for each day. The horizontal components u and v are defined relative to the anemometer orientation. In turn, the anemometer orientation is reported for each day relative to the axis of the grid used for tracer sampling. The directional offset is reported as either 0 or 10 degrees depending upon the sampling day. Thus, in the observational data files described in Appendix IV the wind components reported are based upon a fixed reference system described relative to the sampling grid.

In tables 1-4 of this Appendix VI the five-minute averages of wind and turbulence are reported using a micrometeorological convention for defining component winds. This convention references components in terms of the mean wind direction during each five-minute period. This convention is commonly used in dispersion modeling and is appropriate for description of the wind and turbulence. Here u is defined as the mean horizontal wind speed and v is defined as the component of the horizontal wind that is perpendicular to the mean wind direction as observed during the five-minute period. Mean wind direction is reported in degrees clockwise from true north (such that 90 degrees indicates wind from the east). Based on the sampling of the instantaneous wind (at 20 hertz) the standard deviation of u and v are reported as sigma u and sigma v. This micrometeorological convention for wind reporting requires defining an averaging period for data processing, computing a mean wind direction for each averaging period, and applying a coordinate transformation to the instantaneous wind observations so that the coordinate system is unique for each period.

Micrometeorological analyses may involve use of multiple averaging periods to describe different scales of motion by the reporting of sigma u and sigma v. If the averaging period is redefined (e.g., increased so that sigma v would reflect the meander of wind direction) it is then necessary to return to the original (20 hertz) observations and repeat the data processing steps. Thus for the sake of future analyses the original data (without transformations to micrometeorological reporting conventions) are retained in the files described in Appendix IV.

The distance of tower #1 from obstacles varied with the grid setup as described in Appendices III and IV. The height of sonic anemometer #1 was 0.5 m for all periods. Obstacles were not present on days 17 and 18; obstacles were present on days 19 and 26. On day 17, during the first 20 minutes of sampling, tower #1 was upwind and west of the sample release point as detailed in the schematic for grid setup #1. During all other sampling on days 17 and 18, tower #1 was downwind of the sampling array, as detailed by schematics for grids #3-4. On day 19, tower #1 was 0.9 m downwind of the tracer release point (and obstacles collocated with the release point) as detailed by schematics for grids #5-8. On day 26, tower #1 was immediately downwind of the barrel array as detailed by schematics for grids #9-11.

Table 1: Sigma u, v, and w, July 17, 2001

Start	End	sigma u	sigma v	sigma w	wind direction	wind speed
18:45	18:50	0.99	0.95	0.42	-21.95	7.52
18:50	19:55	1.00	0.98	0.41	-19.22	7.47
18:55	19:00	1.06	0.88	0.40	-18.91	7.16
19:00	19:05	1.08	0.84	0.39	-17.64	7.01
19:19	19:24	0.99	0.89	0.48	-9.53	5.91
19:24	19:29	1.05	0.88	0.44	-6.83	6.23
19:29	19:34	1.01	0.82	0.42	-6.97	6.23
19:34	19:39	0.99	0.78	0.41	-7.60	6.04
19:39	19:44	0.99	0.77	0.40	-8.58	5.98
19:44	19:49	0.97	0.80	0.39	-10.19	5.94
19:49	19:54	0.98	0.78	0.39	-10.36	6.03
19:54	19:59	0.99	0.79	0.40	-9.93	6.07
19:59	20:04	0.98	0.78	0.40	-9.54	6.07
20:04	20:09	0.98	0.80	0.40	-8.88	6.09
20:09	20:14	0.97	0.80	0.40	-8.25	6.10
20:14	20:19	0.96	0.79	0.40	-8.05	6.08
20:19	20:24	0.97	0.78	0.39	-8.41	6.03
20:24	20:29	0.98	0.79	0.39	-9.00	5.97
20:29	20:34	0.98	0.79	0.38	-9.45	5.92
20:34	20:39	0.84	0.53	0.35	-14.89	5.80
20:39	20:44	0.91	0.49	0.34	-16.56	5.38
20:44	20:49	0.90	0.46	0.33	-16.76	5.10
20:49	20:54	0.87	0.44	0.32	-17.05	4.92

Table 2: Sigma u, v, and w, July 18, 2001

Start	End	sigma u	sigma v	sigma w	wind direction	wind speed
19:06	19:11	1.00	0.80	0.40	-8.79	6.76
19:11	19:16	1.06	0.69	0.35	-7.95	5.93
19:16	19:21	1.09	0.65	0.33	-7.73	5.52
19:21	19:26	1.21	0.73	0.36	-5.94	5.79

Table 3: Sigma u, v, w, July 19, 2001

Start	End	sigma u	sigma v	sigma w	wind direction	wind speed
15:28	15:33	1.43	1.57	0.80	26.41	2.65
15:33	15:38	1.34	1.75	0.84	3.32	2.63
15:38	15:43	1.27	1.58	0.77	-9.01	2.57
15:43	15:48	1.27	1.76	0.78	-6.71	2.49
15:48	15:53	1.29	1.70	0.78	-10.62	2.52
15:53	15:58	1.35	1.63	0.78	-14.60	2.63
15:58	16:03	1.34	1.58	0.76	-15.33	2.52
16:03	16:08	1.31	1.63	0.74	-13.99	2.42
16:08	16:13	1.32	1.69	0.76	-12.68	2.41
16:13	16:18	1.32	1.71	0.76	-10.40	2.34
16:18	16:23	1.31	1.66	0.73	-12.11	2.28
16:23	16:28	1.30	1.67	0.72	-9.87	2.21
16:28	16:33	1.29	1.85	0.72	-2.77	2.24
16:33	16:38	1.31	1.90	0.73	1.91	2.31
16:38	16:43	1.31	1.89	0.75	3.97	2.33
16:43	16:48	1.32	1.88	0.76	5.92	2.35
16:48	16:53	1.31	1.86	0.75	5.32	2.30
16:53	16:58	1.34	1.88	0.77	6.33	2.33
16:58	17:03	1.34	1.87	0.77	8.38	2.37
17:03	17:08	1.34	1.90	0.78	7.78	2.37
17:11	17:16	1.79	0.87	0.73	66.27	2.09
17:16	17:21	1.86	1.06	0.91	68.19	2.11
17:21	17:26	1.96	1.23	1.00	74.59	1.47
17:26	17:31	1.97	1.26	1.01	75.54	1.31
17:31	17:36	1.97	1.31	0.99	74.12	1.01
17:36	17:41	2.09	1.28	0.96	68.41	1.40
17:41	17:46	2.07	1.29	1.00	70.42	1.44
17:46	17:51	2.08	1.28	1.01	69.98	1.54
17:51	17:56	2.17	1.30	1.04	68.39	1.74
17:56	18:01	2.24	1.30	1.05	67.13	1.90
18:01	18:06	2.25	1.28	1.04	65.96	2.04
18:06	18:11	2.21	1.26	1.03	66.19	2.04
18:11	18:16	2.21	1.25	1.02	65.41	2.15
18:16	18:21	2.20	1.23	1.01	64.72	2.24
18:21	18:26	2.23	1.25	1.02	65.42	2.11
18:26	18:31	2.26	1.28	1.01	65.40	1.95
18:31	18:36	2.26	1.29	1.02	66.37	1.85
18:36	18:41	2.24	1.28	1.02	67.21	1.78
18:42	18:47	1.62	1.39	0.83	47.27	0.81
18:47	18:52	1.78	1.17	0.87	54.99	1.55
18:52	18:57	1.77	1.12	0.92	58.16	1.51
18:57	19:02	1.82	1.10	0.94	58.95	1.50
19:02	19:07	1.88	1.08	0.93	58.28	1.62
19:07	19:12	1.86	1.05	0.92	57.37	1.81
19:12	19:17	1.84	1.03	0.91	58.09	1.72
19:17	19:22	1.86	1.03	0.92	57.94	1.78

Table 3 cont'd

Start	End	sigma u	sigma v	sigma w	wind direction	wind speed
19:22	19:27	1.82	1.00	0.91	58.11	1.79
19:27	19:32	1.85	0.99	0.89	57.62	1.95
19:32	19:37	1.84	0.98	0.89	57.90	1.92
19:37	19:42	1.84	0.98	0.89	58.21	1.82
19:42	19:47	1.83	0.99	0.89	58.39	1.72
19:48	19:53	1.07	0.90	0.61	25.62	1.98
19:53	20:58	1.18	1.20	0.73	19.46	2.06
20:58	20:03	1.25	1.14	0.72	22.61	2.25
20:03	20:08	1.33	1.08	0.70	25.99	2.54
20:08	20:13	1.30	1.02	0.68	27.66	2.65
20:13	20:18	1.24	0.95	0.65	28.83	2.60
20:18	20:23	1.20	0.92	0.64	30.63	2.62
20:23	20:28	1.18	0.90	0.63	31.94	2.68
20:28	20:33	1.16	0.87	0.62	31.96	2.64
20:33	20:38	1.16	0.86	0.61	32.06	2.66
20:38	20:43	1.15	0.84	0.61	32.43	2.68
20:43	20:48	1.00	0.70	0.58	34.03	2.97
20:48	20:53	1.02	0.69	0.57	31.83	2.94
20:55	21:00	0.92	0.66	0.52	33.64	2.04
21:00	21:05	0.86	0.62	0.49	35.26	1.96
21:05	21:10	0.81	0.59	0.46	36.32	1.96
21:10	21:15	0.82	0.59	0.46	36.43	1.96
21:15	21:20	0.83	0.60	0.48	35.62	1.97
21:20	21:25	0.83	0.60	0.48	35.19	1.93
21:25	21:30	0.85	0.61	0.49	34.41	1.93
21:30	21:35	0.87	0.62	0.50	33.97	1.96
21:37	21:42	0.94	0.65	0.57	32.72	2.26
21:42	21:47	1.02	0.72	0.62	32.29	2.48
21:47	21:52	1.04	0.74	0.62	32.53	2.54
21:52	21:57	1.02	0.72	0.62	32.50	2.50
21:57	22:02	1.01	0.72	0.61	32.76	2.51
22:02	22:07	1.01	0.73	0.62	33.08	2.54
22:07	22:12	1.01	0.73	0.62	33.21	2.55
22:12	22:17	1.01	0.74	0.62	33.41	2.58
22:17	22:22	1.02	0.74	0.63	33.54	2.59
22:23	22:28	1.07	0.72	0.59	31.91	3.11
22:28	22:33	1.09	0.74	0.59	31.36	3.09
22:33	22:38	1.12	0.75	0.59	30.88	3.08
22:38	22:43	1.11	0.74	0.59	30.67	3.05
22:43	22:48	1.10	0.73	0.59	30.37	3.03
22:48	22:53	1.12	0.72	0.58	30.10	2.94
22:53	22:58	1.14	0.73	0.58	29.58	2.82
22:58	23:03	1.21	0.77	0.58	27.76	2.62
23:03	23:08	1.25	0.80	0.58	25.87	2.46

Table 4: Sigma u, v, w, July 26, 2001

Start	End	sigma u	sigma v	sigma w	wind direction	wind speed
15:59	16:04	1.47	1.15	0.78	46.48	4.55
16:04	16:09	1.46	1.10	0.79	44.49	4.40
16:09	16:14	1.48	1.05	0.77	43.17	4.32
16:14	16:19	1.49	1.04	0.76	44.54	4.30
16:19	16:24	1.49	1.08	0.77	44.78	4.39
16:24	16:29	1.51	1.09	0.78	45.04	4.47
16:29	16:34	1.51	1.07	0.77	44.76	4.37
16:34	16:39	1.48	1.05	0.76	45.25	4.34
16:43	16:48	1.27	0.98	0.76	45.91	4.43
16:48	16:53	1.26	0.95	0.72	46.35	4.30
16:53	16:58	1.26	0.94	0.72	47.23	4.34
16:58	17:03	1.32	0.98	0.73	47.95	4.44
17:03	17:08	1.30	0.97	0.72	47.81	4.36
17:08	17:13	1.28	0.95	0.71	47.39	4.27
17:13	17:18	1.28	0.92	0.70	46.93	4.14
17:18	17:23	1.31	0.91	0.69	45.95	4.05
17:23	17:28	1.31	0.91	0.69	45.72	4.07
17:28	17:33	1.35	0.93	0.71	45.14	4.13
17:33	17:38	1.43	0.95	0.72	44.43	4.06
17:38	17:43	1.42	0.94	0.72	43.95	4.05
17:43	17:48	1.43	0.94	0.73	44.04	4.08
17:48	17:53	1.44	0.95	0.73	44.04	4.08
17:53	17:58	1.46	0.95	0.73	43.66	4.02
17:58	18:03	1.46	0.94	0.72	43.52	3.98
18:03	18:08	1.45	0.94	0.72	43.70	3.98
18:08	18:13	1.44	0.94	0.72	43.51	3.96
18:13	18:18	1.43	0.93	0.72	43.55	3.94
18:18	18:23	1.42	0.93	0.71	43.75	3.92
18:23	18:28	1.41	0.92	0.71	43.93	3.90
18:31	18:36	1.07	0.75	0.60	48.60	3.55
18:36	18:41	1.02	0.76	0.61	47.84	3.52
18:41	18:46	1.07	0.74	0.59	46.44	3.34
18:46	18:51	1.03	0.73	0.57	46.84	3.26
18:51	18:56	1.02	0.77	0.56	48.29	3.20
18:56	19:01	1.00	0.76	0.55	47.53	3.18
19:01	19:06	1.01	0.74	0.55	48.00	3.13
19:06	19:11	1.03	0.76	0.55	46.88	3.06
19:11	19:16	1.12	0.77	0.54	45.63	2.91
19:16	19:21	1.13	0.76	0.54	44.71	2.84

APPENDIX B

13.1 THE DEVELOPMENT AND EVALUATION OF A DISPERSION MODEL FOR URBAN AREAS

Akula Venkatram *, Jeetendra K. Upadhyay, Jing Yuan, James Heumann and Joseph Klewicki [+]

University of California, Riverside, CA

[+]University of Utah, Salt Lake City, UT

1. INTRODUCTION:

There is a need for a model to estimate concentrations of releases within the urban canopy at scales of meters from the source. This has motivated several experiments (Davidson et al, 1995; McDonald et al, 1998; Mavroidis and Griffiths, 2001) to understand dispersion within a model urban canopy constructed with cubical or cylindrical obstacles with dimensions of the order of a meter. Results from such studies will eventually result in parameterizations that can be incorporated into models such as ISC or AERMOD.

This paper describes preliminary results from experiments to understand the role of source characteristics on dispersion within a model urban canopy. This is the first stage of a program to develop a practical dispersion model for urban areas. The parameterization resulting from the model study will be evaluated with tracer data from a field study in a real urban area.

2. DUGWAY EXPERIMENT:

The small-scale experiment was conducted at Dugway Proving Ground, Utah from 12th July 2001 to 26th July 2001. The urban canopy was simulated with a 5 × 9 rectangular array of 45 barrels with height H=0.91m and diameter d=0.57m, and a center-to-center spacing S=1.8m. The experiment corresponds roughly to a model length scale ratio of 1:10 and plan area density of 16%, which is typical of an urban canopy.

Propylene (C_2H_6), a tracer, was released through a 25.4mm diameter pipe, both upstream and within the barrel array. The release rate was 15 standard liters/minute. The tracer was sampled on receptor arcs at 1.5S, 2.5S, and 4.5S from the source. Each arc contained 11 photo-ionization detectors (PIDs), 5° apart at 0.23H. The furthest distance of 4.5S scales up to approximately 100 meters in a real urban area. One PID was placed at 0.5S to sample the cavity region of the obstacle where the source is located. At 4.5S, two PIDs were placed at 0.5H and 1.5H, where H is the height of the obstacle. The vertical array of three PIDs at 4.5S provided information to construct the vertical profile of concentrations.

* Corresponding author address: Akula Venkatram, College of Engineering, University of California, Riverside, CA 92521; e-mail: venky@engr.ucr.edu

Turbulence, velocity, and temperature measurements were made with sonic anemometers at three locations. Three sonics at 0.5H, 1.0H, and 2.0H on an upwind tower provided information on the approach flow. One sonic at 0.5H, behind the source obstacle, provided flow and turbulence information in the cavity region of the source. Two sonics at 0.5H and 1.5H located at 4.5S from the source provided information on the fully developed flow in the urban canopy.

The tracer source was located at either ground-level or at 1H. For each source location, four different barrel configurations were arranged near the source. In the first and second configurations, the source was placed directly upwind of a single barrel and two barrels placed side by side, respectively. In the third configuration, four barrels surrounded the source. In the final configuration, the source was located directly upwind of a three barrel pyramid.

The model experiment was designed to understand the effects of source configuration on dispersion. The second major objective was to explore the possibility of using turbulence measurements within the urban canopy to estimate plume dispersion.

3. RESULTS AND DISCUSSION:

Figures 4.1-4.4 compare the variation of plume parameters for releases within the canopy with those in the absence of the canopy. These plume parameters were obtained by averaging over all the experiments corresponding to a particular source configuration. They thus represent an average over a variety of meteorological conditions. The horizontal plume spread was obtained by a fitting a Gaussian profile to the concentrations on each arc, while the vertical plume spread, σ_z, was inferred from ground-level concentrations.

Figure 4.1 shows the effect of the obstacle array on σ_y. These figures indicate that σ_y grows more or less linearly with distance even when the release is behind an obstacle. There is no apparent effect of the obstacle on the horizontal plume spread. However, the growth rate is substantially larger in the obstacle array than that in flat terrain. This corresponds to the increase in σ_v/U from about 0.14 in the absence of the array to about 0.5 within the array measured just behind the source at a height of 0.5H. The value of σ_v/U just downwind of the source is about 0.26, which is more consistent with the σ_y growth rate. It appears that σ_y is governed more by the average turbulent intensity within the canopy rather than that in the cavity of the source. The behavior of σ_y, when the

release is at 1H is very similar to that for the ground release, again suggesting the dependence of σ_y on average urban canopy intensities.

The effect of the source is more apparent in the growth of σ_z with distance from the source. Figure 4.3 indicates that σ_z grows rapidly close to the source, and then appears to grow more slowly beyond x/H=5. In the absence of the obstacle, σ_z grows linearly. The behavior of σ_z for a release at H was qualitatively similar to that of the ground-level release.

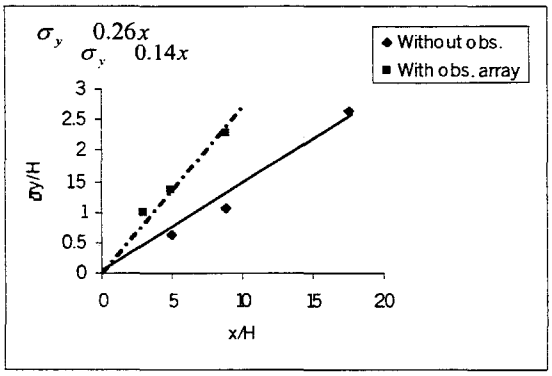

Fig. 4.1: Variation of σ_y/H with x/H with source at ground level

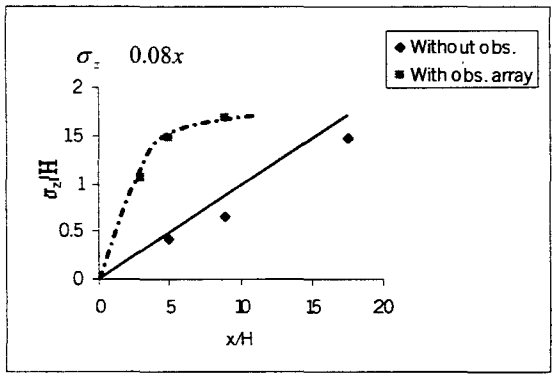

Fig. 4.2: Variation of σ_z/H with x/H with source at ground level

Fig. 4.3 and 4.4 compare the variation of the normalized concentration, C/Q in the obstacle array with that without the obstacles. We see that the concentrations for both the ground-level and the elevated releases are 3 to 5 times lower than those over flat terrain. We expect the concentration in the wake of the obstacle to be higher for an elevated release than that in the absence of the obstacle. A more detailed analysis of the data might provide evidence of this.

In the future, the behavior of plume parameters in the model urban canopy will be related to the measured turbulence parameters.

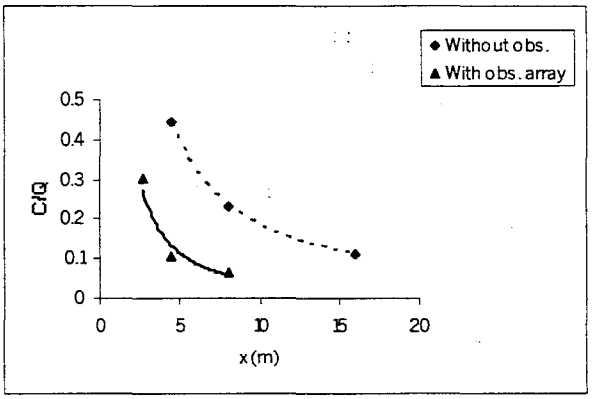

Fig. 4.3: Variation of C/Q with x/H with source at ground level

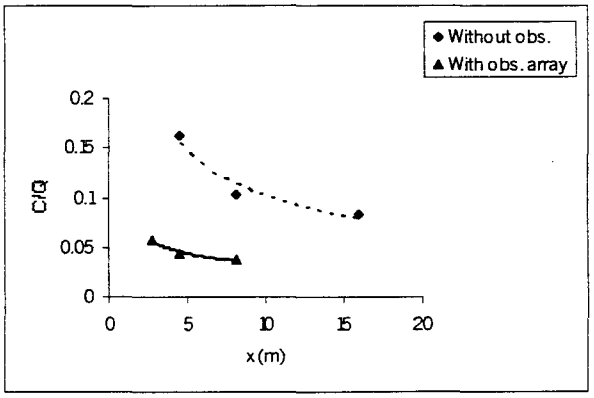

Fig. 4.4: Variation of C/Q with x/H with source at 1H level

Acknowledgements

The research described in this paper is funded by the California Air Resources Board (ARB). We would like to thank the ARB project monitor, Jim Pederson, for his support and encouragement.

REFERENCES:

Davidson, M. J., Mylne, K. R., Jones, C. D., Phillips, J. C., Fung, J. C. H and Hunt, J. C. R., 1995: Plume dispersion through large groups of obstacles-A field investigation. *Atmos. Environ.*, **29**, 3245-3256.

MacDonald, R. W., Griffiths, R. F. and Hall, D. J., 1998: A comparison of results from scaled field and wind tunnel modelling of dispersion in arrays of obstacles. *Atmos. Environ.*, **32**, 3845-3862.

Mavroidis, I and Griffiths, R. F., 2001: Local characteristics of atmospheric dispersion within building arrays. *Atmos. Environ.*, **35**, 2941-2954.

APPENDIX C

Appendix C
Model Input Files for Simulations of CECERT Experiment

Seven text files are available containing model input data used in simulating the tracer concentrations at CE-CERT as reported in the main body of the report. Four files contain source configuration input data. Three files contain meteorological input data. These files are available upon request.

Activation of the PRIME algorithm is by inclusion of building dimensions within the input file that describes the source configuration. Source configuration input files that do not include buildings do not activate the PRIME algorithm.

ISCST3.INP
Input file for ISCST3
(Source configuration without buildings i.e., PRIME algorithm not in effect)

ISCPRIME.INP
Input file for ISCST3
(Source configuration with buildings, i.e., PRIME algorithm in effect)

AERMOD_NOB.INP
Input file for AERMOD
(Source configuration without buildings, i.e., PRIME algorithm not in effect)

AERMOD_BLD.INP
Input file for AERMOD-PRIME
(Source configuration with buildings, i.e., PRIME algorithm in effect)

Running a simulation with AERMOD requires two meteorological input files, one for surface meteorological observations and one for profiles of aloft observations. ISCST 3 requires one meteorological input file.

CECERT01.MET
Meteorological input file for ISCST3

AERMET.SFC
Meteorological input file for AERMOD (surface met data)

AERMET.PFL
Meteorological input file for AERMOD (aloft-profile met data)